

DIGITAL ACCESS TO SCHOLARSHIP AT HARVARD
DASH.HARVARD.EDU

HARVARD LIBRARY


Probing Synovial Sarcomas and the Ubiquitin-Proteasome System With Small Molecules

Citation

Garcia-Rivera, Enrique Miguel. 2017. Probing Synovial Sarcomas and the Ubiquitin-Proteasome System With Small Molecules. Doctoral dissertation, Harvard University, Graduate School of Arts & Sciences.

Link

http://nrs.harvard.edu/urn-3:HUL.InstRepos:41141313

Terms of use

This article was downloaded from Harvard University's DASH repository, and is made available under the terms and conditions applicable to Other Posted Material (LAA), as set forth at
https://harvardwiki.atlassian.net/wiki/external/NGY5NDE4ZjgzNTc5NDQzMGIzZWZhMGFlOWI2M2EwYTg

Accessibility

https://accessibility.huit.harvard.edu/digital-accessibility-policy

Share Your Story

The Harvard community has made this article openly available.
Please share how this access benefits you. Submit a story

Probing Synovial Sarcomas and the Ubiquitin-Proteasome System with Small Molecules

A dissertation presented

by

Enrique Miguel García-Rivera

to

The Division of Medical Sciences

in partial fulfillment of the requirements

for the degree of

Doctor of Philosophy

in the subject of

Biological and Biomedical Sciences

Harvard University

Cambridge, Massachusetts

April 2017

© This work by Enrique Miguel García-Rivera is licensed under the Creative Commons Attribution-NonCommercial-NoDerivatives 4.0 International License. To view a copy of this license, visit http://creativecommons.org/licenses/by-nc-nd/4.0/.



Dissertation Advisors: Enrique Miguel García-Rivera

Dr. Stuart Schreiber

Dr. Cigall Kadoch

Probing Synovial Sarcomas and the Ubiquitin-Proteasome System with Small Molecules

Abstract

Chemical probes have radically transformed our ability to modulate cellular activity by providing robust and reversible disruption of select biological processes. To uncover a novel set of these tools, I first performed a small molecule screen to identify compounds that could selectively prevent the growth of synovial sarcoma (SS) cell lines and observed that MET inhibitors could target a distinct subset. This MET sensitivity was defined by amplification of the MET gene and an active AKT pathway. Through immunohistochemistry of SS patient tumor samples, I discovered that MET is only expressed in the glandular component of biphasic SS, the same histological subtype of the SS cell lines that were sensitive to MET inhibition. Furthermore, this dependency could be targeted *in vivo*, with the MET inhibitor SGX-523 preventing the growth of a biphasic SS xenograft in mice. I also compared the transcriptional changes caused by MET inhibition to loss of SS18-SSX1, the fusion protein understood to initiate SS

oncogenesis. These two perturbations were found to behave very similarly, altering pathways associated to the epithelial to mesenchymal transition, cell-cycle progression, and differentiation. This is one of the first targetable dependencies discovered in this cancer and it could have a marked impact in the future of SS treatment.

Second I executed a screen to identify compounds that could increase the protein levels of the tumor suppressor BAF47 in SS cells and discovered BRD1732, a novel probe of the ubiquitin-proteasome pathway with a novel mechanism of action (MOA) and a yet to be identified target. Cellular treatment with BRD1732 causes a profound increase in the levels of free cellular ubiquitin alongside various protein level increases (e.g. of p21/p27), inhibition of NFκB signaling, and inhibition of the unfolded protein response. The compound does not inhibit the human 26S proteasome, E1 or most E2 enzymes *in vitro*, suggesting a unique MOA distinct from canonical proteasome inhibition. BRD1732 can also prevent the growth of various cancer cell lines, indicating a potential for translation into the clinic. This probe could uncover novel biology surrounding protein homeostasis and further the therapeutic relevance of the ubiquitin-proteasome pathway.

Table of Contents

CHAPTER 1: INTRODUCTION TO SYNOVIAL SARCOMAS AND THE UBIQUITIN-PROTEASOME SYSTEM 1

CHAPTER 1.1: SYNOVIAL SARCOMA 2

Chapter 1.1.1: Pathology of Synovial Sarcomas 2

Chapter 1.1.2: Synovial Sarcoma Fusion Protein SS18-SSX 9

Chapter 1.1.3: Chromatin Remodeling Complex BAF 10

Chapter 1.1.4: Polycomb-mediated Transcriptional Repression 13

Chapter 1.1.5: SS18-SSX-mediated Transcriptional Regulation 15

Chapter 1.1.6: Synovial Sarcoma Standard of Care 17

Chapter 1.1.7: BAF Subunit Regulation by the Proteasome 18

CHAPTER 1.2: THE UBIQUITIN PROTEASOME SYSTEM 19

Chapter 1.2.1: Protein Degradation by the Proteasome 19

Chapter 1.2.2: Ubiquitin as a Degradation Signal 22

Chapter 1.2.3: Ubiquitin Conjugation and Ligation 23

Chapter 1.2.4: Ubiquitin Recognition and Processing 26

Chapter 1.2.5: Inhibitors of the Ubiquitin-Proteasome System as Cancer Therapeutics 29

Chapter 1.2.5.1: Inhibitors of the Proteasome 29

Chapter 1.2.5.2: Inhibitors of Ubiquitin Ligation 32

REFERENCES 34

CHAPTER 2: SMALL MOLECULE PROFILING OF SYNOVIAL SARCOMA CANCER CELL LINES 52

CHAPTER 2.1: INTRODUCTION 53

CHAPTER 2.2: IDENTIFYING PATHWAY DEPENDENCIES IN SS USING SMALL-MOLECULE PROFILING 54

CHAPTER 2.3: MET IS A SPECIFIC LETHAL DEPENDENCE IN SENSITIVE SS CELL LINES 60

CHAPTER 2.4: SS CELL LINES EXHIBIT DIFFERENTIAL EXPRESSION OF RTKS 65

CHAPTER 2.5: METHODS 70

Chapter 2.5.1: Cancer cell-line profiling 70

Chapter 2.5.2: Immunoblotting 70

Chapter 2.5.3: RNA Extraction and RNA-Seq 71

Chapter 2.5.4: Sequencing data processing & analysis 72

CHAPTER 2.6: CONCLUSIONS 73

REFERENCES 74

CHAPTER 3: MET POTENTIATION OF SS18-SSX IN BIPHASIC SYNOVIAL SARCOMAS 77

CHAPTER 3.1: INTRODUCTION 78

CHAPTER 3.2: BIPHASIC SS BIOPSIES SHOW HIGH LEVELS OF MET EXPRESSION 79

CHAPTER 3.3: THE MET INHIBITOR SGX-523 REDUCES TUMOR VOLUME AND EXTENDS SURVIVAL IN VIVO IN A BIPHASIC TUMOR XENOGRAFT MODEL 82

CHAPTER 3.4: LOSS OF SS18-SSX1 REGULATES SIMILAR PATHWAYS TO MET INHIBITION 84
CHAPTER 3.5: METHODS 90
Chapter 3.5.1: RNA Extraction and RNA-Seq 90
Chapter 3.5.2: Sequencing data processing & analysis 90
Chapter 3.5.3: Immunohistochemistry of patient biopsies 90
Chapter 3.5.4: Cell line xenograft 91
CHAPTER 3.6: CONCLUSIONS 92
REFERENCES 95
CHAPTER 4: SCREEN FOR PROTEIN STABILIZERS OF BAF47 99
CHAPTER 4.1: INTRODUCTION 100
CHAPTER 4.2: GENERATING A REPORTER OF BAF47 PROTEIN LEVELS 101
CHAPTER 4.3: SCREEN OF A PERFORMANCE-DIVERSE LIBRARY OF SMALL MOLECULES 102
CHAPTER 4.4: METHODS 109
Chapter 4.4.1: Reporter Construct Generation 110
Chapter 4.4.2: Cell Culture and Lentiviral Production 110
Chapter 4.4.3: Phenotypic Screening 111
Chapter 4.4.4: Immunofluorescence 111
Chapter 4.4.5: Immunoblotting 112
Chapter 4.4.6: Protease Profiling 113

CHAPTER 4.4: CONCLUSIONS 113

REFERENCES 114

CHAPTER 5: BRD1732 IS A CHEMICAL PROBE OF THE UBIQUITIN-PROTEASOME SYSTEM 116

CHAPTER 5.1: INTRODUCTION 117

CHAPTER 5.2: BRD1732 DISRUPTS THE UBIQUITIN-PROTEASOME SYSTEM 118

CHAPTER 5.3: BRD1732 DOES NOT PREVENT *IN VITRO* UBIQUITIN LIGATION 129

CHAPTER 5.4: BRD1732 INDUCES TRANSCRIPTIONAL AND PROTEOME-WIDE CHANGES THAT ARE DISTINCT FROM PROTEASOME INHIBITION 131

CHAPTER 5.5: BRD1732 INDUCES CELL-CYCLE ARREST 138

CHAPTER 5.6: TARGET ID EFFORTS FOR BRD1732 141

Chapter 5.6.1: Biotinylated Analogs of BRD1732 141

Chapter 5.6.2: Identifying Resistance Mechanisms to BRD1732 using CRISPR 144

CHAPTER 5.7: METHODS 146

Chapter 5.7.1: Cell Culture 146

Chapter 5.7.2: Immunoblotting and Compound Treatment 146

Chapter 5.7.3: In vitro Proteasome Activity 147

Chapter 5.7.4: NFκB Activity Reporter 147

Chapter 5.7.5: Aggresome Formation 148

Chapter 5.7.6: Transcriptional Profiling 148

Chapter 5.7.7: Whole-lysate Proteomics 149

Chapter 5.7.8: Cell-cycle Profiling 150

Chapter 5.7.9: CRISPR Resistance Screen 150

CHAPTER 5.8: CONCLUSIONS 151

REFERENCES 155

CHAPTER 6: CONCLUDING REMARKS 158

CHAPTER 6.1: SUMMARY AND IMPACT OF DISSERTATION 159

CHAPTER 6.2: FUTURE DIRECTIONS 161

REFERENCES 164

Acknowledgements

The work here presented could not have been possible without the advising and mentorship of Dr. Cigall Kadoch, who has been a terrific advisor throughout the development of this thesis. In addition, I wouldd like to thank Dr. Stuart Schreiber for given me the flexibility and the opportunity to express myself as a scientist in such a creative way. I would also like to acknowledge members of the Schreiber and Kadoch groups who have contributed to this work, both as co-workers and as friends, and in helping to keep myself grounded in times of hardship. There are also the folks who made graduate school that much more enjoyable, and I thank Steven Poynter, Micah Maetani, Dr. Zarko Boskovic, Sebastian Stark, Dr. Max Majireck, Daniel Tarjan, Tyler Huycke, Anna Maurer, Dr. Jason Law, Jessica Heslin, Ramon Rios, Ricardo Peña, David Jaramillo, and the many other friends I have in Boston for stepping up to the task.

Dedicated to my parents, for their unwavering support of my curiosity.

Chapter 1: Introduction to Synovial Sarcomas and the Ubiquitin-Proteasome System

Chapter 1.1: Synovial Sarcoma

Chapter 1.1.1: Pathology of Synovial Sarcomas

A rare form of cancer, Synovial Sarcoma (SS) is an aggressive soft-tissue malignancy that occurs mostly in young patients (Thway & Fisher, 2014). Despite its name, SS is a clinically and morphologically well-defined entity that is rarely found in joint cavities and occurs most frequently in areas with no relation to synovial structures (Goldblum, Weiss, & Folpe, 2013). These areas are primarily the para-articular regions of the extremities, usually around tendon sheaths, bursae, and joint capsules (Goldblum et al., 2013). Its designation as “synovial” stems from its microscopic resemblance to developing synovium in early literature, but there is little evidence that this is in fact the tissue of origin. The descriptive nature of earlier sarcoma work wrongfully attributed SS to the synovium, with mounting evidence suggesting a marked difference between SS and this tissue, both through immunophenotypic and ultrastructural observations.

Synovial Sarcoma accounts for roughly 5-10% of all soft-tissue sarcomas, making it fourth most common form of this cancer subtype (Herzog, 2005; W. Shi et al., 2013). About 12,390 new soft-tissue sarcomas are diagnosed in the U.S. every year, and 4,990 patients are expected to die of soft-tissue sarcomas

(American Cancer Society, 2016). It is most prevalent in young adults between the ages of 15 and 40, with a mean age of incidence of 34 (Ladanyi et al., 2002). Males are more frequently afflicted with SS, with a male-to-female ratio of 1.2 to 1.0 (Goldblum et al., 2013). Prognosis for SS patients is quite poor, with reported 5-year and 10-year survival rates as low as 36 and 20%, respectively (Haldar, Randall, & Capecchi, 2008).

Most often SS presents itself as a palpable swelling or mass associated with pain in more than 50% of cases (Pollock & Society, 2002). Motion is largely unperturbed, with tumors growing slowly and insidiously for a pre-operative period of 2-4 years (Goldblum et al., 2013). It is most often misdiagnosed as arthritis, synovitis, and bursitis due to the similarity of their symptoms and presentation. As previously mentioned, synovial sarcomas occur most frequently in the extremities, and they are tightly associated with tendons, tendon sheaths, and bursal structures. A study from the Armed Forces Institute of Pathology (AFIP) of 345 cases found the following distribution of anatomic locations for SS:

Table 1.1. Distribution of anatomic locations where SS was found.

Adapted from: (Goldblum et al., 2013)

ANATOMIC LOCATION	NO. OF CASES
Head-Neck	**31 (9.0%)**
Neck	12
Pharynx	7
Larynx	7
Other	5
Trunk	**28 (8.1%)**
Chest	10
Abdominal wall	9
Other	9
Upper Extremities	**80 (23.2%)**
Forearm-wrist	24
Shoulder	22
Elbow-upper arm	20
Hand	14
Lower Extremities	**206 (59.7%)**
Thigh-knee	102
Foot	45
Lower leg-ankle	33
Hip-groin	22
Other	4
Total	**345 (100.0%)**

85-95% of SS cases occur in the extremities, with a higher frequency observed in the lower extremities. This is dominated by cases in the area surrounding the knee, followed by cases in the foot and lower leg-ankles. The upper extremities are the second most common location for SS, with cases equally distributed across the wrist, shoulders and elbow-upper arm region. Outside of the extremities cases of the head and neck are most common, accounting for 5-10% of all cases. These cases seem to arise from the paravertebral connective tissue spaces and manifest as masses near the carotid bifurcation (Al-Daraji, Lasota, Foss, & Miettinen, 2009). Despite these clear tendencies, SS cases have been reported in almost all anatomic sites, including the heart, pleuropulmonary region, kidney, prostate, retroperitoneum, gastrointestinal tract and peripheral nerve. This adds difficulty to the diagnosis of synovial sarcoma, requiring additional molecular genetic testing.

There are two major categories of SS from a histological point of view: monophasic and biphasic (Vlenterie, Jones, & van der Graaf, 2015). The biphasic SS are characterized by having two distinct epithelial and spindle cell components (**Figure 1.1**), with the epithelial part presenting itself as glands. These epithelial cells resemble those of carcinoma, while the spindle cells are more akin to a fibrosarcoma (**Figure 1.2**). Monophasic SS is on the other hand completely composed of spindle cells. SS can also be identified as poorly

differentiated round cell sarcoma, seen in a pericytomatous pattern (also known as poorly differentiated synovial sarcoma), but this is not a true subtype but rather a form of SS progression that can arise from both monophasic and biphasic SS ("Poorly Differentiated Synovial Sarcoma: A Unique Presentation," 2015).

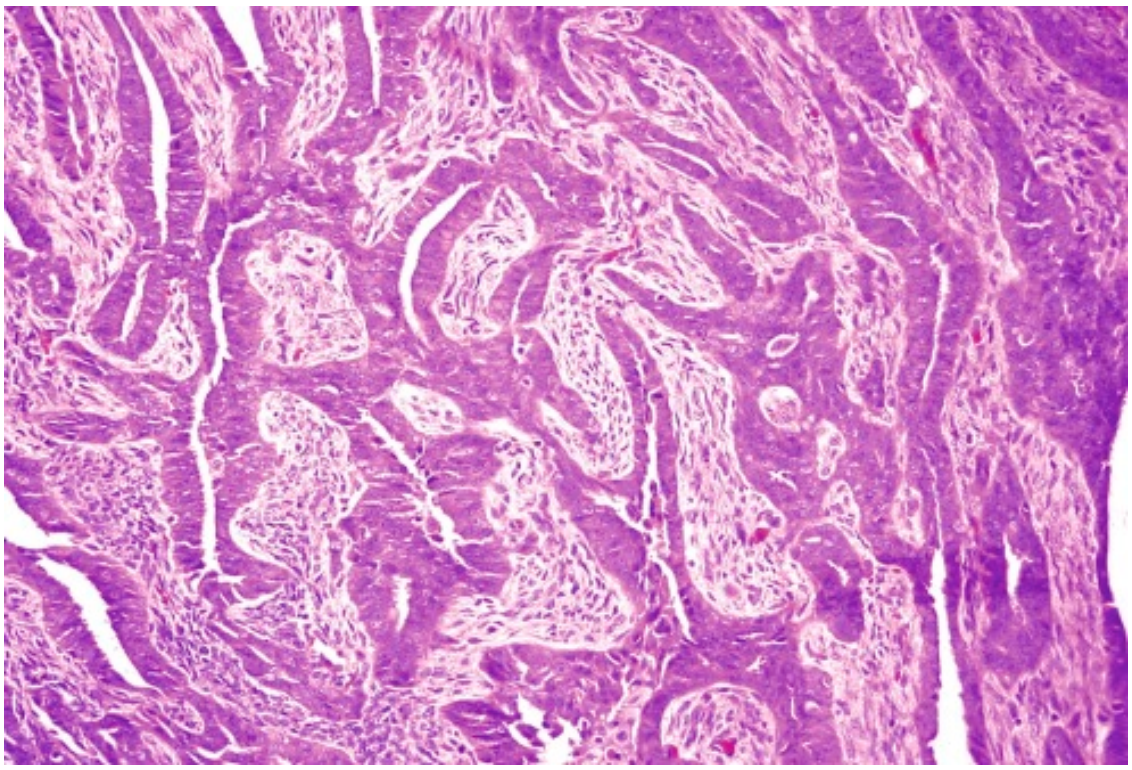


Figure 1.1. Biphasic SS. H&E staining from a biphasic SS tumor biopsy showing clear distinction between glandular epithelial structures and spindle cell elements. Adapted from: (Goldblum et al., 2013)

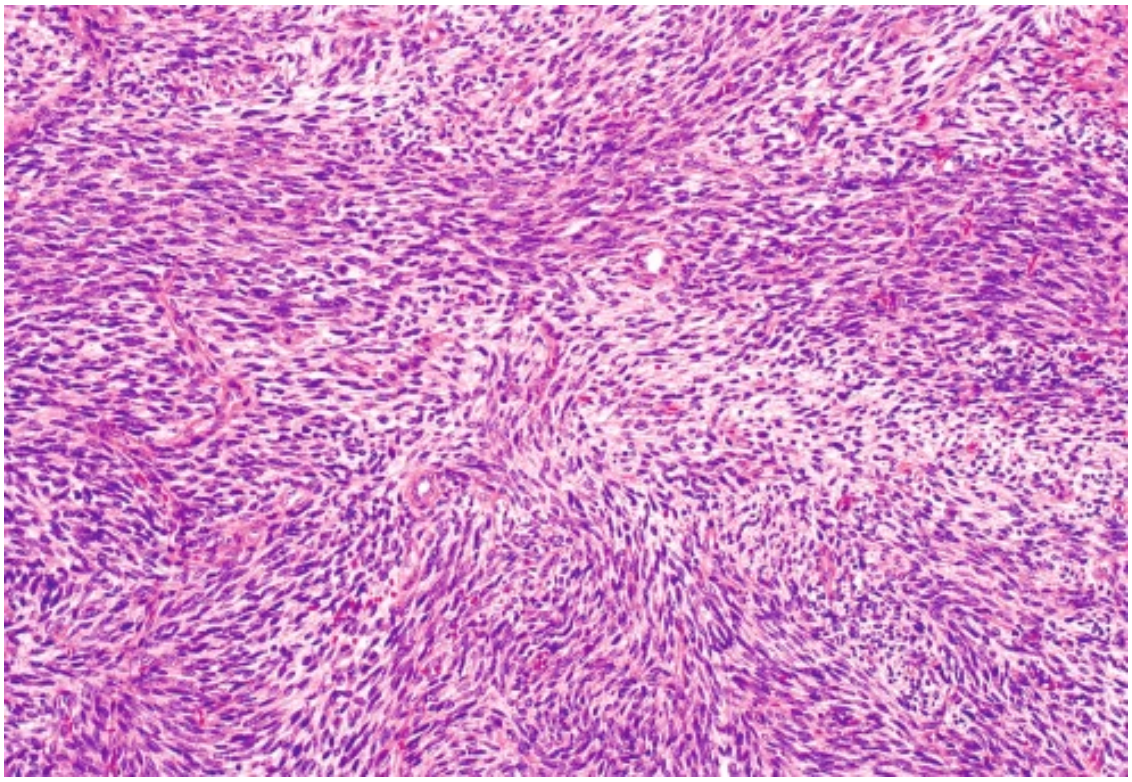


Figure 1.2. Monophasic SS. H&E staining from a monophasic SS tumor biopsy showing a homogenous population of spindle-like cells arranged in distinct fascicles. Adapted from: (Goldblum et al., 2013)

Synovial sarcomas are genetically well-defined, with a single chromosomal translocation, t (X;18) (p11.2;q11.2), occurring in virtually all patients (Ladanyi et al., 2002). This aberration was originally identified through screening of a synovial sarcoma cDNA library with a yeast artificial chromosome spanning the X chromosome breakpoint (Clark et al., 1994). This generated a transcript with sequences that mapped to both chromosome X and chromosome 18. Candidate genes were narrowed to the following two: SSX, so named for **S**ynovial **S**arcoma

X chromosome breakpoint, and SYT, named for **Sy**novial Sarcoma **T**ranslocation, generating the fusion protein SYT-SSX. This fusion was confirmed in multiple independent studies and expanded to include fusion of SYT with three homologs of SSX: SSX1, SSX2 or SSX4 (Brodin et al., 2001; Crew et al., 1995; Fligman et al., 1995). Interestingly there is some evidence suggesting that the specific SSX fusion is correlated with unique histological subtypes. In one study, all biphasic tumors had the SYT-SSX1 fusion, whereas the monophasic tumors harbored SYT-SSX2 (Antonescu et al., 2000). The gene name for SYT was later changed to SSXT and ultimately SS18, for synovial sarcoma chromosome 18, hence the fusion is most commonly and appropriately referred to as SS18-SSX (Yates et al., 2017). Expression of the fusion protein can be reliably detected with either RT-PCR or FISH (Nikiforova, Groen, Mutema, Nikiforov, & Witte, 2005; Surace et al., 2004), and it is instrumental in the diagnosis of SS.

Prognosis for synovial sarcoma patients is favorable in the absence of metastasis, with one study reporting a 5-year survival rate of 75% for patients with a localized disease that drops to 10% for patients with metastatic disease (Palmerini et al., 2009). There are three major factors that appear to associate with a low rate of SS metastasis: age (less than 25 years), tumor size (less than 5cm), and tumor differentiation (absence of poorly differentiated areas) (Goldblum et al., 2013). The proportion of epithelial versus spindled areas does

not seem to associate with prognosis (Machen, Easley, & Goldblum, 1999), though there has not been a definitive study on the matter due to irregularities in the classification of SS subtypes.

Chapter 1.1.2: Synovial Sarcoma Fusion Protein SS18-SSX

Due the prevalence of the fusion protein in all SS cases, understanding the mechanistic function of SS18-SSX is imperative for advancing the treatment of the disease. Information has been slowly accumulating over the years and we are only now beginning to understand the oncogenesis program initiated by SS18-SSX. Initial insights came from the cellular localization of SS18 and SSX, both found to be predominantly expressed in the nuclear compartment (Brett et al., 1997). SS18 displays a punctate staining pattern, while SSX1 is uniformly distributed across the nucleus. This diffuse pattern is preserved in the staining pattern of exogenously expressed SS18-SSX1 (Brett et al., 1997), suggesting that SS18 and its associated factors are recruited to SSX1 sites when the fusion is expressed. The SS18 protein has two major domains: the SS18 NH_2-terminal homology (SNH) domain, conserved among a wide variety of species, and the glutamine-, proline-, glycine-, and tyrosine-rich QPGY domain (Thaete et al., 1999). SS18 itself was found to colocalize with various proteins of the ATP-dependent chromatin remodeler BAF (also known as SWI/SNF) (Perani, Ingram,

Cooper, Garrett, & Goodwin, 2003), displaying an interaction with BAF core subunits hBRM and BRG1 through its SNH domain.

Chapter 1.1.3: Chromatin Remodeling Complex BAF

Being one of the most studied ATP-dependent chromatin remodeling complexes, the activity of BAF (SWI/SNF) has traditionally been associated with gene activation (Peterson & Herskowitz, 1992), with a number of subunits forming part of the historical *Trithorax* group (trxG) genes (Francis & Kingston, 2001). It was originally discovered in yeast through screens aimed at finding genes responsible for sucrose fermentation (Carlson, Osmond, & Botstein, 1981) (SNF) and mating type switching (SWI) (Stern, Jensen, & Herskowitz, 1984), and it was subsequently found that these proteins form a multi-subunit complex capable of regulating gene expression (Peterson & Tamkun, 1995). These complexes utilize the energy of ATP to remodel nucleosomes, altering their interactions with DNA that are necessary for transcriptional activity by repositioning histone octamers (Vignali, Hassan, Neely, & Workman, 2000). In higher eukaryotes, homologs of the SWI/SNF ATPase SWI2 were found in both *Drosophila* and mammals (Brm and Brg1, respectively), also as parts of large protein complexes. Because the subunit composition of these complexes differed in many parts from its yeast counterpart, these complexes were subsequently named after their respective

ATPase subunit; e.g. those associated with Brg1 were coined Brg1 Associated Factors (BAF) (Wang, Cote, Xue, Zhou, & Khavari, 1996).

BAF complexes are divided into two broad types: BAF and polybromo-associated BAF (PBAF), the latter distinguished by the inclusion of polybromo and ARID subunits. BAF is composed of a single central ATPase, BRG (SMARCA4) or BRM (SMARCA2), in combination with several other BAF subunits. In addition to yeast SWI/SNF homologs, several subunits appear to be mammalian specific, such as: SS18, BCL7, BCL11, and BRD9 (Hodges, Kirkland, & Crabtree, 2016). BAF was initially characterized through affinity purification of Brg1, which yielded two distinct complexes with an apparent non-identical subunit composition (Wang et al., 1996). One of these complexes was later shown to be defined by the inclusion of BAF180, a polybromo domain containing protein, hence it was renamed to Polybromo BAF or PBAF (Xue et al., 2000). PBAF complexes contain PBRM1 but lack ARID1A/B, in addition to having BRD7 in place of BRD9 (Hodges et al., 2016). In contrast to BAF, PBAF shows some similarity to the yeast RSC complex, sharing its cellular localization at kinetochores of chromosomes during mitosis and playing a key role in cell division (Xue et al., 2000).

The changes in gene expression enabled by BAF complexes have far reaching consequences, including establishment of self-renewal and differentiated states in different cell types. In the former, the complex takes on a specific subunit assembly (esBAF) that is required for embryonic stem-cell (ES) self-renewal and pluripotency, and it can also facilitate reprogramming of cells to iPSCs (Ho et al., 2009; Singhal et al., 2010). Similarly, BAF plays an important role in neural development and differentiation, acting through a different combination of subunits (nBAF) to determine neuronal cell fate (Ronan, Wu, & Crabtree, 2013). Cancer cells could then exploit this function of defining cell states through combinatorial assembly by altering the subunit composition to resemble that of complexes found in proliferative cells (e.g. esBAF). Not surprisingly mutations in BAF subunits are found in nearly 20% of all human cancers (**Figure 1.3**), highlighting the importance of this complex in oncogenesis (Kadoch et al., 2013).

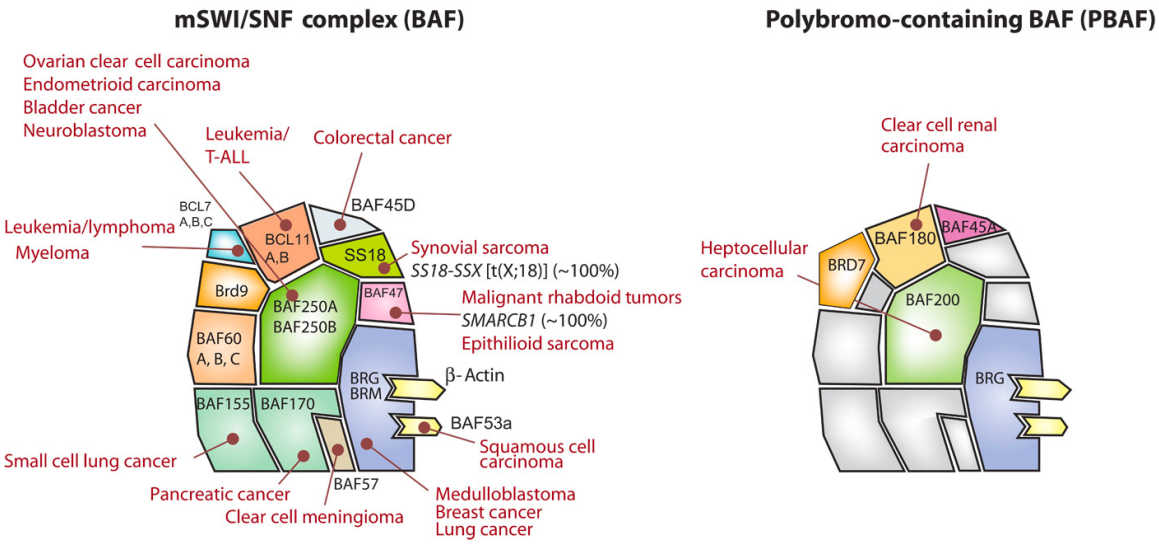


Figure 1.3. Diseases in which BAF mutations have been identified. These mutations and their corresponding diseases, highlighted in red, have been mapped to specific subunits of either BAF (left) or PBAF (right) complexes, and includes missense mutations and chromosomal aberrations that lead to loss of function. Adapted from: (Kadoch & Crabtree, 2015)

Chapter 1.1.4: Polycomb-mediated Transcriptional Repression

SSX has only one major protein domain: an N-terminal region that shows homology to the Kruppel-associated box (KRAB) domain (de Bruijn et al., 2006), known for its association with transcriptional repression (Urrutia, 2003). As a nuclear protein it colocalizes with Polycomb Group (PcG) proteins RING1 and BMI-1, both as SSX and SS18-SSX1, whereas SS18 does not (Soulez, Saurin, Freemont, & Knight, 1999). Identified via dominant mutations that induced the

production of extra sex combs in *Drosophila* (P. H. Lewis, 1949), the *Polycomb* (Pc) genes were observed to act as repressors of the *Bithorax* complex (BX-C) of genes, which directed development of the fly's thoracic and abdominal segments (E. B. Lewis, 1978). Several other mutations were later identified that displayed transcription repressor roles similar to Pc genes, including modulators of the *zeste* eye phenotype that also showed the same capacity to induce homeotic transformations in the fly (R. S. Jones & Gelbart, 1990). Together with the trxG genes, which act antagonistically to Pc, these helped establish how certain genes are maintained on or off transcriptionally, with Pc proteins maintaining the off state and trxG proteins responsible for the active state (J. Müller et al., 2002).

Biochemical characterization of Pc-related proteins revealed that a select group formed a multi-subunit complex with histone methyltransferase (HMT) activity (J. Müller et al., 2002). In *Drosophila*, the complex's catalytic subunit was determined to be Enhancer of Zeste (E (Z)), E (Z) homolog 2 (EZH2) in mammals, with the major substrate being histone 3 lysine 27 (H3K27) (Cao & Zhang, 2004). This interacts with three other core-subunits of the complex: Extra Sex Combs (ESC), NURF-55, and Suppressor of Zeste 12 (SU (Z)12) in *Drosophila* (Schuettengruber, Chourrout, Vervoort, Leblanc, & Cavalli, 2007); with human homologs Embryonic Ectoderm Development (EED), RbAp48/46,

and SUZ12, respectively (Schuettengruber et al., 2007). The complex was named the Polycomb Repressive Complex 2 (PRC2), and it is the only known enzyme that catalyzes the formation of H3K27 tri-methyl (H3K27me3) (Margueron & Reinberg, 2011), which imparts a structural change in chromatin is associated with transcriptional repression (Margueron & Reinberg, 2011). Similarly, trxG proteins were found to be part of a HMT that catalyzed H3K4me3 (Hughes et al., 2004), an activating mark, and also the major chromatin-remodeling complex SWI/SNF (Francis & Kingston, 2001), showcasing modification of chromatin structure as a vital mechanism for gene regulation.

Chapter 1.1.5: SS18-SSX-mediated Transcriptional Regulation

SS18 itself was later found to be present in BAF complexes, with purification of SS18-SSX1 displaying similar affinity to the chromatin remodeler (Middeljans et al., 2012). Prior to this study, only the SS18 homolog SS18L1 was known to bind the BAF complex, identified through a similar mass spectrometry based approach (Ho et al., 2009). Interaction of SS18 with the BAF complex paired with SSX1 co-localization with transcriptional repressors suggested that SS18-SSX functions through global chromatin remodeling changes ultimately changing the transcriptional profile of the cells that transform into SS. Evidence for this mechanism came in early 2013, when Kadoch et.al. showed SS18-SSX1

incorporates into the BAF complex as a stable subunit, changes its subunit composition, and induces profound changes in gene expression (Kadoch & Crabtree, 2013).

Once the fusion protein is incorporated into the BAF complex, this leads to the ejection of tumor suppressor BAF47 as a subunit, which is subsequently degraded by the proteasome (Kadoch & Crabtree, 2013). BAF47, also known as INI1 and SNF5, is a bona-fide tumor suppressor found to be biallelically inactivated in malignant rhabdoid tumors (MRT) (Knutson et al., 2013). Its inactivation in mice is highly penetrant with a rapid onset of tumor development, in a manner that positions BAF47 as one of the most potent tumor suppressors known (Roberts, Leroux, Fleming, & Orkin, 2002). Decreased expression of BAF47 has been independently verified as a correlate with SS disease, serving as a rapid and accurate confirmation of SS diagnosis (Ito, Asano, Kawai, & Yoshida, 2016). This oncogenic complex, containing SS18-SSX and not BAF47, has altered activity and can be recruited to the Sox2 locus when the fusion protein is expressed in 293T cells (Kadoch & Crabtree, 2013), providing a mechanistic explanation of the fusion protein's oncogene phenotype.

Chapter 1.1.6: Synovial Sarcoma Standard of Care

Despite these advances in understanding the molecular function of SS18-SSX, identification of effective targeted therapeutics in this disease remains particularly challenging. Because of this, current treatment is quite dated and relies almost exclusively on surgery and subsequent chemotherapy or radiotherapy (Sherman et al., 2014). Recent clinical trials for the multi-target receptor-tyrosine kinase (RTK) inhibitor pazopanib in the treatment of SS have been encouraging, with pazopanib displaying an increased PFS than control (van der Graaf et al., 2012); cediranib, sunitinib and sorafenib trials also show early promise (Fox et al., 2010; George et al., 2009; Hong et al., 2014; R. G. Maki et al., 2009). The studies for pazopanib, cediranib and sunitinib were prompted by the observation that higher serum levels of VEGF were associated with a worse prognosis and poor cellular differentiation in soft-tissue sarcomas[19]. Sorafenib was additionally motivated by observations of apoptosis and growth inhibition in cancer cell line models of SS (Yanni Zhang, Du, & Zhang, 2016a). An alternative therapy that has gained traction in SS is trabectedin, a small molecule with anti-proliferative properties but an otherwise unknown MOA (Uboldi et al., 2017). In a Phase II study comparing trabectedin and best supportive care in 18 patients with SS, trabectedin reduced the risk of progression or death by 86% (Martín Broto, Le Cesne, & Reichardt, 2017).

Chapter 1.1.7: BAF Subunit Regulation by the Proteasome

Following incorporation of SS18-SSX into the BAF complex BAF47 is ejected and subsequently degraded by the proteasome. This was shown in SS cancer cell lines using the proteasome inhibitor MG132 to illustrate that BAF47 protein levels were highly dependent on proteasome activity (Kadoch & Crabtree, 2013). Other BAF subunits interact intimately with the proteasome, such as BAF155 (SRG3), which can act as a negative regulator of BAF subunit degradation through blocking of CHFR-mediated ubiquitination and protein degradation (Jung et al., 2012; Luo et al., 2014). This encompasses regulation of most BAF core subunits, including BRG1, SNF5 and BAF60a, which are targets of proteasomal degradation (Jung et al., 2012). The catalytic activity of the proteasome was also shown to fine-tune the kinetics of inflammatory gene transcription through inhibition of BAF complex activity via protein degradation of ATPase Brg1 (Cullen, Ponnappan, & Ponnappan, 2009). Nonetheless, this interplay between proteasome activity and chromatin remodeling remains relatively unexplored.

Chapter 1.2: The Ubiquitin Proteasome System

Chapter 1.2.1: Protein Degradation by the Proteasome

Protein levels in cells are dictated by their rate of synthesis and degradation. In eukaryotic cells the ATP-dependent proteasome is responsible for the degradation of most cellular proteins (Coux, Tanaka, & Goldberg, 1996), and is responsible for a wide variety of cellular processes including apoptosis, cell survival, cell-cycle progression, DNA repair, and antigen presentation (Manasanch & Orlowski, 2017). It is a multi-subunit complex that is very abundant in cells, representing up to 1% of a cell's protein mass (Tanaka, Ii, Ichihara, Waxman, & Goldberg, 1986). It was discovered through proteolytic activity monitoring of protein fractions of tissue homogeneates, independently by many groups, one example being as a high-molecular weight protease named ingensin (Yamamoto, Nojima, Ishiura, & Sugita, 1986). Further biochemical characterization of this protease determined that it is composed of two major components: a 700-kDa and a larger 1500-kDa complex, the former of which was shown to be a part of the bigger complex, also named 20S and 26S for their sedimentation coefficients, respectively (Driscoll & Goldberg, 1990). Over 21 names were used in the past for the complex before "proteasome" was arrived at

to indicate its proteolytic and particulate nature (Arrigo, Tanaka, Goldberg, & Welch, 1988; Coux et al., 1996).

The 20S proteasome core is made up of 28 protein subunits which harbor the catalytic activity of the proteasome (Bhattacharyya, Yu, Mim, & Matouschek, 2014). Crystal structures of the complex revelead that the core particle is arranged into four seven-subunit rings: two that contain α-subunits and two that contain β-subunits (Groll et al., 1997). Three out of the seven β-subunits harbor catalytic activity: β1, β2, and β5, each of which has a distinct type of proteolytic activity: caspase-like, trypsin-like, and chymotrypsin-like, respectively (Saeki, 2017). These sites have a poor preference for specific amino acids and can cleave virtually any peptide sequence (Bhattacharyya et al., 2014). Specificity is thus achieved through regulation of protein access to the catalytic sites, which are in the hollow center of the ring structure (Groll et al., 1997).

In addition to the 20S core, the 26S proteasome particle contains a distinct sub complex of proteins called the 19S complex or regulatory particle (Coux et al., 1996). These make up the pores of the proteasome that allow access to the catalytic core. They recognize ubiquitin tags and use the energy of ATP to unfold protein substrates and feed them into the 20S core (Bhattacharyya et al., 2014). The 19S regulatory particle is comprised of at least 19 subunits, and also harbors

proteolytic activity that removes ubiquitin tags from substrate proteins (Finley, 2009). Structurally it is broadly separated into a base component and a lid component, which together form the regulatory particle. The base on its own can activate the core particle to degrade peptides, while the lid is responsible for ubiquitin-dependent degradation (Glickman et al., 1998). In contrast to the 19S particle, the 11S particle can also act a regulator of the proteasome and stimulates protein degradation without ATP hydrolysis or ubiquitin recognition (Finley, 2009). The 11S alternate cap, a heptameric protein complex, binds the proteasome similarly to the 19S particle and promotes degradation of small peptides, but not of complete proteins. The core and regulatory particles come together to form the full 26S proteasome (**Figure 1.4**).

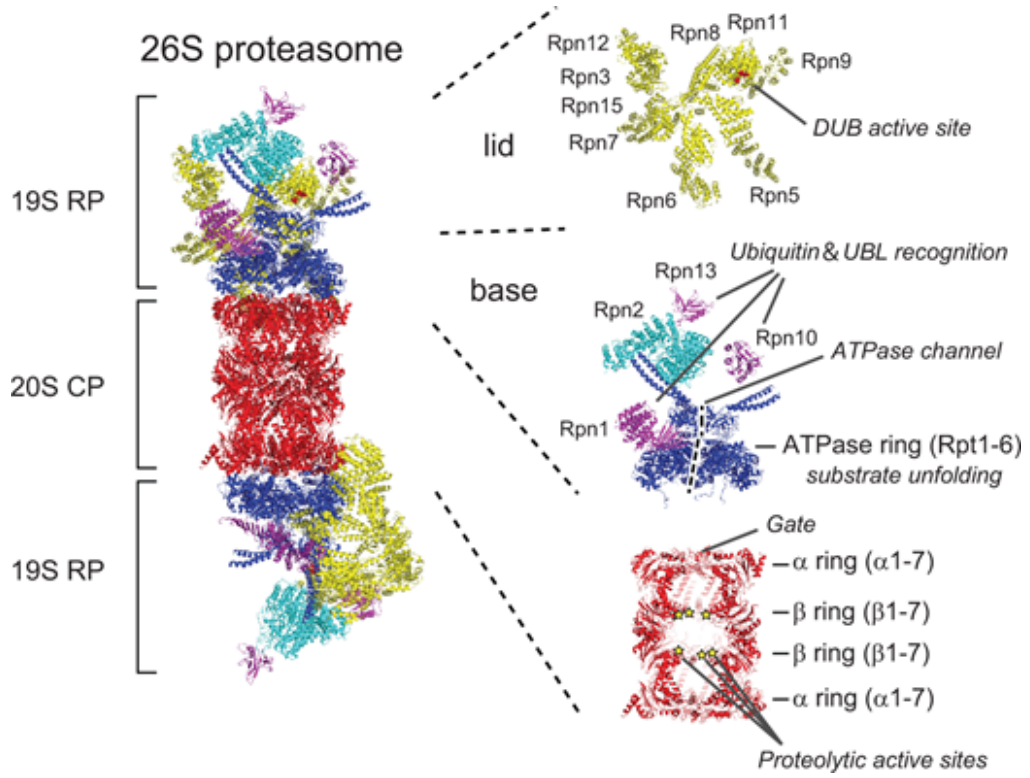


Figure 1.4. Structure and key subunits of the proteasome. The 26S proteasome is divided into three components: two regulatory particles and a central core particle that harbors catalytic activity. The regulatory particle is further subdivided into a lid component and a base component. Adapted from: (Saeki, 2017).

Chapter 1.2.2: Ubiquitin as a Degradation Signal

Ubiquitin is a small, 76 amino acid globular protein used by the cell to mark protein substrates for degradation by the proteasome. It was originally isolated as a protein able to induce T-cell and B-cell differentiation in mouse lymphoid cells

that also displayed ubiquitous expression in animal tissues (Kagan, O'Neill, Incefy, Goldstein, & Good, 1977; Schlesinger, Goldstein, & Niall, 1975). In the first established systems of proteasome proteolytic activity from rabbit reticulocytes an ATP-dependent proteolysis factor (APF-1) was identified to be essential, which later studies showed that it was in fact ubiquitin, the same protein identified by Goldstein et. al. showing wide-spread tissue expression (Wilkinson, Urban, & Haas, 1980). This was further evidenced by co-migration of APF-1 and ubiquitin in gel electrophoresis and amino acid sequencing. In addition, ubiquitin was also found conjugated to endogenous reticulocyte proteins, and was later suggested as an intermediary in the ATP-dependent hydrolysis process in reticulocytes (Wilkinson et al., 1980).

Chapter 1.2.3: Ubiquitin Conjugation and Ligation

Ubiquitin is conjugated to proteins through the concerted action of multiple enzymes consisting of three central classes: ubiquitin-activating enzymes (also called E1 enzymes), ubiquitin-transferring enzymes (E2), and ubiquitin ligases (E3) (Saeki, 2017). Together these enzymes dictate which proteins in the cell are to be degraded by the proteasome. In most cases ubiquitin is found in the form of poly-ubiquitin chains, that is ubiquitin conjugated to other ubiquitin molecules in a linear pattern. There are at least seven known lysine (K) residues where

ubiquitin can be found conjugated to itself: K6, K11, K27, K29, K33, K48 and K64 (Saeki, 2017). Chains of each type are also exclusive of other linkages (e.g. ubiquitin in K48-linked chains are all linked at K48) (Saeki, 2017). Most common among these is K48-linked chains, which are highly abundant in cells and target cellular proteins for degradation by the proteasome (Finley, 2009). Among these 7 Lys residues of ubiquitin, only K48 was shown to be essential for cell growth and protein degradation in yeast (Finley et al., 1994). The chains need to be at least four ubiquitin moieties long to bind the proteasome (Thrower, Hoffman, Rechsteiner, & Pickart, 2000), and can be much longer in cells. Targeting is thus achieved through an increase in substrate affinity that is caused by binding of the polyubiquitin chain. This further enables flexibility in the cellular roles of ubiquitin by assigning protein degradation signaling to polyubiquitin chains and not to ubiquitin monomers.

The enzymes that conjugate ubiquitin to proteins work in concert to activate ubiquitin and ultimately ligate it to the substrate. A central E1 enzyme first activates ubiquitin by adenylating it on its C-terminal glycine residue, which later becomes charged as a thiol ester, and then transfers ubiquitin to one of several E2 ubiquitin-conjugating enzymes through another thiol ester bond (Nalepa, Rolfe, & Harper, 2006). Two common E1 enzymes activate most ubiquitin utilized by the cell. E2 enzymes then come into complex with one of several hundred E3s

(>600) to ubiquitinate protein substrates (W. Li et al., 2008). The mechanism of ubiquitination varies depending on which E2 and E3s are involved. Broadly E3s belong to three major classes: really interesting new gene (RING) E3s, homology to E6AP C terminus (HECT) E3s, and U-box E3s (Nalepa et al., 2006). E3s function to bring the E2 enzyme into proximity with the target protein, providing specificity to the ubiquitin conjugation process, in addition to catalyzing the transfer of ubiquitin. The mechanism of conjugation varies by E3, with RING ligases transferring the ubiquitin from the E2 to a substrate lysine via an aminolysis reaction, in contrast to HECT ligases which transfer first to the E3 itself through a transthioesterification reaction (Berndsen & Wolberger, 2014).

Several ubiquitin-like proteins exist that follow a similar protein conjugation mechanism to ubiquitin. These include small ubiquitin modifier (SUMO), neural prescursor cell expressed developmentally downregulated 8 (NEDD8), and ISG15 (Cappadocia & Lima, 2017). SUMO is a key post-translational modification in many proteins, and it has been implicated in the regulation of transcription factors that mediate the transition between epithelial and mesenchymal states (Bogachek, De Andrade, & Weigel, 2015). Neddylation, i.e. the conjugation of NEDD8 to a target protein, is essential in the function of cullin-containing ubiquitin ligases, also known as cullin-RING ligases (CRLs) (Pan, Kentsis, Dias, Yamoah, & Wu, 2004). Cullins are covalently bound to NEDD8,

and this modification is necessary for CRL ubiquitin ligase activity, thus making NEDD8 a regulator of ubiquitination (Pan et al., 2004). Like ubiquitin, a distinct E1 enzyme exists for each ubiquitin-like protein that activates it and transfers it to an E2 enzyme.

Chapter 1.2.4: Ubiquitin Recognition and Processing

The proteasome recognizes ubiquitin through two canonical receptors: PSMD4 (Rpn10 in yeast) and ADRM1 (Rpn13 in yeast) (Elsasser, Chandler-Militello, Müller, Hanna, & Finley, 2004; Husnjak et al., 2008). Given the structure of a tetra-ubiquitin chain, it is possible that one chain can bind both Rpn10 and Rpn13 simultaneously. This recognition by two spatially separated subunits could allow for the distinction between proteins with mono-ubiquitin and those with poly-ubiquitin chains (Lander et al., 2012). Nonetheless this is not enough to distinguish between the type of ubiquitin linkage, e.g. K48 vs K63 linked, and loss of a single ubiquitin receptor is not enough to prevent growth in yeast (Bhattacharyya et al., 2014). It is reasonable to then expect that other subunits in the proteasome handle chain-type recognition. In addition to these two canonical receptors, Rpn1 was recently identified as an additional receptor of ubiquitin (Y. Shi et al., 2016).

Following recognition by the proteasome, ubiquitin-chains are cleaved off from the target substrate at a single cleavage point by the enzyme Rpn11, releasing the entire poly-ubiquitin chain (Verma et al., 2002). This enzyme contains a highly-conserved metalloisopeptidase domain, and the process is ATP-dependent and tightly coupled to protein degradation (Verma et al., 2002). In the 26S proteasome structure Rpn11 is found close to the catalytic core entrance, and it is strategically positioned to cleave poly-ubiquitin chains once the substrate is translocated into the degradation channel (Bhattacharyya et al., 2014). Outside of the proteasome ubiquitin is removed from proteins by deubiquitinating enzymes (DUBs), which can also process free ubiquitin chains through catalytic cleavage into free ubiquitin. There are more than 100 annotated DUBs in the human genome classified into the following families: ubiquitin-specific proteases (USPs), ubiquitin COOH-terminal hydrolases (UCHs), ovarian tumor proteases (OTUs), Josephins, the JAB1/MPN/MOV34 family (JAMMs) and motif interacting with Ub-containing novel DUB family (MINDYs) (He, Zhou, Wu, Chen, & Wan, 2017). DUBs, in conjunction with E1 enzymes, E2 enzymes, E3 enzymes and the 26S proteasome, form the Ubiquitin-Proteasome System, responsible for the majority of protein degradation in the cell (**Figure 1.5**).

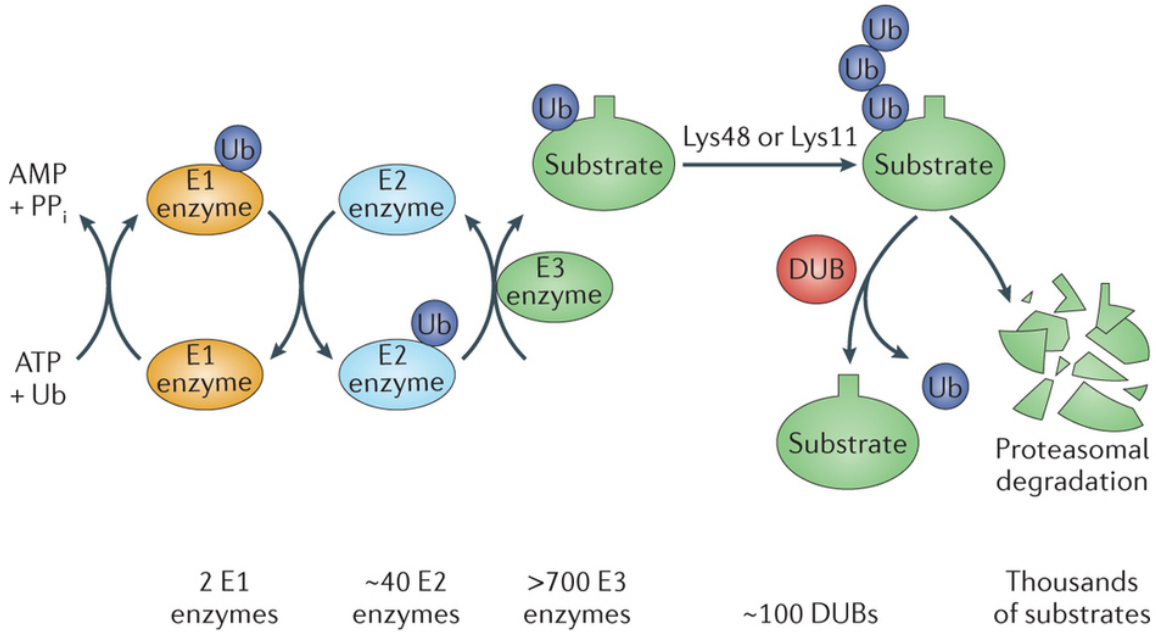


Figure 1.5. Overview of Ubiquitin-Proteasome System. Ubiquitin is first activated by an E1 enzyme in an ATP-dependent manner. It is later transferred to an E2 enzyme which together with an E3 enzyme they ubiquitinate protein substrates in the cell. If said modification is of the K48-linkage or K11-linkage type, the substrate is subsequently recognized and degraded by the proteasome. Alternatively, deubiquitinating enzymes, or DUBs, can prevent this process by catalyzing the removal of ubiquitin chains from proteins. The number of proteins believed to belong to each enzyme class is noted at the bottom. Adapted from: (Skaar, Pagan, & Pagano, 2014)

Chapter 1.2.5: Inhibitors of the Ubiquitin-Proteasome System as Cancer Therapeutics

Chapter 1.2.5.1: Inhibitors of the Proteasome

Despite being an essential cellular process, inhibition of the ubiquitin proteasome system through pharmacological means has proven to be an unexpected success in the treatment of certain cancers (Manasanch & Orlowski, 2017). Sensitivity to proteasome inhibition has been attributed to an imbalance between the degradation capacity of the proteasome and the amount of proteins that need to be degraded, in other words the proteasome load. This provides a therapeutic window for diseases that harbor an extraordinarily high proteasome load, which in turn can lead to downregulation of key cell-cycle regulators, such as p53, suggesting proteasome inhibition as a therapeutic strategy (C. G. Maki, Huibregtse, & Howley, 1996).

The initial interest in proteasome inhibitors came from the hypothesis by Alfred Goldberg that proteasome inhibition could be used to treat muscle wasting, or cachexia, due to the role of the proteasome in protein turnover (Manasanch & Orlowski, 2017). This lead to development of a series of peptide aldehyde molecules, most notably MG132 (named after the company Myogenics, later

named ProScript and ultimately acquired by Millennium Pharmaceuticals), that could reversibly inhibit the 26S proteasome (Lee & Goldberg, 1996). Additional medicinal chemistry efforts led to MG-341/PS-341 (later renamed bortezomib), which is a dipeptide boronate inhibitor of the proteasome with sub-nanomolar potency that showed promise early on as an anti-proliferative agent in pre-clinical cancer models (Hideshima et al., 2001; Palombella et al., 1998; Shah et al., 2001). In addition to p53 stabilization, blocking degradation of NF-kB inhibitor IkB was also hypothesized to be responsible for the apoptotic phenotypes seen with proteasome inhibitors (Palombella et al., 1998).

Bortezomib is a pseudo-covalent (i.e. slowly reversible) inhibitor of the chymotrypsin-like (β5) catalytic activity of the 26S proteasome (Groll, Berkers, Ploegh, & Ovaa, 2006). It can also, to a lesser degree, inhibit the trypsin-like (β2) and caspase-like activities (β1) (Groll et al., 2006). In a Phase I trial of patients with refractory hematologic malignancies, bortezomib displayed a promising response in 9 out of 9 patients that were fully assessable (Orlowski et al., 2002), which launched subsequent studies into its efficacy. It was first approved for treatment of refractory multiple myeloma patients, where for the first time progression-free survival was observed in this population after treatment (Richardson et al., 2003), and this was subsequently confirmed with a Phase III trial that turned bortezomib into a first line treatment for relapsing or refractory

multiple myeloma patients (Richardson et al., 2005). Bortezomib is also approved for treatment of patients with refractory or relapsed mantle cell lymphoma (Manasanch & Orlowski, 2017).

Despite the success of bortezomib in the clinic, development of new proteasome inhibitors continued, made relevant by the observation of bortezomib-resistance in the clinic in addition to the development of peripheral neuropathy in patients receiving high-doses of bortezomib (Dimopoulos et al., 2011). Other boronic acids that were developed include ixazomib, which is an orally available proteasome inhibitor and FDA approved for patients with relapsed or refractory multiple myeloma (Landgren & Iskander, 2017). Another class of peptides that can also inhibit the proteasome with the same mechanism of action as bortezomib (i.e. binding to the N-terminal threonines of the catalytic subunits) are epoxyketones. These compounds can bind irreversibly to the proteasome, displaying a longer period of inhibition than reversible inhibitors (Gozzetti et al., 2016), and one of these drugs (carfilzomib) has received FDA approval for treatment of patients with refractory or relapsed multiple myeloma (Landgren & Iskander, 2017).

Chapter 1.2.5.2: Inhibitors of Ubiquitin Ligation

Another avenue of inhibition of the ubiquitin-proteasome system is through disruption of ubiquitin conjugation and ligation, even though there are no molecules available in the clinic that function via this mechanism, some have been reported in the literature. Given the success of bortezomib in the clinic, there exists a wide spread interested in developing alternative inhibitory molecules of ubiquitin-mediated degradation. This includes inhibitors of all three ubiquitin conjugating enzyme families: E1, E2 and E3.

PYR-41 is a cell-permeable inhibitor of the human E1 enzyme UBE1 that irreversibly binds its active cysteine (Yang et al., 2007). It prevents global protein ubiquitination of all linkage-types, and this leads to accumulation of canonical proteasome targets such as IkB-a and p53, causing anti-proliferative effects in cancer cell lines that depend on these oncogenic pathways (Yang et al., 2007). Similarly, MLN7243 is a potent inhibitor of UBE1 activity, with single-digit nanomolar acitivty in vitro and double-digit potency in cellular models. Other inhibitors targeting ubiquitin-like E1 enzymes have been developed, particularly those that work with NEDD8 and SUMO1. MLN4924 is a selective small molecule inhibitor of NEDD8 activating enzyme (NAE), the E1 enzyme responsible for NEDD8 activation, and it is an adenosine analog that covalently

binds the nucleotide binding site of NAE (Soucy et al., 2009). It shows anti-proliferative activity in several cancer models, most likely through inhibition of CRLs (e.g. Skp/Cullin/F-box complexes, or SCF) and stabilization of cell-cycle inhibitors (e.g. p27) (Lan, Tang, Jin, & Sun, 2016; Yi Zhang, Shi, Zhang, Li, & Li, 2016b). It is also one of the first ubiquitin-proteasome system inhibitors that does not target the proteasome to be in the clinic, with one Phase I study in patients with acute myeloid leukaemia (AML) reporting moderate clinical responses for MLN4924 (renamed to Pevonedistat) (Swords et al., 2015).

E2 inhibitors have also been developed, including an inhibitor of Cdc34 (CC0651) and one for UBE2N (NSC697923) (Landré, Rotblat, Melino, Bernassola, & Melino, 2014). Inhibition of Cdc34 has a negative impact on SCF ubiquitin ligase activity, and stabilizes the cell cycle inhibitor p27, which could be a promising therapeutic target (Ceccarelli et al., 2011). Similarly pharmacological inhibition of UBE2N leads to potent cancer cell line toxicity, potentially through re-activation and accumulation of monomeric p53, activation of the JNK pathway, and inhibition of NF-kB signaling (Cheng et al., 2014; Pulvino et al., 2012). Inhibition of E3 enzymes provides its own unique problems, in part because RING and U-box E3s do not have intrinsic catalytic activity, and inhibitors of these enzymes would have to be allosteric. While HECT E3 ligases posses catalytic activity, little effort has been made in developing inhibitors for them.

Nonetheless, several inhibitors do exist for various E3s including: MDM2, Skp2, IAP, XIAP, Frataxin, VHL, SCF-Cdc4, SCF-Met30, Itch, and E6AP, the majority of which are RING-finger E3 ligases (Landré et al., 2014).

References

Al-Daraji, W., Lasota, J., Foss, R., & Miettinen, M. (2009). Synovial sarcoma involving the head: analysis of 36 cases with predilection to the parotid and temporal regions. *The American Journal of Surgical Pathology*, *33* (10), 1494–1503. http://doi.org/10.1097/PAS.0b013e3181aa913f

American Cancer Society. (2016). Cancer Facts and Figures 2016. Atlanta. http://doi.org/10.1111/j.1742-4658.2005.04900.x/full

Antonescu, C. R., Kawai, A., Leung, D. H., Lonardo, F., Woodruff, J. M., Healey, J. H., & Ladanyi, M. (2000). Strong association of SYT-SSX fusion type and morphologic epithelial differentiation in synovial sarcoma. *Diagnostic Molecular Pathology : the American Journal of Surgical Pathology, Part B*, *9* (1), 1–8.

Arrigo, A. P., Tanaka, K., Goldberg, A. L., & Welch, W. J. (1988). Identity of the 19S “prosome” particle with the large multifunctional protease complex of mammalian cells (the proteasome). *Nature*, *331* (6152), 192–194. http://doi.org/10.1038/331192a0

Berndsen, C. E., & Wolberger, C. (2014). New insights into ubiquitin E3 ligase mechanism. *Nature Structural & Molecular Biology*, *21* (4), 301–307. http://doi.org/10.1038/nsmb.2780

Bhattacharyya, S., Yu, H., Mim, C., & Matouschek, A. (2014). Regulated protein turnover: snapshots of the proteasome in action. *Nature Reviews Molecular Cell Biology*, *15* (2), 122–133. http://doi.org/10.1038/nrm3741

Bogachek, M. V., De Andrade, J. P., & Weigel, R. J. (2015). Regulation of epithelial-mesenchymal transition through SUMOylation of transcription factors. *Cancer Research*, *75* (1), 11–15. http://doi.org/10.1158/0008-5472.CAN-14-2824

Brett, D., Whitehouse, S., Antonson, P., Shipley, J., Cooper, C., & Goodwin, G. (1997). The SYT protein involved in the t (X;18) synovial sarcoma translocation is a transcriptional activator localised in nuclear bodies. *Human Molecular Genetics*, *6* (9), 1559–1564.

Brodin, B., Haslam, K., Yang, K., Bartolazzi, A., Xie, Y., Starborg, M., et al. (2001). Cloning and characterization of spliced fusion transcript variants of synovial sarcoma: SYT/SSX4, SYT/SSX4v, and SYT/SSX2v. Possible regulatory role of the fusion gene product in wild type SYT expression. *Gene*, *268* (1-2), 173–182.

Cao, R., & Zhang, Y. (2004). The functions of E (Z)/EZH2-mediated methylation of lysine 27 in histone H3. *Current Opinion in Genetics & Development*, *14* (2), 155–164. http://doi.org/10.1016/j.gde.2004.02.001

Cappadocia, L., & Lima, C. D. (2017). Ubiquitin-like Protein Conjugation: Structures, Chemistry, and Mechanism. *Chemical Reviews*, acs.chemrev.6b00737. http://doi.org/10.1021/acs.chemrev.6b00737

Carlson, M., Osmond, B. C., & Botstein, D. (1981). Mutants of yeast defective in sucrose utilization. *Genetics*, *98* (1), 25–40.

Ceccarelli, D. F., Tang, X., Pelletier, B., Orlicky, S., Xie, W., Plantevin, V., et al. (2011). An allosteric inhibitor of the human Cdc34 ubiquitin-conjugating enzyme. *Cell*, *145* (7), 1075–1087. http://doi.org/10.1016/j.cell.2011.05.039

Cheng, J., Fan, Y.-H., Xu, X., Zhang, H., Dou, J., Tang, Y., et al. (2014). A small-molecule inhibitor of UBE2N induces neuroblastoma cell death via activation of p53 and JNK pathways. *Cell Death & Disease*, *5* (2), e1079. http://doi.org/10.1038/cddis.2014.54

Clark, J., Rocques, P. J., Crew, A. J., Gill, S., Shipley, J., Chan, A. M., et al. (1994). Identification of novel genes, SYT and SSX, involved in the t (X;18) (p11.2;q11.2) translocation found in human synovial sarcoma. *Nature Genetics*, *7* (4), 502–508. http://doi.org/10.1038/ng0894-502

Coux, O., Tanaka, K., & Goldberg, A. L. (1996). Structure and functions of the 20S and 26S proteasomes. *Annual Review of Biochemistry*, *65* (1), 801–847. http://doi.org/10.1146/annurev.bi.65.070196.004101

Crew, A. J., Clark, J., Fisher, C., Gill, S., Grimer, R., Chand, A., et al. (1995). Fusion of SYT to two genes, SSX1 and SSX2, encoding proteins with homology to the Kruppel-associated box in human synovial sarcoma. *The EMBO Journal*, *14* (10), 2333–2340.

Cullen, S. J., Ponnappan, S., & Ponnappan, U. (2009). Catalytic activity of the proteasome fine-tunes Brg1-mediated chromatin remodeling to regulate the expression of inflammatory genes. *Molecular Immunology*, *47* (2-3), 600–605. http://doi.org/10.1016/j.molimm.2009.09.008

de Bruijn, D. R. H., Allander, S. V., van Dijk, A. H. A., Willemse, M. P., Thijssen, J., van Groningen, J. J. M., et al. (2006). The synovial-sarcoma-associated SS18-SSX2 fusion protein induces epigenetic gene (de)regulation. *Cancer Research*, *66* (19), 9474–9482. http://doi.org/10.1158/0008-5472.CAN-05-

3726

Dimopoulos, M. A., Mateos, M.-V., Richardson, P. G., Schlag, R., Khuageva, N. K., Shpilberg, O., et al. (2011). Risk factors for, and reversibility of, peripheral neuropathy associated with bortezomib-melphalan-prednisone in newly diagnosed patients with multiple myeloma: subanalysis of the phase 3 VISTA study. *European Journal of Haematology*, *86* (1), 23–31. http://doi.org/10.1111/j.1600-0609.2010.01533.x

Driscoll, J., & Goldberg, A. L. (1990). The proteasome (multicatalytic protease) is a component of the 1500-kDa proteolytic complex which degrades ubiquitin-conjugated proteins. *The Journal of Biological Chemistry*, *265* (9), 4789–4792.

Elsasser, S., Chandler-Militello, D., Müller, B., Hanna, J., & Finley, D. (2004). Rad23 and Rpn10 serve as alternative ubiquitin receptors for the proteasome. *The Journal of Biological Chemistry*, *279* (26), 26817–26822. http://doi.org/10.1074/jbc.M404020200

Finley, D. (2009). Recognition and processing of ubiquitin-protein conjugates by the proteasome. *Annual Review of Biochemistry*, *78*, 477–513. http://doi.org/10.1146/annurev.biochem.78.081507.101607

Finley, D., Sadis, S., Monia, B. P., Boucher, P., Ecker, D. J., Crooke, S. T., & Chau, V. (1994). Inhibition of proteolysis and cell cycle progression in a multiubiquitination-deficient yeast mutant. *Molecular and Cellular Biology*, *14* (8), 5501–5509.

Fligman, I., Lonardo, F., Jhanwar, S. C., Gerald, W. L., Woodruff, J., & Ladanyi, M. (1995). Molecular diagnosis of synovial sarcoma and characterization of a variant SYT-SSX2 fusion transcript. *The American Journal of Pathology*, *147* (6), 1592–1599.

Fox, E., Aplenc, R., Bagatell, R., Chuk, M. K., Dombi, E., Goodspeed, W., et al. (2010). A phase 1 trial and pharmacokinetic study of cediranib, an orally bioavailable pan-vascular endothelial growth factor receptor inhibitor, in children and adolescents with refractory solid tumors. *Journal of Clinical Oncology : Official Journal of the American Society of Clinical Oncology*, *28* (35), 5174–5181. http://doi.org/10.1200/JCO.2010.30.9674

Francis, N. J., & Kingston, R. E. (2001). *Nature Reviews Molecular Cell Biology*, *2* (6), 409. http://doi.org/10.1038/35073039

George, S., Merriam, P., Maki, R. G., Van den Abbeele, A. D., Yap, J. T., Akhurst, T., et al. (2009). Multicenter phase II trial of sunitinib in the treatment of nongastrointestinal stromal tumor sarcomas. *Journal of Clinical Oncology : Official Journal of the American Society of Clinical Oncology*, *27* (19), 3154–3160. http://doi.org/10.1200/JCO.2008.20.9890

Glickman, M. H., Rubin, D. M., Coux, O., Wefes, I., Pfeifer, G., Cjeka, Z., et al. (1998). A subcomplex of the proteasome regulatory particle required for ubiquitin-conjugate degradation and related to the COP9-signalosome and eIF3. *Cell*, *94* (5), 615–623.

Goldblum, J. R., Weiss, S. W., & Folpe, A. L. (2013). Enzinger and Weiss's Soft Tissue Tumors (6 ed.). Philadelphia: Elsevier Health Sciences.

Gozzetti, A., Papini, G., Candi, V., Brambilla, C. Z., Sirianni, S., & Bocchia, M. (2016). Second generation proteasome inhibitors in multiple myeloma. *Anti-Cancer Agents in Medicinal Chemistry*.

Groll, M., Berkers, C. R., Ploegh, H. L., & Ovaa, H. (2006). Crystal structure of the boronic acid-based proteasome inhibitor bortezomib in complex with the

yeast 20S proteasome. *Structure (London, England : 1993)*.

Groll, M., Ditzel, L., Löwe, J., Stock, D., Bochtler, M., Bartunik, H. D., & Huber, R. (1997). Structure of 20S proteasome from yeast at 2.4 A resolution. *Nature*, *386* (6624), 463–471. http://doi.org/10.1038/386463a0

Haldar, M., Randall, R. L., & Capecchi, M. R. (2008). Synovial sarcoma: from genetics to genetic-based animal modeling. *Clinical Orthopaedics and Related Research*, *466* (9), 2156–2167. http://doi.org/10.1007/s11999-008-0340-2

He, M., Zhou, Z., Wu, G., Chen, Q., & Wan, Y. (2017). Emerging role of DUBs in tumor metastasis and apoptosis: Therapeutic implication. *Pharmacology & Therapeutics*. http://doi.org/10.1016/j.pharmthera.2017.03.001

Herzog, C. E. (2005). Overview of sarcomas in the adolescent and young adult population. *Journal of Pediatric Hematology/Oncology*, *27* (4), 215–218.

Hideshima, T., Richardson, P., Chauhan, D., Palombella, V. J., Elliott, P. J., Adams, J., & Anderson, K. C. (2001). The proteasome inhibitor PS-341 inhibits growth, induces apoptosis, and overcomes drug resistance in human multiple myeloma cells. *Cancer Research*, *61* (7), 3071–3076.

Ho, L., Ronan, J. L., Wu, J., Staahl, B. T., Chen, L., Kuo, A., et al. (2009). An embryonic stem cell chromatin remodeling complex, esBAF, is essential for embryonic stem cell self-renewal and pluripotency. *Proceedings of the National Academy of Sciences of the United States of America*, *106* (13), 5181–5186. http://doi.org/10.1073/pnas.0812889106

Hodges, C., Kirkland, J. G., & Crabtree, G. R. (2016). The Many Roles of BAF (mSWI/SNF) and PBAF Complexes in Cancer. *Cold Spring Harbor Perspectives in Medicine*, *6* (8), a026930.

http://doi.org/10.1101/cshperspect.a026930

Hong, D. S., Garrido-Laguna, I., Ekmekcioglu, S., Falchook, G. S., Naing, A., Wheler, J. J., et al. (2014). Dual inhibition of the vascular endothelial growth factor pathway: a phase 1 trial evaluating bevacizumab and AZD2171 (cediranib) in patients with advanced solid tumors. *Cancer*, *120* (14), 2164–2173. http://doi.org/10.1002/cncr.28701

Hughes, C. M., Rozenblatt-Rosen, O., Milne, T. A., Copeland, T. D., Levine, S. S., Lee, J. C., et al. (2004). Menin associates with a trithorax family histone methyltransferase complex and with the hoxc8 locus. *Molecular Cell*, *13* (4), 587–597.

Husnjak, K., Elsasser, S., Zhang, N., Chen, X., Randles, L., Shi, Y., et al. (2008). Proteasome subunit Rpn13 is a novel ubiquitin receptor. *Nature*, *453* (7194), 481–488. http://doi.org/10.1038/nature06926

Ito, J., Asano, N., Kawai, A., & Yoshida, A. (2016). The diagnostic utility of reduced immunohistochemical expression of SMARCB1 in synovial sarcomas: a validation study. *Human Pathology*, *47* (1), 32–37. http://doi.org/10.1016/j.humpath.2015.09.010

Jones, R. S., & Gelbart, W. M. (1990). Genetic analysis of the enhancer of zeste locus and its role in gene regulation in Drosophila melanogaster. *Genetics*, *126* (1), 185–199.

Jung, I., Sohn, D. H., Choi, J., Kim, J. M., Jeon, S., Seol, J. H., & Seong, R. H. (2012). SRG3/mBAF155 stabilizes the SWI/SNF-like BAF complex by blocking CHFR mediated ubiquitination and degradation of its major components. *Biochemical and Biophysical Research Communications*, *418* (3), 512–517. http://doi.org/10.1016/j.bbrc.2012.01.057

Kadoch, C., & Crabtree, G. R. (2013). Reversible disruption of mSWI/SNF (BAF) complexes by the SS18-SSX oncogenic fusion in synovial sarcoma. *Cell*, *153* (1), 71–85. http://doi.org/10.1016/j.cell.2013.02.036

Kadoch, C., & Crabtree, G. R. (2015). Mammalian SWI/SNF chromatin remodeling complexes and cancer: Mechanistic insights gained from human genomics. *Science Advances*, *1* (5), e1500447–e1500447. http://doi.org/10.1126/sciadv.1500447

Kadoch, C., Hargreaves, D. C., Hodges, C., Elias, L., Ho, L., Ranish, J., & Crabtree, G. R. (2013). Proteomic and bioinformatic analysis of mammalian SWI/SNF complexes identifies extensive roles in human malignancy. *Nature Genetics*, *45* (6), 592–601. http://doi.org/10.1038/ng.2628

Kagan, W. A., O'Neill, G. J., Incefy, G. S., Goldstein, G., & Good, R. A. (1977). Induction of human granulocyte differentiation in vitro by ubiquitin and thymopoietin. *Blood*, *50* (2), 275–288.

Knutson, S. K., Warholic, N. M., Wigle, T. J., Klaus, C. R., Allain, C. J., Raimondi, A., et al. (2013). Durable tumor regression in genetically altered malignant rhabdoid tumors by inhibition of methyltransferase EZH2. *Proceedings of the National Academy of Sciences of the United States of America*, *110* (19), 7922–7927. http://doi.org/10.1073/pnas.1303800110

Ladanyi, M., Antonescu, C. R., Leung, D. H., Woodruff, J. M., Kawai, A., Healey, J. H., et al. (2002). Impact of SYT-SSX fusion type on the clinical behavior of synovial sarcoma: a multi-institutional retrospective study of 243 patients. *Cancer Research*, *62* (1), 135–140.

Lan, H., Tang, Z., Jin, H., & Sun, Y. (2016). Neddylation inhibitor MLN4924 suppresses growth and migration of human gastric cancer cells. *Scientific Reports*, *6*, 24218. http://doi.org/10.1038/srep24218

Lander, G. C., Estrin, E., Matyskiela, M. E., Bashore, C., Nogales, E., & Martin, A. (2012). Complete subunit architecture of the proteasome regulatory particle. *Nature*, *482* (7384), 186–191. http://doi.org/10.1038/nature10774

Landgren, O., & Iskander, K. (2017). Modern multiple myeloma therapy: deep, sustained treatment response and good clinical outcomes. *Journal of Internal Medicine*, *281* (4), 365–382. http://doi.org/10.1111/joim.12590

Landré, V., Rotblat, B., Melino, S., Bernassola, F., & Melino, G. (2014). Screening for E3-ubiquitin ligase inhibitors: challenges and opportunities. *Oncotarget*, *5* (18), 7988–8013. http://doi.org/10.18632/oncotarget.2431

Lee, D. H., & Goldberg, A. L. (1996). Selective inhibitors of the proteasome-dependent and vacuolar pathways of protein degradation in Saccharomyces cerevisiae. *The Journal of Biological Chemistry*, *271* (44), 27280–27284.

Lewis, E. B. (1978). A gene complex controlling segmentation in Drosophila. *Nature*, 565–570.

Lewis, P. H. (1949). Pc: Polycomb. *Drosophila Information Service*, *21*, 69.

Li, W., Bengtson, M. H., Ulbrich, A., Matsuda, A., Reddy, V. A., Orth, A., et al. (2008). Genome-wide and functional annotation of human E3 ubiquitin ligases identifies MULAN, a mitochondrial E3 that regulates the organelle's dynamics and signaling. *PloS One*, *3* (1), e1487. http://doi.org/10.1371/journal.pone.0001487

Luo, X., Wang, B., Tang, F., Zhang, J., Zhao, Y., Li, H., & Jin, Y. (2014). Wwp2 targets SRG3, a scaffold protein of the SWI/SNF-like BAF complex, for

ubiquitination and degradation. *Biochemical and Biophysical Research Communications*, *443* (3), 1048–1053. http://doi.org/10.1016/j.bbrc.2013.12.089

Machen, S. K., Easley, K. A., & Goldblum, J. R. (1999). Synovial sarcoma of the extremities: a clinicopathologic study of 34 cases, including semi-quantitative analysis of spindled, epithelial, and poorly differentiated areas. *The American Journal of Surgical Pathology*, *23* (3), 268–275.

Maki, C. G., Huibregtse, J. M., & Howley, P. M. (1996). In vivo ubiquitination and proteasome-mediated degradation of p53 (1). *Cancer Research*, *56* (11), 2649–2654.

Maki, R. G., D'Adamo, D. R., Keohan, M. L., Saulle, M., Schuetze, S. M., Undevia, S. D., et al. (2009). Phase II study of sorafenib in patients with metastatic or recurrent sarcomas. *Journal of Clinical Oncology : Official Journal of the American Society of Clinical Oncology*, *27* (19), 3133–3140. http://doi.org/10.1200/JCO.2008.20.4495

Manasanch, E. E., & Orlowski, R. Z. (2017). Proteasome inhibitors in cancer therapy. *Nature Reviews. Clinical Oncology*, *28*, 9270. http://doi.org/10.1038/nrclinonc.2016.206

Margueron, R., & Reinberg, D. (2011). The Polycomb complex PRC2 and its mark in life. *Nature*, *469* (7330), 343–349. http://doi.org/10.1038/nature09784

Martín Broto, J., Le Cesne, A., & Reichardt, P. (2017). The importance of treating by histological subtype in advanced soft tissue sarcoma. *Future Oncology (London, England)*, *13* (1s), 23–31. http://doi.org/10.2217/fon-2016-0500

Middeljans, E., Wan, X., Jansen, P. W., Sharma, V., Stunnenberg, H. G., & Logie, C. (2012). SS18 together with animal-specific factors defines human BAF-type SWI/SNF complexes. *PloS One*, *7* (3), e33834. http://doi.org/10.1371/journal.pone.0033834

Müller, J., Hart, C. M., Francis, N. J., Vargas, M. L., Sengupta, A., Wild, B., et al. (2002). *Cell*, *111* (2).

Nalepa, G., Rolfe, M., & Harper, J. W. (2006). Drug discovery in the ubiquitin-proteasome system. *Nature Reviews. Drug Discovery*, *5* (7), 596–613. http://doi.org/10.1038/nrd2056

Nikiforova, M. N., Groen, P., Mutema, G., Nikiforov, Y. E., & Witte, D. (2005). Detection of SYT-SSX rearrangements in synovial sarcomas by real-time one-step RT-PCR. *Pediatric and Developmental Pathology : the Official Journal of the Society for Pediatric Pathology and the Paediatric Pathology Society*, *8* (2), 162–167. http://doi.org/10.1007/s10024-004-8097-4

Orlowski, R. Z., Stinchcombe, T. E., Mitchell, B. S., Shea, T. C., Baldwin, A. S., Stahl, S., et al. (2002). Phase I trial of the proteasome inhibitor PS-341 in patients with refractory hematologic malignancies. *Journal of Clinical Oncology : Official Journal of the American Society of Clinical Oncology*, *20* (22), 4420–4427. http://doi.org/10.1200/JCO.2002.01.133

Palmerini, E., Staals, E. L., Alberghini, M., Zanella, L., Ferrari, C., Benassi, M. S., et al. (2009). Synovial sarcoma: retrospective analysis of 250 patients treated at a single institution. *Cancer*, *115* (13), 2988–2998. http://doi.org/10.1002/cncr.24370

Palombella, V. J., Conner, E. M., Fuseler, J. W., Destree, A., Davis, J. M., Laroux, F. S., et al. (1998). Role of the proteasome and NF-kappaB in streptococcal cell wall-induced polyarthritis. *Proceedings of the National Academy of Sciences*, *95* (26), 15671–15676.

Pan, Z.-Q., Kentsis, A., Dias, D. C., Yamoah, K., & Wu, K. (2004). Nedd8 on cullin: building an expressway to protein destruction. *Oncogene*, *23* (11), 1985–1997. http://doi.org/10.1038/sj.onc.1207414

Perani, M., Ingram, C. J. E., Cooper, C. S., Garrett, M. D., & Goodwin, G. H. (2003). Conserved SNH domain of the proto-oncoprotein SYT interacts with components of the human chromatin remodelling complexes, while the QPGY repeat domain forms homo-oligomers. *Oncogene*, *22* (50), 8156–8167. http://doi.org/10.1038/sj.onc.1207031

Peterson, C. L., & Herskowitz, I. (1992). Characterization of the yeast SWI1, SWI2, and SWI3 genes, which encode a global activator of transcription. *Cell*, *68* (3), 573–583.

PETERSON, C., & TAMKUN, J. (1995). The SWI-SNF complex: a chromatin remodeling machine? *Trends in Biochemical Sciences*, *20* (4), 143–146. http://doi.org/10.1016/S0968-0004 (00)88990-2

Pollock, R. E., & Society, A. C. (2002). Soft Tissue Sarcomas. PMPH-USA.

Poorly Differentiated Synovial Sarcoma: A Unique Presentation. (2015). Poorly Differentiated Synovial Sarcoma: A Unique Presentation. *American Journal of Clinical Pathology*. http://doi.org/10.1093/ajcp/142.suppl1.285

Pulvino, M., Liang, Y., Oleksyn, D., DeRan, M., Van Pelt, E., Shapiro, J., et al. (2012). Inhibition of proliferation and survival of diffuse large B-cell lymphoma cells by a small-molecule inhibitor of the ubiquitin-conjugating enzyme Ubc13-Uev1A. *Blood*, *120* (8), 1668–1677. http://doi.org/10.1182/blood-2012-02-406074

Richardson, P. G., Barlogie, B., Berenson, J., Singhal, S., Jagannath, S., Irwin, D., et al. (2003). A phase 2 study of bortezomib in relapsed, refractory myeloma. *The New England Journal of Medicine*, *348* (26), 2609–2617. http://doi.org/10.1056/NEJMoa030288

Richardson, P. G., Sonneveld, P., Schuster, M. W., Irwin, D., Stadtmauer, E. A., Facon, T., et al. (2005). Bortezomib or high-dose dexamethasone for relapsed multiple myeloma. *The New England Journal of Medicine*, *352* (24), 2487–2498. http://doi.org/10.1056/NEJMoa043445

Roberts, C. W. M., Leroux, M. M., Fleming, M. D., & Orkin, S. H. (2002). Highly penetrant, rapid tumorigenesis through conditional inversion of the tumor suppressor gene Snf5. *Cancer Cell*, *2* (5), 415–425.

Ronan, J. L., Wu, W., & Crabtree, G. R. (2013). From neural development to cognition: unexpected roles for chromatin. *Nature Reviews. Genetics*, *14* (5), 347–359. http://doi.org/10.1038/nrg3413

Saeki, Y. (2017). Ubiquitin recognition by the proteasome. *Journal of Biochemistry*, mvw091. http://doi.org/10.1093/jb/mvw091

Schlesinger, D. H., Goldstein, G., & Niall, H. D. (1975). The complete amino acid sequence of ubiquitin, an adenylate cyclase stimulating polypeptide probably universal in living cells. *Biochemistry*, *14* (10), 2214–2218.

Schuettengruber, B., Chourrout, D., Vervoort, M., Leblanc, B., & Cavalli, G. (2007). Genome regulation by polycomb and trithorax proteins. *Cell*, *128* (4), 735–745. http://doi.org/10.1016/j.cell.2007.02.009

Shah, S. A., Potter, M. W., McDade, T. P., Ricciardi, R., Perugini, R. A., Elliott, P. J., et al. (2001). 26S proteasome inhibition induces apoptosis and limits

growth of human pancreatic cancer. *Journal of Cellular Biochemistry*, *82* (1), 110–122.

Sherman, K. L., Wayne, J. D., Chung, J., Agulnik, M., Attar, S., Hayes, J. P., et al. (2014). Assessment of multimodality therapy use for extremity sarcoma in the United States. *Journal of Surgical Oncology*, *109* (5), 395–404. http://doi.org/10.1002/jso.23520

Shi, W., Indelicato, D. J., Morris, C. G., Scarborough, M. T., Gibbs, C. P., & Zlotecki, R. A. (2013). Long-term treatment outcomes for patients with synovial sarcoma: a 40-year experience at the University of Florida. *American Journal of Clinical Oncology*, *36* (1), 83–88. http://doi.org/10.1097/COC.0b013e31823fe450

Shi, Y., Chen, X., Elsasser, S., Stocks, B. B., Tian, G., Lee, B.-H., et al. (2016). Rpn1 provides adjacent receptor sites for substrate binding and deubiquitination by the proteasome. *Science (New York, N.Y.)*, *351* (6275), aad9421–aad9421. http://doi.org/10.1126/science.aad9421

Singhal, N., Graumann, J., Wu, G., Araúzo-Bravo, M. J., Han, D. W., Greber, B., et al. (2010). Chromatin-Remodeling Components of the BAF Complex Facilitate Reprogramming. *Cell*, *141* (6), 943–955. http://doi.org/10.1016/j.cell.2010.04.037

Skaar, J. R., Pagan, J. K., & Pagano, M. (2014). SCF ubiquitin ligase-targeted therapies. *Nature Reviews. Drug Discovery*, *13* (12), 889–903. http://doi.org/10.1038/nrd4432

Soucy, T. A., Smith, P. G., Milhollen, M. A., Berger, A. J., Gavin, J. M., Adhikari, S., et al. (2009). An inhibitor of NEDD8-activating enzyme as a new approach to treat cancer. *Nature*, *458* (7239), 732–736. http://doi.org/10.1038/nature07884

Soulez, M., Saurin, A. J., Freemont, P. S., & Knight, J. C. (1999). SSX and the synovial-sarcoma-specific chimaeric protein SYT-SSX co-localize with the human Polycomb group complex. *Oncogene*, *18* (17), 2739–2746. http://doi.org/10.1038/sj.onc.1202613

Stern, M., Jensen, R., & Herskowitz, I. (1984). Five SWI genes are required for expression of the HO gene in yeast. *Journal of Molecular Biology*, *178* (4), 853–868. http://doi.org/10.1016/0022-2836 (84)90315-2

Surace, C., Panagopoulos, I., Pålsson, E., Rocchi, M., Mandahl, N., & Mertens, F. (2004). A novel FISH assay for SS18-SSX fusion type in synovial sarcoma. *Laboratory Investigation; a Journal of Technical Methods and Pathology*, *84* (9), 1185–1192. http://doi.org/10.1038/labinvest.3700142

Swords, R. T., Erba, H. P., DeAngelo, D. J., Bixby, D. L., Altman, J. K., Maris, M., et al. (2015). Pevonedistat (MLN4924), a First-in-Class NEDD8-activating enzyme inhibitor, in patients with acute myeloid leukaemia and myelodysplastic syndromes: a phase 1 study. *British Journal of Haematology*, *169* (4), 534–543. http://doi.org/10.1111/bjh.13323

Tanaka, K., Ii, K., Ichihara, A., Waxman, L., & Goldberg, A. L. (1986). A high molecular weight protease in the cytosol of rat liver. I. Purification, enzymological properties, and tissue distribution. *The Journal of Biological Chemistry*, *261* (32), 15197–15203.

Thaete, C., Brett, D., Monaghan, P., Whitehouse, S., Rennie, G., Rayner, E., et al. (1999). Functional domains of the SYT and SYT-SSX synovial sarcoma translocation proteins and co-localization with the SNF protein BRM in the nucleus. *Human Molecular Genetics*, *8* (4), 585–591.

Thrower, J. S., Hoffman, L., Rechsteiner, M., & Pickart, C. M. (2000). Recognition of the polyubiquitin proteolytic signal. *The EMBO Journal*, *19* (1),

94–102. http://doi.org/10.1093/emboj/19.1.94

Thway, K., & Fisher, C. (2014). Synovial sarcoma: defining features and diagnostic evolution. *Annals of Diagnostic Pathology*, *18* (6), 369–380. http://doi.org/10.1016/j.anndiagpath.2014.09.002

Uboldi, S., Craparotta, I., Colella, G., Ronchetti, E., Beltrame, L., Vicario, S., et al. (2017). Mechanism of action of trabectedin in desmoplastic small round cell tumor cells. *BMC Cancer*, *17* (1), 107. http://doi.org/10.1186/s12885-017-3091-1

Urrutia, R. (2003). KRAB-containing zinc-finger repressor proteins. *Genome Biology*, *4* (10), 231. http://doi.org/10.1186/gb-2003-4-10-231

van der Graaf, W. T. A., Blay, J.-Y., Chawla, S. P., Kim, D.-W., Bui-Nguyen, B., Casali, P. G., et al. (2012). Pazopanib for metastatic soft-tissue sarcoma (PALETTE): a randomised, double-blind, placebo-controlled phase 3 trial. *Lancet (London, England)*, *379* (9829), 1879–1886. http://doi.org/10.1016/S0140-6736 (12)60651-5

Verma, R., Aravind, L., Oania, R., McDonald, W. H., Yates, J. R., Koonin, E. V., & Deshaies, R. J. (2002). Role of Rpn11 metalloprotease in deubiquitination and degradation by the 26S proteasome. *Science (New York, N.Y.)*, *298* (5593), 611–615. http://doi.org/10.1126/science.1075898

Vignali, M., Hassan, A. H., Neely, K. E., & Workman, J. L. (2000). ATP-Dependent Chromatin-Remodeling Complexes. *Molecular and Cellular Biology*, *20* (6), 1899–1910. http://doi.org/10.1128/MCB.20.6.1899-1910.2000

Vlenterie, M., Jones, R. L., & van der Graaf, W. T. A. (2015). Synovial sarcoma diagnosis and management in the era of targeted therapies. *Current Opinion*

in Oncology, *27* (4), 316–322. http://doi.org/10.1097/CCO.0000000000000198

Wang, W., Cote, J., Xue, Y., Zhou, S., & Khavari, P. A. (1996). Purification and biochemical heterogeneity of the mammalian SWI-SNF complex. *The EMBO …*.

Wilkinson, K. D., Urban, M. K., & Haas, A. L. (1980). Ubiquitin is the ATP-dependent proteolysis factor I of rabbit reticulocytes. *The Journal of Biological Chemistry*, *255* (16), 7529–7532.

Xue, Y., Canman, J. C., Lee, C. S., Nie, Z., Yang, D., Moreno, G. T., et al. (2000). The human SWI/SNF-B chromatin-remodeling complex is related to yeast rsc and localizes at kinetochores of mitotic chromosomes. *Proceedings of the National Academy of Sciences*, *97* (24), 13015–13020. http://doi.org/10.1073/pnas.240208597

Yamamoto, T., Nojima, M., Ishiura, S., & Sugita, H. (1986). Purification of the two forms of the high-molecular-weight neutral proteinase ingensin from rat liver. *Biochimica Et Biophysica Acta*, *882* (3), 297–304.

Yang, Y., Kitagaki, J., Dai, R.-M., Tsai, Y. C., Lorick, K. L., Ludwig, R. L., et al. (2007). Inhibitors of ubiquitin-activating enzyme (E1), a new class of potential cancer therapeutics. *Cancer Research*, *67* (19), 9472–9481. http://doi.org/10.1158/0008-5472.CAN-07-0568

Yates, B., Braschi, B., Gray, K. A., Seal, R. L., Tweedie, S., & Bruford, E. A. (2017). Genenames.org: the HGNC and VGNC resources in 2017. *Nucleic Acids Research*, *45* (D1), D619–D625. http://doi.org/10.1093/nar/gkw1033

Zhang, Yanni, Du, Z., & Zhang, M. (2016a). Biomarker development in MET-

targeted therapy. *Oncotarget*, *7* (24), 37370–37389. http://doi.org/10.18632/oncotarget.8276

Zhang, Yi, Shi, C.-C., Zhang, H.-P., Li, G.-Q., & Li, S.-S. (2016b). MLN4924 suppresses neddylation and induces cell cycle arrest, senescence, and apoptosis in human osteosarcoma. *Oncotarget*, *7* (29), 45263–45274. http://doi.org/10.18632/oncotarget.9481

Chapter 2: Small Molecule Profiling of Synovial Sarcoma Cancer Cell Lines

Chapter 2.1: Introduction

To identify SS-specific therapeutic opportunities comprehensively, I screened SS cell lines for high specific lethality among 860 total cell lines using a panel of 481 small molecules with known bioactivity. This set of compounds included 70 FDA-approved drugs, 100 clinical candidates and 311 small-molecule probes targeting a wide array of biological pathways. This well-annotated informer set from the Cancer Target Discovery and Development (CTD^2) program has been used previously for large scale cancer cell line (CCL) profiling (Seashore-Ludlow et al., 2015). With this approach, I identified the receptor tyrosine kinase (RTK) MET as a novel target in biphasic SS which I demonstrate potentiates the oncogenic activity of SS18-SSX.

MET, also known as the hepatocyte growth-factor receptor (HGFR), mediates key biological pathways including embryogenesis, tissue regeneration and wound healing (Fajardo-Puerta, Mato Prado, Frampton, & Jiao, 2016). Its misregulation is tightly associated with oncogenesis, as binding of its ligand, HGF, can induce proliferation, cell survival, cell motility, and stimulation of angiogenesis (Gherardi, Birchmeier, Birchmeier, & Vande Woude, 2012). There are currently two approved non-specific small-molecule MET inhibitors in the

clinic that could be repurposed for biphasic SS, cabozantinib and crizotinib, with several others under early-stage evaluation (Ariyawutyakorn, Saichaemchan, & Varella-Garcia, 2016). In the context of SS, MET has previously been observed to be expressed in a significant number of cases (Kuhnen, Tolnay, Steinau, Voss, & Müller, 1998), and recently its activity was implicated in SS cell line proliferation (Imura et al., 2016), but the mechanistic details and connection to SS18-SSX remain poorly understood.

Chapter 2.2: Identifying pathway dependencies in SS using small-molecule profiling

To identify compounds that may exhibit selective potency in SS, I screened three SS cell lines across the full the CTD^2 informer set and compared viability scores quantified using the area under the growth curve (AUC) from SS with those from 860 other CCLs (**Figure 2.1A**). The median AUC value of all compounds screened in SS lines was similar to that observed in other CCLs (**Figure 2.2A**), indicating similar global screening results. I then selected compounds with an AUC in SS significantly below their median AUC across all other CCLs for further study (**Table 2.1**). Among this set of compounds, I observed that MET was the most common target, with 6 out of 7 MET inhibitors reaching statistical significance ($p < 0.05$) (**Figure 2.1B**). For the most potent MET inhibitors, SGX-

523 and cabozantinib, sensitivity was exclusive to the biphasic SS lines, Aska and Yamato ($p < 0.0001$, ANOVA), and moreover, the sensitivity in these lines was among the highest across all 860 CCLs screened (**Figure 2.1C**). I next validated the high- throughput screening results to validate potency and to obtain the concentration of compound resulting in half-maximal growth (IC_{50}). To this re-test I included three additional SS lines: SYO1, Fuji and HSSY2, in addition to three sarcoma lines of other types (HOS (osteosarcoma), RH18 (rhabdomyosarcoma) and TE125T (rhabdomyosarcoma)) for comparison. Five compounds were found to significantly prevent cell growth in all SS lines: JQ-1, clorafarabine, ouabain, i-BET, and SNS-032, though these compounds were also active in non-SS lines (**Figure 2.1D**), as well as cell lines across several lineages. More notably, MET inhibitors clustered together, showing high activity in the two biphasic SS lines, Aska and Yamato, confirming high-throughput screen results. MET inhibition was highly selective for Aska and Yamato over other SS lines, with the MET inhibitor SGX-523 showing a >100-fold selectivity and cabozantinib showing a >10-fold selectivity (**Figure 2.1E**). This difference in sensitivity is likely due to the reported target specificity of these inhibitors for MET (Buchanan et al., 2009; Grüllich, 2014) (**Figure 2.2B**).

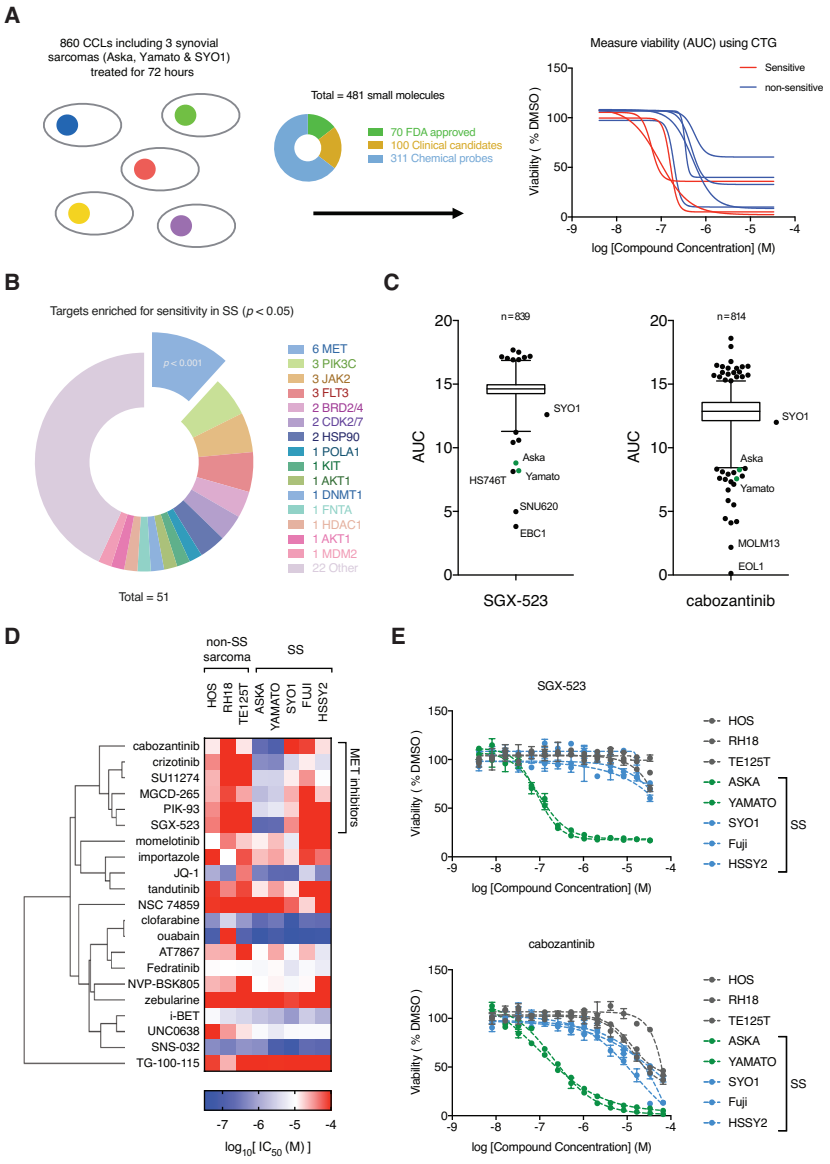


Figure 2.1. MET is a targetable dependency in a subset of synovial sarcoma (SS) cell lines. (A) Outline of performed high-throughput screen for small molecules that can prevent the proliferation of SS cell lines.

Figure 2.1 (Continued). (B) Breakdown of the small molecule targets that were enriched for growth sensitivity in SS at a p-value < 0.05 (Fisher's test). Significance of MET enrichment was ascertained through random sampling of the compound-target list. (C) Distribution of AUCs for two MET inhibitors across all cancer cell lines tested, with the 3 SS lines highlighted. (D) Heatmap of the half-maximal growth inhibitory concentration (IC50) for top compounds identified in the screen in 3 non-SS sarcoma (HOS, RH18 and TE125T) lines and 5 SS cell lines (Aska, Yamato, SYO1, Fuji and HSSY2). An apparent cluster of MET inhibitors is highlighted. (E) Growth curves used to derive IC50 values in previous heatmap for two MET inhibitors.

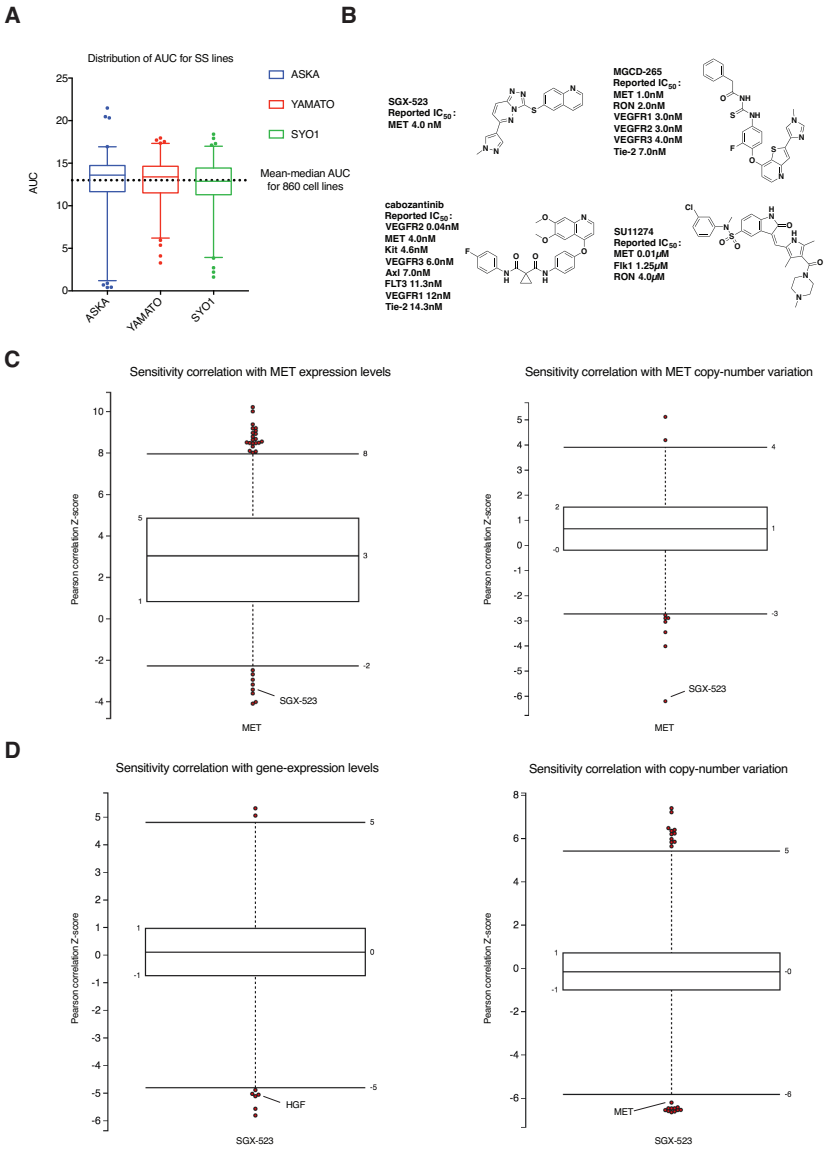


Figure 2.2. MET inhibitors have varied specificity, and low AUC for SGX-523 correlates with high MET or HGF expression. (A) Distribution of AUC values from the screen for the 3 SS lines tested. Line highlights the mean-median AUC value observed across all 860 cell lines.

Figure 2.2 (Continued). (B) Literature reporter in vitro specificity of re-tested MET inhibitors across various RTKs, with their respective chemical structure. (C) Compounds determined to correlate the most with MET expression and copy number variation from the screen. (D) Genes whose expression levels or copy-number variation correlated negatively with SGX-523 AUC.

Table 2.1. Identification and selection of hits from small molecule screen.

List of compounds that were identified as having a lower AUC in SS lines as compared to the rest of the cell lines and chosen for IC_{50} determination. Fisher's test was used to determine statistical significance, with a cutoff of p-value < 0.05 in addition to manual inspection of the growth curves. Column name descriptions are as follows: compound.median.AUC (the median AUC value for that compound across all cell lines), n.features.tested (number of SS lines killed at the cutoff), n.features.total (total number of SS lines the compound saw, i.e. <= 4), AUC (AUC value at the cutoff), cutoff (number of total cell lines below the cutoff, both synovial and not), total.cell.lines (total number of lines the compound saw), and fisher.pval (p-value from Fisher's test).

compound	compound.median.AUC	n.features.tested	n.features.total	AUC	cutoff	total.cell.lines	fisher.pval	targets	direction
TG-100-115	14.469	3	4	12.392	13	647	2.52E-05	PIK3CD;PIK3CG	sensitive
SGX-523	14.609	3	4	12.559	16	646	4.93E-05	MET	sensitive
momelotinib	12.529	4	4	11.503	89	628	0.000380372	JAK1;JAK2	sensitive
tandutinib	13.577	4	4	12.005	101	641	0.000585899	FLT3;KIT	sensitive
AT7867	12.7365	4	4	11.497	105	630	0.000735261	AKT1;AKT2;AKT3;RPS6KB2	sensitive
crizotinib	11.689	2	4	7.5016	9	643	0.001031312	ALK;MET	sensitive
cabozantinib	12.998	2	4	8.2736	9	633	0.001063933	FLT3;KDR;MET;RET	sensitive
zebularine	14.544	3	4	12.975	45	653	0.001169171	DNMT1	sensitive
clofarabine	11.5485	4	4	8.8344	124	656	0.001226976		sensitive
ouabain	5.89515	4	4	4.107	132	654	0.001599775	ATP1A1;ATP1A2;ATP1A3;ATP1A4;ATP1B1;ATP1B2;ATP1B3;ATP1B4	sensitive
UNC0638	13.985	4	4	12.943	135	642	0.00188708	EHMT1;EHMT2	sensitive
PIK-93	12.593	2	4	9.7854	12	635	0.001926045	PIK3CG	sensitive
SNS-032	9.7692	4	4	8.1915	140	615	0.002597091	CDK16;CDK17;CDK2;CDK7;CDK9;CDKL5	sensitive
NVP-BSK805	12.647	4	4	11.996	151	646	0.002894857	JAK2	sensitive
MGCD-265	13.7655	2	4	10.104	16	656	0.003256391	FLT1;FLT3;KDR;MET	sensitive
SU11274	14.0265	2	4	11.177	16	644	0.003377146	MET	sensitive
JQ-1	11.877	3	4	9.3364	73	655	0.004906627	BRDT	sensitive
importazole	13.361	3	4	11.257	68	607	0.004968469	KPNB1	sensitive

Chapter 2.3: MET is a specific lethal dependence in sensitive SS cell lines

I next leveraged the CTRP (Clincal Trials Reporting Program) database to identify features that correlate with sensitivity to SGX-523 to help explain the observed discrepancy in the SS lines. Both MET and HGF expression showed strong negative correlations with SGX-523 AUC, as well as MET copy-number variations (**Figure 2.2C-D**). I assessed MET protein levels in the SS lines and found high expression in Aska and Yamato cell lines, but low to absent expression in the rest of SS lines (**Figure 2.3A**). MET was also activated, as measured by Y1234/35 phosphorylation, in conjunction with its downstream target AKT (pAKT S473). This AKT activation, as measured by S473 phosphorylation, was diminished with SGX-523 treatment in a dose-dependent manner (**Figure 2.3B, Figure 2.4A**). Of note, Aska and Yamato were modestly sensitive to AKT inhibition in the screen (**Figure 2.4B**). Interestingly, AKT activation was present in SYO1 and Fuji, suggesting alternative routes of activation in these cells, e.g. a different RTK, albeit substantially weaker. To validate this MET dependency, I stably infected Aska cell lines with shRNAs directed against the MET gene, which achieved ~50-75% loss of MET expression after 3 days (**Figure 2.3C**). MET knockdown was sufficient to ablate AKT activation, with the most potent MET knockdown resulting in almost complete

loss of pAKT S473 (**Figure 2.3D**). In addition, MET knockdown significantly halted Aska cell proliferation in culture, in a manner which corresponded directly to knock-down efficiency (**Figure 2.3E**). To identify if any other major RTKs were active in the SS lines, I profiled SS lines using a phospho-RTK array to detect levels of active RTKs (including downstream targets). Out of all targets examined, the highest level of activation were seen in AKT (pS473), S6 and Src in all SS lines, with AKT-pS473 highest in Aska and Yamato biphasic SS cell lines, likely correlating with their pattern of MET activation and METi sensitivity (**Figure 2.4C**).

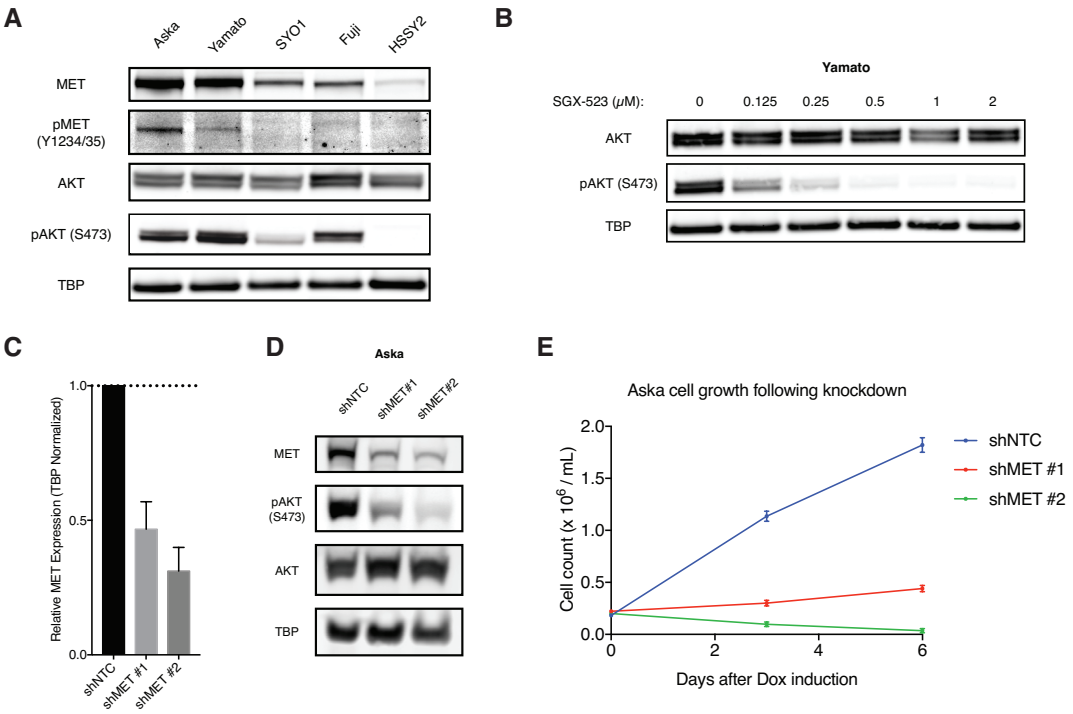


Figure 2.3. MET expression and activity are required for proliferation in biphasic SS. (A) Whole-cell immunoblot for MET, AKT and their activated phosphorylated forms from 5 SS cell lines. (B) Whole-cell immunoblot for AKT/pAKT of Yamato cells treated in dose with the MET inhibitor SGX-523 for 24 hours. (C) Real-time PCR quantification of MET expression levels following shRNA mediated knockdown of MET or a non-targeting control (NTC) in Aska cells after 3 days. (D) Whole-cell immunoblot of MET/AKT following 3-day knockdown of MET or NTC in Aska cells. (E) Growth curve for Aska cells that have been induced for MET or NTC knockdown (n=3 for all data points).

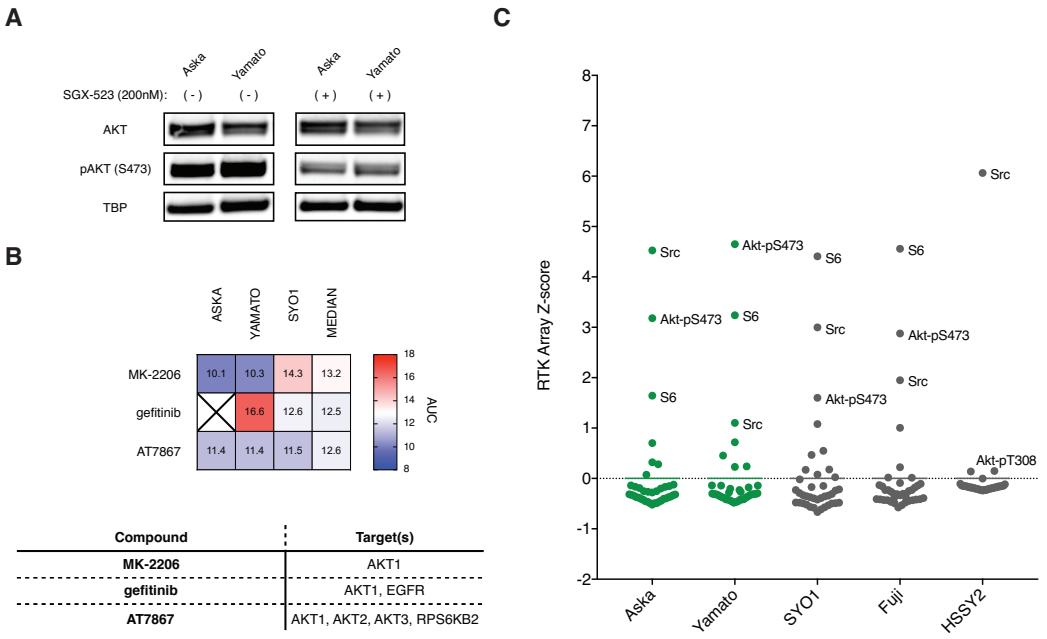


Figure 2.4. AKT activation and dependency is observed in Aska and Yamato. (A) Whole-cell immunoblot for AKT and pAKT S473 following MET inhibition with SGX-523 for 24 hours. (B) AUC values taken from the original screen for several AKT inhibitors with various specificities (listed in the table below) from the 3 SS lines screened and the median AUC across all 860 lines. (C) Whole-cell lysates from 5 SS lines were analyzed for RTK activation using a Phospho-RTK array (CellSignaling).

Chapter 2.4: SS cell lines exhibit differential expression of RTKs

To further understand the observed differential responses to MET inhibition, I performed mRNA profiling via RNA-seq across all five SS lines. Gene expression profiles were most similar between Aska and Yamato cell lines, as demonstrated by principal component analysis (PCA) (**Figure 2.5A**). Interestingly, RTK gene expression was highly heterogeneous across all lines, including Aska and Yamato (**Figure 2.5B**), however elevated MET expression was seen exclusively in Aska and Yamato. While these two shared *MET* expression, Aska cells have high levels of *KIT* and *LTK* not seen in Yamato. This extended to the rest of the lines, with unique expression of *PDGFRA* in Yamato, *KDR* in SYO1, *FLT1* in Fuji, and *FGFR2* in HSSY2.

Gene set enrichment analysis (GSEA) performed in Aska and Yamato as well as the other 3 additional SS cell lines demonstrated selective enrichment of gene sets associated with the MET and AKT pathways in Aska and Yamato cell lines (**Figure 2.5C**). Importantly, expression of the MET receptor ligand, *HGF*, was only highly expressed in Aska and Yamato cell lines (**Figure 2.5D**). Concordant expression of *MET* and *HGF* has been reported to be indicative of autocrine signaling, suggesting an active MET/HGF pathway in these cells (Toiyama et al., 2012). Using whole-exome sequencing, I further identified that these high

expression levels are due to a focal amplification of the MET gene on Chr 7, but not of HGF, in Aska and Yamato biphasic SS cell lines (**Figure 2.5E, Figure 2.6A**).

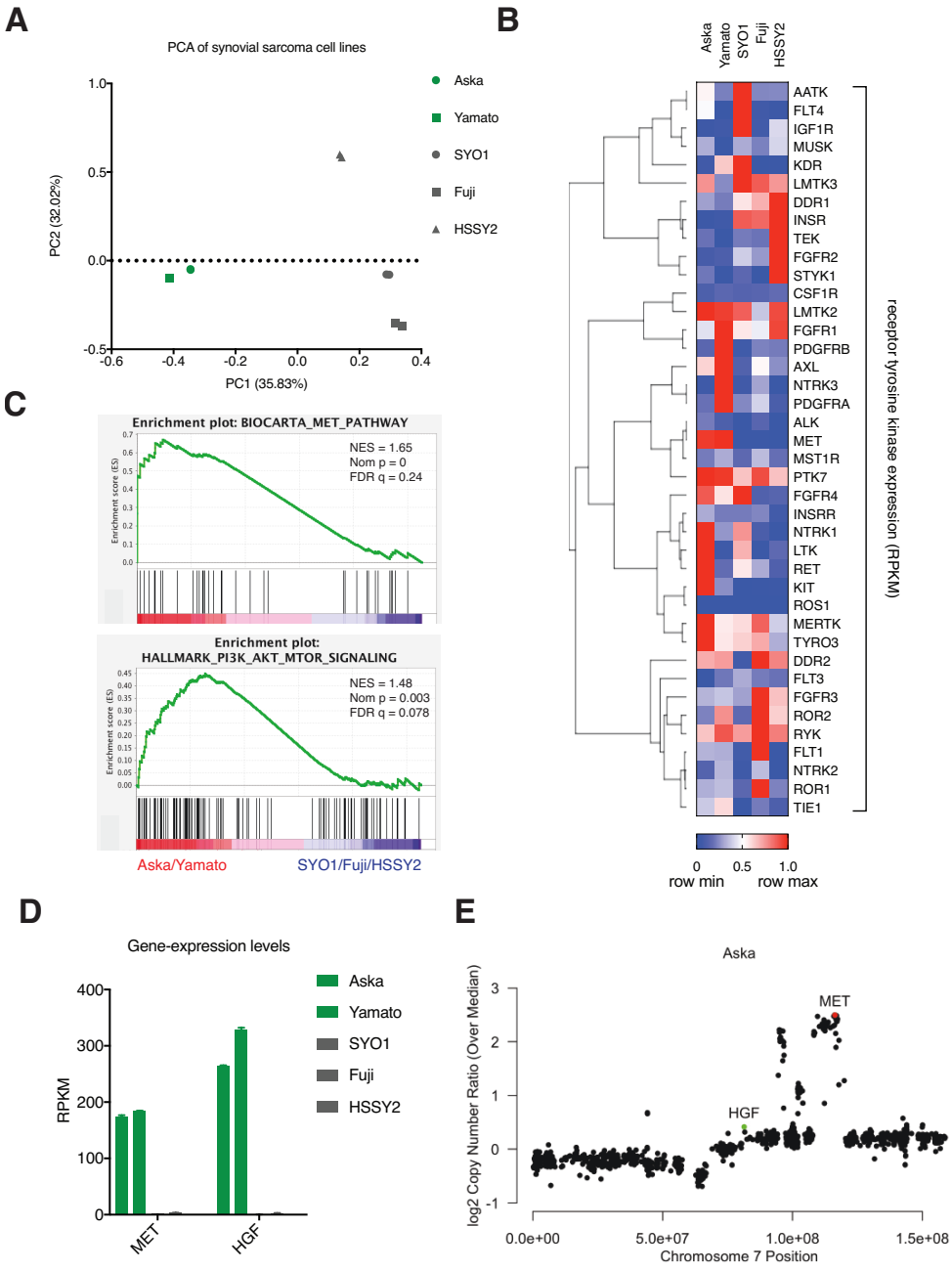


Figure 2.5. SS CCLs have differential expression of RTKs, with Aska and Yamato harboring a MET chromosomal amplification. (A) Principal component analysis (PCA) of RNA-Seq data from each SS line in this study. Highlighted in green are the cell lines sensitive to MET inhibition.

Figure 2.5 (Continued). (B) Heatmap showing relative abundance in RPKM units of RTKs in SS CCLs. (C) GSEA of the MET-inhibition sensitive cell lines (Aska & Yamato) compared to the rest of SS cells (SYO1, Fuji & HSSY2). (D) Expression levels (RPKM) of MET and HGF in the SS lines. (E) Plot of copy number variation with respect to chromosomal position for the Aska line, derived from whole-exome sequencing.

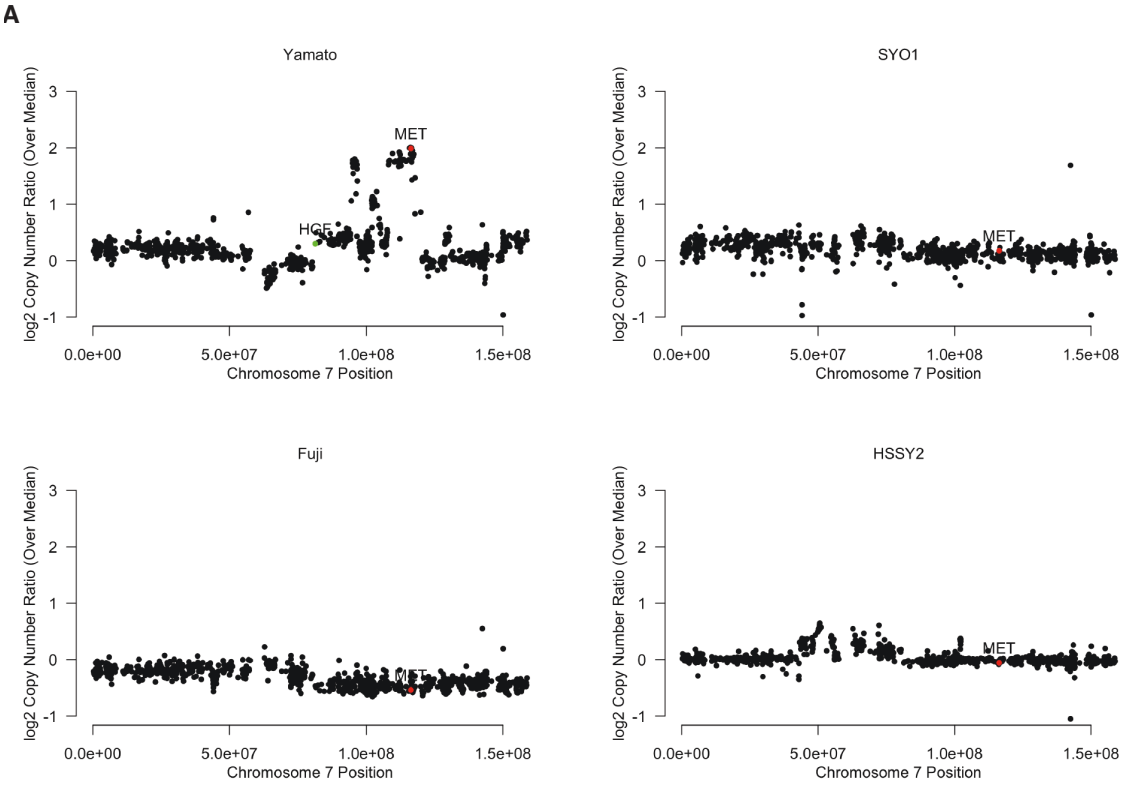


Figure 2.6. MET amplification is only observed in Aska and Yamato. (A) Copy-number variation levels in chromosome 7 for 4 SS cell lines derived from whole-exome sequencing data. Highlighted are the genes MET (red) and HGF (green).

Chapter 2.5: Methods

Chapter 2.5.1: Cancer cell-line profiling

Screening has been described in detail in a previous study, including data analysis and interpretation (Seashore-Ludlow et al., 2015). In brief, cells were grown in DMEM (supplemented with 20% FBS (Omega Scientific), 1mg/mL Penicillin-streptomycin (Gibco), 1mM sodium pyruvate (Gibco)) and plated at a density of 1000 cells per well in white 384-well TC-treated plates (Corning). Compounds were added after 24 hours using a pinning-tool (CyBio) and cellular ATP levels measured after 72 hours using the CellTiterGlo (Promega) reagent with detection on an Envision Multiplate Reader (Perkin Elmer). Effects on ATP levels were tested in a 16-point (2-fold dilution) dose curve for every compound in duplicate. Follow up studies for lead compounds were performed in triplicate under the same conditions.

Chapter 2.5.2: Immunoblotting

Cells were grown in DMEM supplemented with 10% heat-inactivated FBS (Omega Scientific), 1mg/mL Penicillin-streptomycin (Gibco), and 1mM sodium pyruvate (Gibco) up to full confluence and washed once with PBS before lysis.

100μL of lysis buffer (RIPA + cOmplete Protease Inhibitors (Roche) + PhosSTOP (Roche)) was added to $2x10^6$ cells, incubated on ice for 30 min and cleared in a micro-centrifuge (17,000xg for 15 min). 30μg of the supernatant was separated using gel electrophoresis, transferred into a PVDF membrane (Millipore), blotted for the target protein and analyzed using an IR imaging system (LI-COR Odyssey CLx).

Chapter 2.5.3: RNA Extraction and RNA-Seq

$1x10^6$ cells from each SS cell line were plated in a 6-well dish. To induce shRNA knockdown Dox was added to the media at a final concentration of 1μg/mL. Similarly, for MET inhibition compound was added directly to the media to desired concentration at a final DMSO v/v concentration of 1%. Following perturbation, media was removed and 1mL of TRIzol reagent (ThermoFisher) was added to each well, and RNA was extracted according to the manufacturers protocol. Quantification of the samples was performed using the Qubit RNA HS Assay Kit (ThermoFisher) in a Qubit fluorometer (ThermoFisher). All library preparation and sequencing (75bp single end on Illumina NextSeq 500) was performed in the Molecular Biology Core Facilities at the Dana-Farber Cancer Institute.

Chapter 2.5.4: Sequencing data processing & analysis

RNA-Seq reads were mapped to the human reference genome (hg19) using STAR (Dobin et al., 2013) version 2.3.1 with default parameters. All sequence data is deposited in the Sequence Read Archive under accession number GSE90807. RPKM values for biological duplicate RNA-seq samples were generated using GFold (Feng et al., 2012) version 1.1.0. All error bars represent Mean±SEM. Significance was assessed using the R package DESeq2 (Love, Huber, & Anders, 2014) using raw read counts generated with Rsubread featureCounts against the hg19 refFlat annotation. Significantly changing genes were assessed with a Bonferri-corrected p-value of less than 1e-3 and a two-fold gene expression change (|log2FC|>1) to determine set of significantly changing genes. GSEA was performed using the GSEA Preranked function of the JAVA program (http://www.broadinstitute.org/gsea) as described previously (Subramanian et al., 2005). Rank files for GSEA were generated using RPKMs for duplicate RNA-seq in each cell line, removal of short RNAs, filtering for expressed genes (minimum RPKM value for four samples >= 1), averaging replicates of each condition, then doing a log2 fold change comparison with a pseudocount of 1 in each condition, i.e. log2 (($RPKM^B$ + 1)/ ($RPKM^A$ + 1)). Pairwise correlation was determined using a Pearson correlation coefficient between normalized expression values.

Chapter 2.6: Conclusions

To identify novel therapeutic targets for SS I determined SS cancer cell line dependencies using small molecule profiling, and identified compounds that were selectively toxic to SS CCLs. Out of the hits from the screen, MET was the most abundant target that reached significance, with 6 out of 7 MET inhibitors in the library scoring as selectively toxic in SS lines. This sensitivity was exclusive to 2 out of the 5 SS lines studied, with the MET inhibitor SGX-523 displaying a selectivity of >100-fold for Aska and Yamato. While there were other interesting hits in the screen, e.g. JQ-1 and ouabain, these saw activity in the 3 non-SS control lines used and have relatively complex mechanisms of action.

I validated the sensitivity to MET inhibition genetically using RNAi with two independent guides specific to the MET gene in the Aska cell line. Loss of MET expression induced loss of AKT activation (measured via phosphorylation at S473) and prevented Aska cell line growth, which are the same phenotypes observed with MET inhibition using SGX-523. This difference in sensitivity extends to the cell line's transcriptional profile, with Aska and Yamato having a much closer gene expression state than the other 3 SS lines, evidence by their distance in their Principal Components. This profiling also revealed that HGF is also expressed in Aska and Yamato, indicative of autocrine type signaling in

these cells. Lastly, I observed that MET is amplified in Aska and Yamato using whole-exome sequencing, determining the mechanistic cause of expression differences of MET between Aska/Yamato and the non-sensitive lines to MET inhibition. It remained to be seen whether this discovery was clinically relevant, and I address this in the subsequent chapter of this thesis.

References

Ariyawutyakorn, W., Saichaemchan, S., & Varella-Garcia, M. (2016). Understanding and Targeting MET Signaling in Solid Tumors - Are We There Yet? *Journal of Cancer*, *7* (6), 633–649. http://doi.org/10.7150/jca.12663

Buchanan, S. G., Hendle, J., Lee, P. S., Smith, C. R., Bounaud, P.-Y., Jessen, K. A., et al. (2009). SGX523 is an exquisitely selective, ATP-competitive inhibitor of the MET receptor tyrosine kinase with antitumor activity in vivo. *Molecular Cancer Therapeutics*, *8* (12), 3181–3190. http://doi.org/10.1158/1535-7163.MCT-09-0477

Dobin, A., Davis, C. A., Schlesinger, F., Drenkow, J., Zaleski, C., Jha, S., et al. (2013). STAR: ultrafast universal RNA-seq aligner. *Bioinformatics (Oxford, England)*, *29* (1), 15–21. http://doi.org/10.1093/bioinformatics/bts635

Fajardo-Puerta, A. B., Mato Prado, M., Frampton, A. E., & Jiao, L. R. (2016). Gene of the month: HGF. *Journal of Clinical Pathology*, *69* (7), 575–579. http://doi.org/10.1136/jclinpath-2015-203575

Feng, J., Meyer, C. A., Wang, Q., Liu, J. S., Shirley Liu, X., & Zhang, Y. (2012).

GFOLD: a generalized fold change for ranking differentially expressed genes from RNA-seq data. *Bioinformatics (Oxford, England)*, *28* (21), 2782–2788. http://doi.org/10.1093/bioinformatics/bts515

Gherardi, E., Birchmeier, W., Birchmeier, C., & Vande Woude, G. (2012). Targeting MET in cancer: rationale and progress. *Nature Reviews. Cancer*, *12* (2), 89–103. http://doi.org/10.1038/nrc3205

Grüllich, C. (2014). Cabozantinib: A MET, RET, and VEGFR2 Tyrosine Kinase Inhibitor. In *Small Molecules in Oncology* (Vol. 201, pp. 207–214). Berlin, Heidelberg: Springer Berlin Heidelberg. http://doi.org/10.1007/978-3-642-54490-3_12

Imura, Y., Nakai, T., Yamada, S., Outani, H., Takenaka, S., Hamada, K., et al. (2016). Functional and therapeutic relevance of hepatocyte growth factor/c-MET signaling in synovial sarcoma. *Cancer Science*, *107* (12), 1867–1876. http://doi.org/10.1111/cas.13092

Kuhnen, C., Tolnay, E., Steinau, H. U., Voss, B., & Müller, K. M. (1998). Expression of c-Met receptor and hepatocyte growth factor/scatter factor in synovial sarcoma and epithelioid sarcoma. *Virchows Archiv : an International Journal of Pathology*, *432* (4), 337–342.

Love, M. I., Huber, W., & Anders, S. (2014). Moderated estimation of fold change and dispersion for RNA-seq data with DESeq2. *Genome Biology*, *15* (12), 31. http://doi.org/10.1186/s13059-014-0550-8

Seashore-Ludlow, B., Rees, M. G., Cheah, J. H., Cokol, M., Price, E. V., Coletti, M. E., et al. (2015). Harnessing Connectivity in a Large-Scale Small-Molecule Sensitivity Dataset. *Cancer Discovery*, *5* (11), 1210–1223. http://doi.org/10.1158/2159-8290.CD-15-0235

Subramanian, A., Tamayo, P., Mootha, V. K., Mukherjee, S., Ebert, B. L., Gillette,

M. A., et al. (2005). Gene set enrichment analysis: a knowledge-based approach for interpreting genome-wide expression profiles. *Proceedings of the National Academy of Sciences*, *102* (43), 15545–15550. http://doi.org/10.1073/pnas.0506580102

Toiyama, Y., Yasuda, H., Saigusa, S., Matushita, K., Fujikawa, H., Tanaka, K., et al. (2012). Co-expression of hepatocyte growth factor and c-Met predicts peritoneal dissemination established by autocrine hepatocyte growth factor/c-Met signaling in gastric cancer. *International Journal of Cancer. Journal International Du Cancer*, *130* (12), 2912–2921. http://doi.org/10.1002/ijc.26330

Chapter 3: MET Potentiation of SS18-SSX in Biphasic Synovial Sarcomas

All work, analysis, and interpretation was performed by Enrique Miguel García-Rivera except for the following experiments. Immunohistochemistry of SS patient biopsies was performed by Dr. Jason Hornick. Xenografts of SS cancer cell lines were performed by Dr. Ting Chen and Dr. Fei Li. Knockdown of SS18-SSX1 in the Aska cell line was performed by Matthew McBride, and sequencing data was processed by John Pulice.

Chapter 3.1: Introduction

The results of the small molecule profiling in SS cell lines suggested that MET is required for proliferation in certain subsets of SS. In order to establish the clinical relevance of this finding I decided to explore the expression of MET in SS patient samples. While an interesting discovery, cancer cell lines have their limits in terms of translation into patient treatment. Notably they lack the tumor microenvironment known to have a profound effect in gene expression profiles, giving rise to marked differences between cancer cell lines and tumors of the same histology (Gillet, Varma, & Gottesman, 2013). This is routinely addressed to a certain extent with the use of mouse xenografts, which allow cancer cell lines to grow into tumors that are exposed to a microenvironment, albeit one that is not human (Sampson, Kamara, & Kolb, 2013). For this reason, I established a biphasic SS mouse xenograft model to determine the therapeutic potential of MET inhibition in this cancer.

Given that the expression of SS18-SSX1 is essential for viability in SS cancer cell lines (Kadoch & Crabtree, 2013), it is important to establish the relationship between SS18-SSX function and MET activity. For this reason, I performed a series of experiments designed to compare the transcriptional changes induced by loss of SS18-SSX1 and MET inhibition. Similarities at both the gene and

pathway level could shed light into how the fusion protein leads to oncogenesis, and how the additional dependencies I've uncovered are related to the expression of SS18-SSX. All of this together can inform the therapeutic impact and the clinical path forward of this discovery.

Chapter 3.2: Biphasic SS biopsies show high levels of MET expression

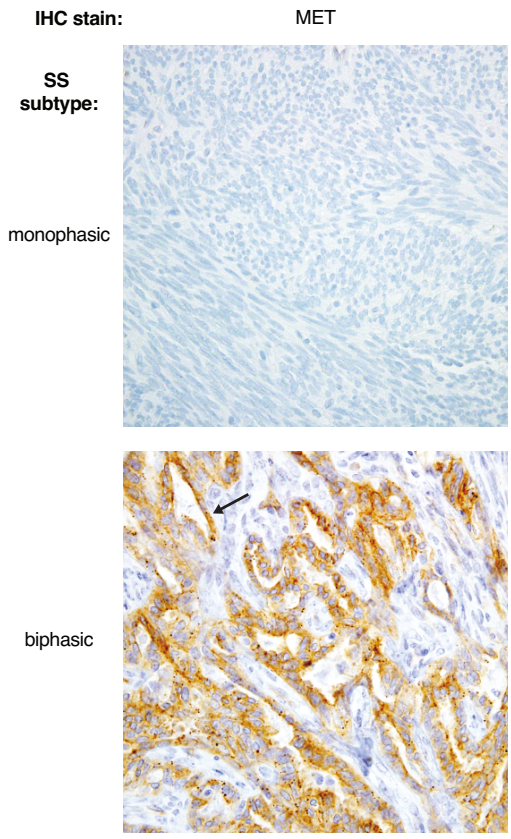
Because the observed dependency can be attributed to MET amplification, I aimed to determine whether MET expression levels are specific to biphasic synovial sarcoma in primary human tumor samples. I used immunohistochemistry from 25 adult SS biopsies, including 15 monophasic and 10 biphasic, to determine if MET protein was significantly expressed. Interestingly, MET was only found to be expressed in biphasic SS samples (7/10, 70%) and not in any of the monophasic samples (0/15, 0%) (**Figure 3.1A**). Surprisingly, this expression was restricted in its entirety to the glandular component of biphasic SS tumors for all samples that were MET positive (**Figure 3.1B**). Staining for pAKT S473 revealed 50% positivity in both monophasic and biphasic tumor samples, indicative of other mechanisms of AKT activation. This staining was not mutually exclusive with MET expression, recapitulating our observations in SS cell lines (**Figure 3.1A**), as Aska and

Yamato cell lines were derived from biphasic samples (Naka et al., 2010), reinforcing the finding that MET is predominantly expressed in this histological subtype of SS (**Figure 3.1C**).

A

Histological Subtype	MET expression	pAKT S473 positive
monophasic	0/15	8/15
biphasic	7/10	5/10

B



C

Cell Line	MET expression	Reported subtype
Aska	+	biphasic
Yamato	+	biphasic
SYO1	-	biphasic
Fuji	-	unknown
HSSY2	-	monophasic

Figure 3.1. MET is exclusively expressed in the glandular compartment of biphasic synovial sarcomas. (A) Results of immunohistochemistry (IHC) performed using primary adult tumor samples of patients with synovial sarcoma, which were stained for MET and pAKT S473. (B) Representative images from the previously described patient samples in (A) for MET in monophasic or biphasic tumors. (C) Description of SS lines used in this study with respect to MET expression and reported SS subtype of the tumor of origin.

Chapter 3.3: The MET inhibitor SGX-523 reduces tumor volume and extends survival in vivo in a biphasic tumor xenograft model

I next determined if I could exploit this MET dependency in vivo using the MET inhibitor SGX-523 in SS cell line xenograft mouse models (**Figure 3.2A**). This compound was chosen due to its proven high bioavailability in mice models (Buchanan et al., 2009). I injected 5 x 10^6 cells into the flank of NOD-SCID mice; tumors developed within 2 weeks. Immunohistochemical analyses of Yamato and SYO-1 tumors following harvesting showed that MET expression differences were recapitulated in vivo, with Yamato exhibiting high levels of MET staining (**Figure 3.2B**). Following SGX-523 treatment, Yamato tumors were significantly decreased in size, with average sizes of 1.04 g (+/- 0.20 g) in DMSO control and 0.47 g (+/- 0.12 g) in SGX-523 (**Figure 3.2C**). As expected, MET inhibition had no effect on the final tumor weight or growth of SYO1 tumors as compared to vehicle (**Figure 3.2D**). In contrast, SGX-523 significantly decreased the final tumor weight and volume of the Yamato xenograft (**Figure 3.2E**). An almost 50% reduction in tumor weight was observed for MET inhibition in Yamato xenografts, with a similar decrease in tumor volume at the end of treatment.

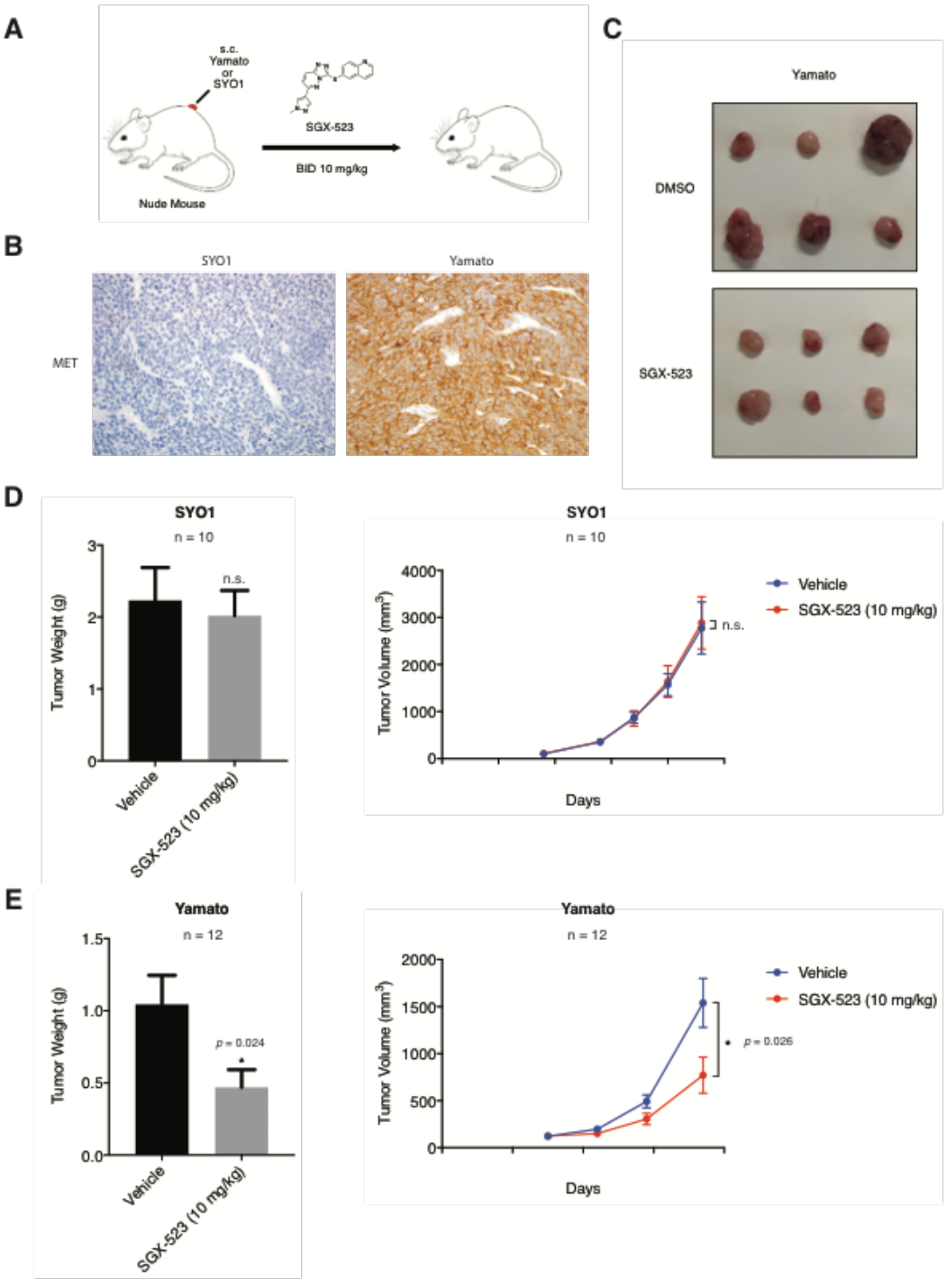


Figure 3.2. MET inhibition prevents tumor growth in an in vivo biphasic SS model. (A) Diagram of performed xenograft experiment using the SS lines

Figure 3.2 (Continued). Yamato and SYO1, which were introduced into nude mice (Charles River) via sub-cutaneous (s.c.) injection. (B) Representative image of IHC performed on tumor samples from xenograft models at the end of treatment, stained for MET. All Yamato samples stained positive for MET expression. (C) Representative image of the tumors obtained from the Yamato xenograft at the end of treatment. (D) SYO1 tumor weight +/- STD at the end of treatment (day 23) for vehicle (n=5) and SGX-523 treated (n=5) samples. Tumor volume curves are shown on the right for the mean volume +/- SEM. (E) Same as (D) at end of treatment (day 37), with vehicle (n=6) and SGX-523 treated (n=6) Yamato tumor samples. An unpaired t-test, or Welch's t-test for volume, was used to determine a statistical difference between treatments in Yamato with p-value of 0.024 for weight and 0.026 for volume.

Chapter 3.4: Loss of SS18-SSX1 regulates similar pathways to MET inhibition

To characterize the mechanism by which MET inhibition functions in tandem with the proliferative effects of the SS18-SSX oncogenic fusion, I performed RNA-Seq studies in the setting of two distinct experiments in the Aska SS cell line: DMSO vs. SGX-523 METi treatment, and shScramble (shScr) vs. shSSX1 shRNA-mediated knockdown (**Figure 3.3A**). SS18-SSX1 was significantly reduced after

knockdown (>90%), and this had no effect on the levels of MET or HGF (**Figure 3.4A-B**). Overall, loss of SS18-SSX1 induced a larger transcriptional change than SGX-523, as assessed by PCA (**Figure 3.3B**). This is expected as the SS18-SSX fusion is the hallmark, driving event in these tumors and controls the genome-wide occupancy of the mSWI/SNF (BAF) chromatin remodeling complex. Interestingly, I found that the perturbations, SGX-523 or shSS18-SSX, produce opposite global directional effects on gene expression (**Figure 3.3C**), and I do not find significant concordance between the two perturbations at the overall transcriptome level (**Figure 3.4C**). Strikingly however, using GSEA analysis I found that several pathways were regulated in the same direction by both perturbations, such as epithelial-mesenchymal transition (EMT) genes, E2F cell cycle genes, MYC targets, and EGFR signaling, pathways required for oncogenic maintenance (Beuran et al., 2015; Cataisson et al., 2016; Duan et al., 2016) (**Figure 3.3D-E, Figure 3.4D**). Importantly, while there are many individual genes such as *E2F1* and *CCNB1*, as well as several other cell cycle genes that are regulated similarly by both SGX-523 and shSS18-SSX (**Figure 3.3F-G**, **Figure 3.4G-K**), I found that these two perturbations regulate oncogenic pathways in a similar direction by affecting the expression of different genes, respectively. This is exemplified by *MYC*, which is only downregulated by SGX-523 MET inhibition, yet its downstream target genes are downregulated in both comparisons (**Figure 3.3H, Figure 3.4E-F**). These results suggest an

independent, collaborative effect of SS18-SSX and MET in promoting oncogenic proliferation in synovial sarcoma cell lines, suggesting that MET is a global, upstream regulator of different individual master genes but similar pathways as the SS18-SSX fusion in bisphasic synovial sarcoma. In a cell line of origin dependent manner, RTKs could potentiate fusion protein-mediated oncogenesis through pathways that render the resulting tumor dependent on both genes (**Figure 3.3l**). Loss of SS18-SSX or inhibition of RTK activity is capable of inducing differentiation in these cells and halting SS cell proliferation.

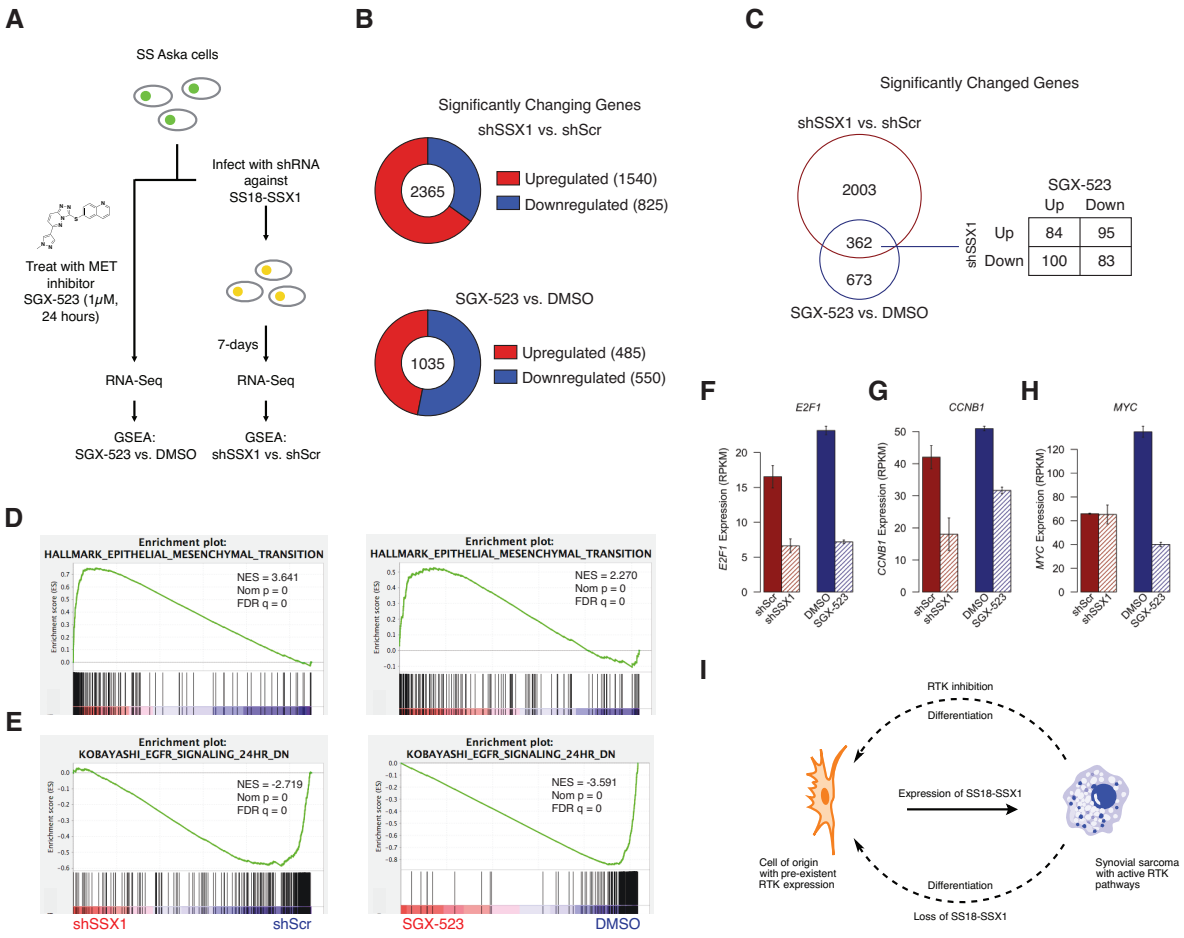


Figure 3.3. MET inhibition and loss of SS18-SSX cause differentiation in SS. (A) Schematic of RNA-Seq experiments performed in Aska cells in shScr and shSSX1 conditions as well as DMSO and SGX-523 settings. (B) Number of significantly changed genes (DESeq2 p<1e-3 and | $\log_2$FC | > 1) in (top) shSSX1 vs. shScr and (bottom) SGX-523 vs. DMSO conditions.

Figure 3.3 (Continued). (C) Overlap of significantly-changed genes in shScr vs. shSSX1 and DMSO vs. SGX-523 conditions with (right) no significant concordance of significant genes ($p = 0.1716$, Fisher exact test). (D-E) GSEA enrichment analysis of ranked genes shows (D) significant positive enrichment of epithelial-mesenchymal transition genes and (E) significant negative enrichment of EGFR genes in (left) shSSX1 vs. shScr and (right) SGX-523 vs. DMSO comparisons. (F-H) RPKM values in Aska shScr and shSSX1 conditions as well as DMSO and SGX-523 settings for cell cycle genes (F) E2F1 and (G) CCNB1, as well as (H) MYC. (I) Proposed model of MET inhibition activity in SS. Inhibition of MET or other RTK causes transcriptional changes that mimic, but are not identical, to loss of SS18-SSX1.

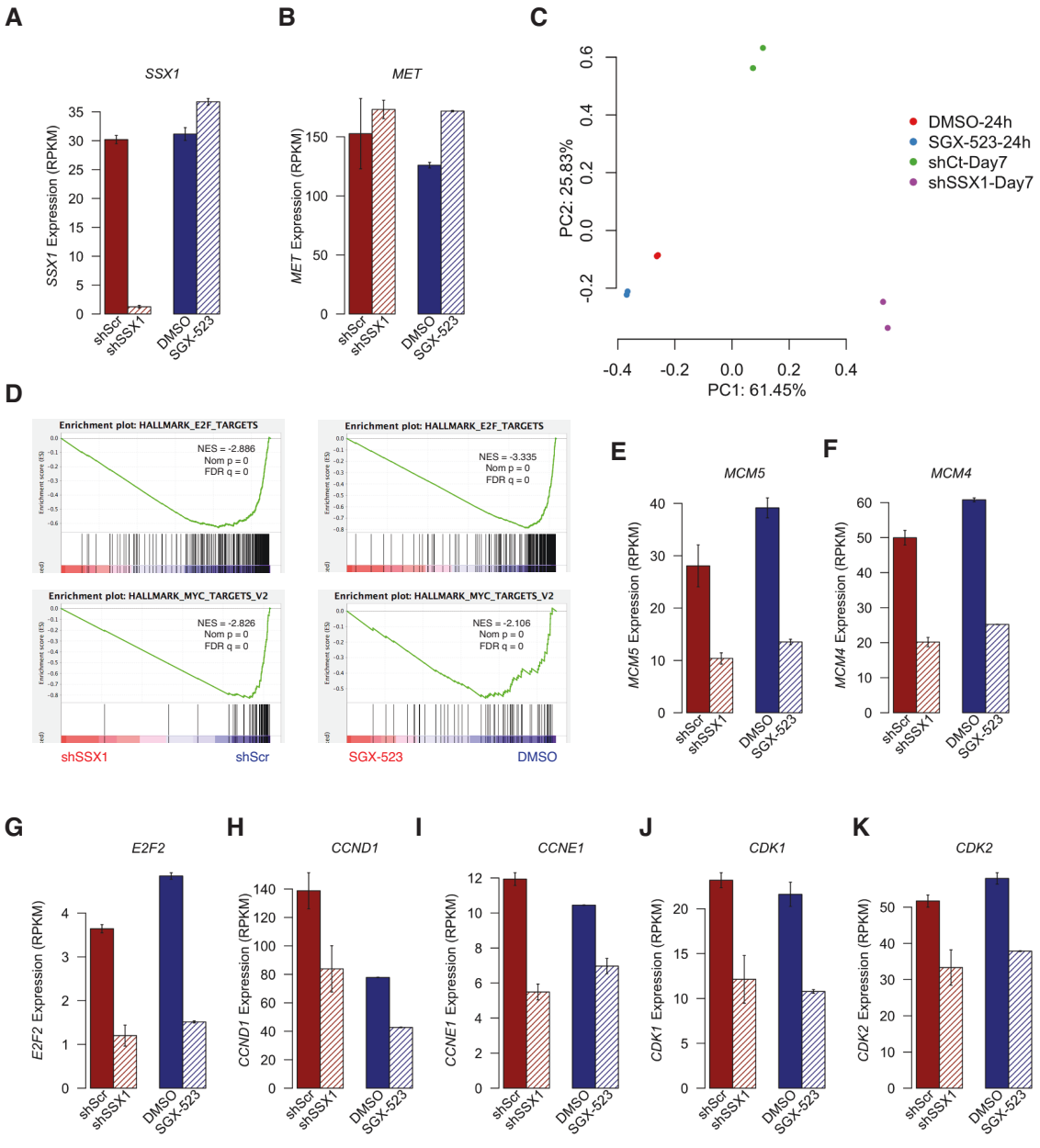


Figure 3.4. MET inhibition and loss of SS18-SSX1 decrease expression of proliferation related genes. (A-B) Expression levels for SSX1 (A), as a proxy for SS18-SSX1, and MET (B) following perturbation in Aska cells: knockdown of SS18-SSX1 for 7 days or MET inhibition with SGX-523 for 24 hours.

Figure 3.4 (Continued). (C) Principal component analysis (PCA) of RNA-Seq data from the performed experiments in Aska cells. (D) GSEA for the gene sets related to E2F and MYC activity which were downregulated in both shSSX1 and SGX-523 conditions. (E-K) Expression levels for genes related to DNA replication (E-F), transcription (G), and cell cycle progression (H-K) following treatment with shSSX1 or SGX-523.

Chapter 3.5: Methods

Chapter 3.5.1: RNA Extraction and RNA-Seq

See Chapter 2.5.3.

Chapter 3.5.2: Sequencing data processing & analysis

See Chapter 2.5.4.

Chapter 3.5.3: Immunohistochemistry of patient biopsies

Immunohistochemistry was performed on 4-micrometer-thick formalin-fixed paraffin-embedded tissue sections following pressure cooker antigen retrieval

(Target Retrieval Solution, pH 6.1; Dako, Carpinteria, CA). Samples were stained using an anti-MET (clone SP44; Spring Biosciences) or anti-pAKT-S473 (clone D9E; Cell Signaling Technology) rabbit monoclonal antibody at 1:100 dilutions for 40 minutes, visualized with EnVision + System-HRP (Dako).

Chapter 3.5.4: Cell line xenograft

Xenograft models were established by subcutaneous (s.c.) injection of 5 x 10^6 SYO1 or Yamato cells in Matrigel Matrix (Corning) into the flank of nude mice (Charles River). Approximately 2 weeks after s.c injections visible tumor nodules appeared. Tumors were measured with a caliper, and when tumor volume reached 100-200 mm^3 mice were randomized into treatment with either 10 mg/kg SGX-523 BID or vehicle BID. Tumor volume and mice weights were measured weekly from treatment start. After the appropriate treatment time mice were sacrificed and tumor samples were obtained for subsequent IHC analysis as previously described in this study.

Chapter 3.6: Conclusions

In the last two chapters, I've described how I identified one of the first reported targetable dependencies in synovial sarcomas. The large-scale approach to identify compounds that could selectively target SS CCLs yielded multiple compounds of interest that have not been previously reported. In particular, I observed that biphasic SS cell lines are highly sensitive to MET inhibition, and this was attributed to MET amplification and HGF overexpression. These cell lines with MET amplification also had active AKT, suggesting that MET is both expressed and active in these cells. In addition, AKT activation was dependent on MET activity. This suggests MET as an attractive therapeutic target in biphasic SS, as MET amplification has been implicated in the proliferation of many other cancers (Cui, 2014; Kawakami et al., 2013). The observation of concurrent HGF expression with MET further signifies the autocrine pathway activation. This co-occurrence is also seen in recurrent cases of glioblastomas (Tabouret et al., 2016), in addition to clear cell renal cell carcinomas in which MET/HGF co-expressing cases correlate with poorest overall survival (Xie et al., 2016).

Interestingly, I did observe AKT activation in cell lines that did not respond to MET inhibition. This could be due to the activity of other RTKs, for which I saw

differential expression across all SS CCLs. The importance of this was further substantiated by the IHC results, where AKT activation was seen in half of all cases. RTKs have also been implicated in other BAF mediated cancers, such as malignant rhabdoid tumors, where a subset of cell lines showcased a distinct FGFR dependency (Wöhrle et al., 2013). Together this suggests that aberrant BAF complex-mediated oncogenesis requires concomitant activity of RTKs to effect its oncogenic changes. One possibility is that expression of the SS18-SSX fusion protein creates a path to proliferation that is highly dependent on the cell of origin and its RTK expression profile, which is to date, unknown for SS. This is substantiated by transcriptional profiling of tumors generated by SS18-SSX2 expression in mice, which shows large heterogeneity between the samples (Jones et al., 2013). I attribute the uniqueness of MET staining in IHC to tissue of origin as well, since it was only present in the glandular component of biphasic SS despite the fact that both phases are thought to harbor the fusion protein (Kasai, 2000; Nishio et al., 2001).

The comparison of MET inhibition and SS18-SSX loss in SS provides one of the first insights into how aberration of BAF complex activity leads to oncogenic proliferation. Because SS has been characterized as having stem cell- like properties (Naka et al., 2010), I was not surprised to observe that differentiation pathways were being activated by both SGX-523 and SS18-SSX fusion

knockdown treatments. This was evidenced by the strong induction of cell cycle inhibitors and differentiation-associated genes. Interestingly the individual genes changed were not shared between MET inhibition and suppression of SS18-SSX, while overall pathways changed were shared, suggesting these two effectors act in parallel to drive oncogenesis. The order of these events, MET amplification and SS18-SSX expression, in SS tumor development remains to be determined.

Lastly, I was able to target MET in vivo using clinically available small-molecule inhibitors, showing that MET inhibition with the SGX-523 compound significantly attenuates the growth of biphasic SS tumors in mice. While development of this particular compound has been halted in the clinic due to unexpected renal toxicity (Infante et al., 2013), its exquisite specificity and bioavailability allowed us to showcase that MET activity was necessary for growth in vivo (Buchanan et al., 2009). For clinical purposes it would be more tractable to repurpose cabozantinib or crizotinib for a trial in biphasic SS with high levels of MET, as both have demonstrated safety and tolerability in human studies (Grüllich, 2014; Poon & Kelly, 2016). Together these findings suggest that SS is a unique and highly heterogeneous tumor type that is amenable to targeted therapeutics. CCLs have proven invaluable in the discovery of driving cancer mutations, and they can provide an accurate representation of cancer subtypes that parallels clinical data

(Wilding & Bodmer, 2014). Further studies should delineate the unique dependencies of each SS subtype. This study also underscores the power of small molecule screens in CCLs to identify pathway dependencies driven by genetic alterations.

References

Beuran, M., Negoi, I., Paun, S., Ion, A. D., Bleotu, C., Negoi, R. I., & Hostiuc, S. (2015). The epithelial to mesenchymal transition in pancreatic cancer: A systematic review. *Pancreatology : Official Journal of the International Association of Pancreatology (IAP) ... [Et Al.]*, *15* (3), 217–225. http://doi.org/10.1016/j.pan.2015.02.011

Buchanan, S. G., Hendle, J., Lee, P. S., Smith, C. R., Bounaud, P.-Y., Jessen, K. A., et al. (2009). SGX523 is an exquisitely selective, ATP-competitive inhibitor of the MET receptor tyrosine kinase with antitumor activity in vivo. *Molecular Cancer Therapeutics*, *8* (12), 3181–3190. http://doi.org/10.1158/1535-7163.MCT-09-0477

Cataisson, C., Michalowski, A. M., Shibuya, K., Ryscavage, A., Klosterman, M., Wright, L., et al. (2016). MET signaling in keratinocytes activates EGFR and initiates squamous carcinogenesis. *Science Signaling*, *9* (433), ra62–ra62. http://doi.org/10.1126/scisignal.aaf5106

Cui, J. J. (2014). Targeting receptor tyrosine kinase MET in cancer: small molecule inhibitors and clinical progress. *Journal of Medicinal Chemistry*, *57* (11), 4427–4453. http://doi.org/10.1021/jm401427c

Duan, Y., Tian, L., Gao, Q., Liang, L., Zhang, W., Yang, Y., et al. (2016). Chromatin remodeling gene ARID2 targets cyclin D1 and cyclin E1 to suppress hepatoma cell progression. *Oncotarget*, *7* (29), 45863–45875. http://doi.org/10.18632/oncotarget.10244

Gillet, J.-P., Varma, S., & Gottesman, M. M. (2013). The clinical relevance of cancer cell lines. *Journal of the National Cancer Institute*, *105* (7), 452–458. http://doi.org/10.1093/jnci/djt007

Grüllich, C. (2014). Cabozantinib: A MET, RET, and VEGFR2 Tyrosine Kinase Inhibitor. In *Small Molecules in Oncology* (Vol. 201, pp. 207–214). Berlin, Heidelberg: Springer Berlin Heidelberg. http://doi.org/10.1007/978-3-642-54490-3_12

Infante, J. R., Rugg, T., Gordon, M., Rooney, I., Rosen, L., Zeh, K., et al. (2013). Unexpected renal toxicity associated with SGX523, a small molecule inhibitor of MET. *Investigational New Drugs*, *31* (2), 363–369. http://doi.org/10.1007/s10637-012-9823-9

Jones, K. B., Su, L., Jin, H., Lenz, C., Randall, R. L., Underhill, T. M., et al. (2013). SS18-SSX2 and the mitochondrial apoptosis pathway in mouse and human synovial sarcomas. *Oncogene*, *32* (18), 2365–71– 2375.e1–5. http://doi.org/10.1038/onc.2012.247

Kadoch, C., & Crabtree, G. R. (2013). Reversible disruption of mSWI/SNF (BAF) complexes by the SS18-SSX oncogenic fusion in synovial sarcoma. *Cell*, *153* (1), 71–85. http://doi.org/10.1016/j.cell.2013.02.036

Kasai, T. (2000). Detection of SYT-SSX fusion transcripts in both epithelial and spindle cell areas of biphasic synovial sarcoma using laser capture microdissection. *Journal of Clinical …*, *53* (2), 107–110. http://doi.org/10.1136/mp.53.2.107

Kawakami, H., Okamoto, I., Arao, T., Okamoto, W., Matsumoto, K., Taniguchi, H., et al. (2013). MET amplification as a potential therapeutic target in gastric cancer. *Oncotarget*, *4* (1), 9–17. http://doi.org/10.18632/oncotarget.718

Naka, N., Takenaka, S., Araki, N., Miwa, T., Hashimoto, N., Yoshioka, K., et al. (2010). Synovial Sarcoma Is a Stem Cell Malignancy. *Stem Cells*, *28* (7), 1119–1131. http://doi.org/10.1002/stem.452

Nishio, J., Iwasaki, H., Ishiguro, M., Ohjimi, Y., Isayama, T., Naito, M., & Kikuchi, M. (2001). Identification of syt-ssx fusion transcripts in both epithelial and spindle cell components of biphasic synovial sarcoma in small tissue samples isolated by membrane-based laser microdissection. *Virchows Archiv : an International Journal of Pathology*, *439* (2), 152–157.

Poon, C. C., & Kelly, J. J. (2016). Development of crizotinib, a rationally designed tyrosine kinase inhibitor for non-small cell lung cancer. *International Journal of Cancer. Journal International Du Cancer*. http://doi.org/10.1002/ijc.30533

Sampson, V. B., Kamara, D. F., & Kolb, E. A. (2013). Xenograft and genetically engineered mouse model systems of osteosarcoma and Ewing's sarcoma: tumor models for cancer drug discovery. *Expert Opinion on Drug Discovery*, *8* (10), 1181–1189. http://doi.org/10.1517/17460441.2013.817988

Tabouret, E., Denicolai, E., Delfino, C., Graillon, T., Boucard, C., Nanni, I., et al. (2016). Changes in PlGF and MET-HGF expressions in paired initial and recurrent glioblastoma. *Journal of Neuro-Oncology*, *130* (3), 431–437. http://doi.org/10.1007/s11060-016-2251-5

Wilding, J. L., & Bodmer, W. F. (2014). Cancer cell lines for drug discovery and development. *Cancer Research*, *74* (9), 2377–2384. http://doi.org/10.1158/0008-5472.CAN-13-2971

Wöhrle, S., Weiss, A., Ito, M., Kauffmann, A., Murakami, M., Jagani, Z., et al. (2013). Fibroblast Growth Factor Receptors as Novel Therapeutic Targets in SNF5-Deleted Malignant Rhabdoid Tumors. *PloS One*, *8* (10), e77652. http://doi.org/10.1371/journal.pone.0077652

Xie, Z., Lee, Y. H., Boeke, M., Jilaveanu, L. B., Liu, Z., Bottaro, D. P., et al. (2016). MET Inhibition in Clear Cell Renal Cell Carcinoma. *Journal of Cancer*, *7* (10), 1205–1214. http://doi.org/10.7150/jca.14604

Chapter 4: Screen for Protein Stabilizers of BAF47

All work, analysis, and interpretation was performed by Enrique Miguel García-Rivera except for the following experiments. Original concept and development of BAF47 fused to Luciferase as a reporter, including verification of response to loss of SS18-SSX1, was performed by Dr. Cigall Kadoch. Protease activity profiling of BRD1732 was performed by BPS Biosciences.

Chapter 4.1: Introduction

The tumor suppressor BAF47 is implicated in the proliferation of various cancers, including malignant rhabdoid tumors and Synovial Sarcomas (Ito, Asano, Kawai, & Yoshida, 2016; Roberts, Leroux, Fleming, & Orkin, 2002). Re-expression of BAF47 in these cancers leads to cell-cycle arrest (Betz, Strobeck, Reisman, Knudsen, & Weissman, 2002), suggesting that restoring BAF47 functionality would be sufficient to treat these cancers. Some cancers like MRT have genetically lost BAF47 through biallelic inactivation, and treating these would require more complex gene therapy. SS on the other hand is a unique case where BAF47 is still expressed following oncogenesis and is only suppressed at the protein level. Overexpression of BAF47 is not sufficient in these cells due to the dominant-negative phenotype of the SS18-SSX, which displaces BAF47 from the BAF complex, causing its proteasomal degradation (Kadoch & Crabtree, 2013).

It naturally followed then that a therapeutic that could prevent the function of SS18-SSX would also cause the restoration of BAF47 protein levels, and this was validated through knockdown of fusion protein expression (Kadoch & Crabtree, 2013). I thus designed a cellular system to monitor BAF47 protein levels, with the goal of identifying small molecules that could stabilize its protein

levels, hypothesizing that some of these could act through direct inhibition of SS18-SSX function.

Chapter 4.2: Generating a Reporter of BAF47 Protein Levels

BAF47 is mostly a nuclear protein whose protein levels are largely suppressed in a SS background. To monitor these levels I designed a luciferase reporter system by fusing BAF47 at its C-terminus to NanoLuc. NanoLuc is a small (19 kDa) and extremely bright luciferase, with a high emission intensity and a relatively narrow spectrum (460nm peak), used extensively as a tool for monitoring protein dynamics (Machleidt et al., 2015). This reporter was introduced into the SS cell line Yamato through lentiviral delivery of the construct. Expression of BAF47-NanoLuc (BAF47-NL) had no impact on the proliferation of these cells. In addition, fusion of BAF47 to luciferase did not inhibit its ability to bind the BAF complex and more importantly it responded to loss of SS18-SSX1 (**Figure 4.1)**.

A

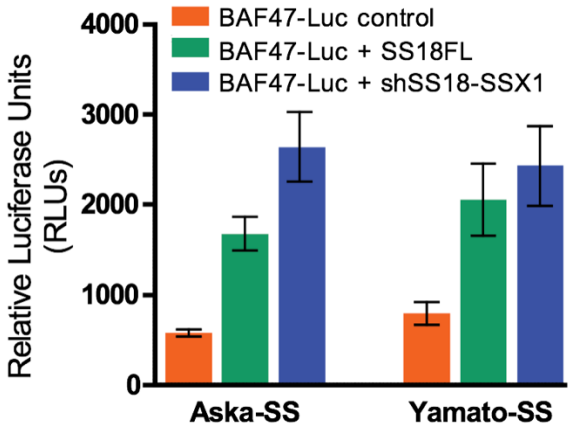


Figure 4.1. BAF47 protein levels can be monitored using luciferase. (A) BAF47-Luciferase protein levels following expression of SS18 or loss of SS18-SSX1 in two synovial sarcoma cell lines: Aska and Yamato. Expression of SS18 and knockdown of SS18-SSX1 were induced with Dox for 3 days, and luciferase signal was measured with the Steady-Glo® reagent. Adapted from work performed by Dr. Cigall Kadoch (unpublished).

Chapter 4.3: Screen of a Performance-Diverse Library of Small Molecules

Using the BAF47-NL reporter I screened a small molecule library of ~3,000 small molecules (**Figure 4.3A**). This unique library was designed on the basis of biological assay performance diversity, and this screen is one of its first applications. Compounds for this collections were selected based on their

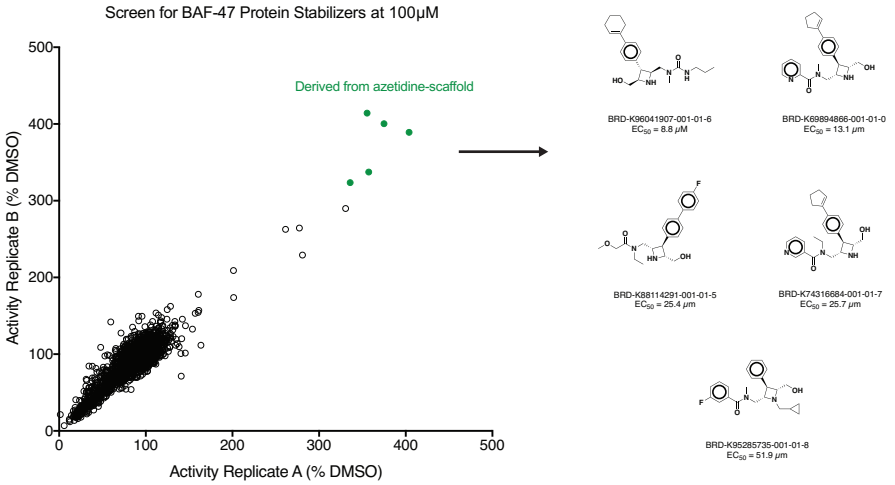
performance in two key assays: high-dimensional image-based cell morphology and gene expression profiles (Wawer et al., 2014). This selection process provides a more diverse set of assay performances than a comparable library built solely on chemical structure diversity (Wawer et al., 2014). This screen yielded 9 compounds that could increase BAF47-NL protein levels more than 2.5-fold when compared to vehicle (**Figure 4.2A, left**). 3 of these compounds were known HDAC inhibitors, while the other 5 were derived from the same chemical scaffold based on an azetidine-ring (**Figure 4.2A, right**). These 5 compounds had not been described as hits before in most of the screens either performed within our group or published in PubChem (**Figure 4.2B**).

While the most potent compound in the screen had significant activity (EC_{50} of 8.8μM in the BAF47-NL assay), I proceeded to coordinate a medicinal chemistry effort to both understand the structure-activity relationships (SAR) in this series as well as identify more potent compounds. After analyzing 1- (((2S,3R,4R)-3- (4- (cyclopent-1-en-1-yl)phenyl)-4- (hydroxymethyl)azetidin-2-yl)methyl)-1-methyl-3-propylurea (BRD1907) and other hit compounds (**Figure 4.2A, right**), I suspected that the cyclopentenyl and urea motifs could be modified to increase potency. For example, changing the urea to a pyridylamide such as N- (((2S,3R,4R)-3- (4- (cyclopent-1-en-1-yl)phenyl)-4- (hydroxymethyl)azetidin-2-yl)methyl)-N-methylpicolinamide (BRD4866) resulted in a loss of potency, and a

medicinal chemistry campaign demonstrated that the unprotected amino alcohol and the N-methyl amide were critical for activity. Ultimately, I decided to move away from unconventional functional groups such as the cyclopentene and settled on N- (((2S,3R,4R)-3- ([1,1'-biphenyl]-4-yl)-4- (hydroxymethyl)azetidin-2-yl)methyl)-3-fluoro-N-methylbenzamide (BRD1732), which had an EC_{50} of 1.5 μM (**Figure 4.3B**).

BRD1732 had significant potency and could increase BAF47-NL levels up to 4-fold, even higher than the canonical proteasome inhibitor MG132 (**Figure 4.3C, left**). Even though MG132 does not have robust specificity as it is known to inhibit some cathepsins, I chose to compare BRD1732 to it due to their similar potency in cells when it came to BAF47 stabilization. I validated the luciferase results using immunofluorescence and this recapitulated what I had seen with the high-throughput assay (**Figure 4.2C**). This increase in protein levels can also be seen using immunoblotting, with BRD1732 showing increases of BAF47-NL at the 1.25μM dose in the Yamato cell line (**Figure 4.3C, right**). As measure of selectivity I profiled the activity of BRD1732 against 36 other proteases in vitro, including USPs, caspases and cathepsins, and saw no activity at 25μM (**Figure 4.4A**).

A



B

Compound	Activity in Broad Assays	Activity in Pubchem Asssays	Promiscuity Probability
BRD-K96041907-001-01-6	0	11	0.042
BRD-K69894866-001-01-0	1	2	0.005
BRD-K88114291-001-01-5	1	0	0.005
BRD-K74316684-001-01-7	1	0	0.005
BRD-K95285735-001-01-8	0	0	0

C

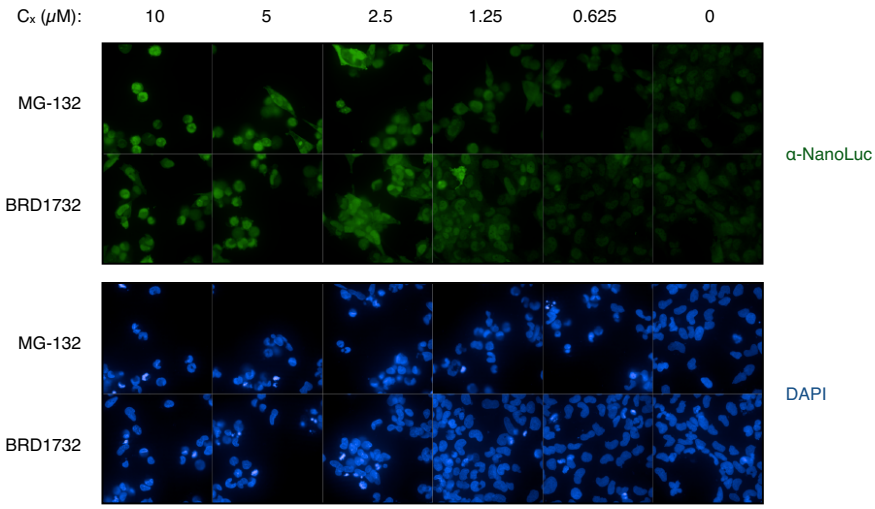


Figure 4.2. HTS identifies small molecules that can increase the protein levels of BAF47 in cells. (A) Scatter plot of HTS results performed in duplicate following 48 hour treatment with 100μM of each compound.

Figure 4.2 (Continued). Highlighted in green are 5 HTS hits that are derived from the same chemical scaffold. These hits were repeated in dose to obtain its EC50 value. (B) Activity of the aforementioned 5 hits in previous assays performed at the Broad Institute and reported in PubChem. Promiscuity Probability is the probability the compound would score as active in at least 25% of all screens, and it was calculated based on proportion of screens it was active in. (C) Immunofluorescence for the reporter protein using anti-NanoLuc and DAPI nuclear stain following 24 hours of treatment with MG132 or BRD1732.

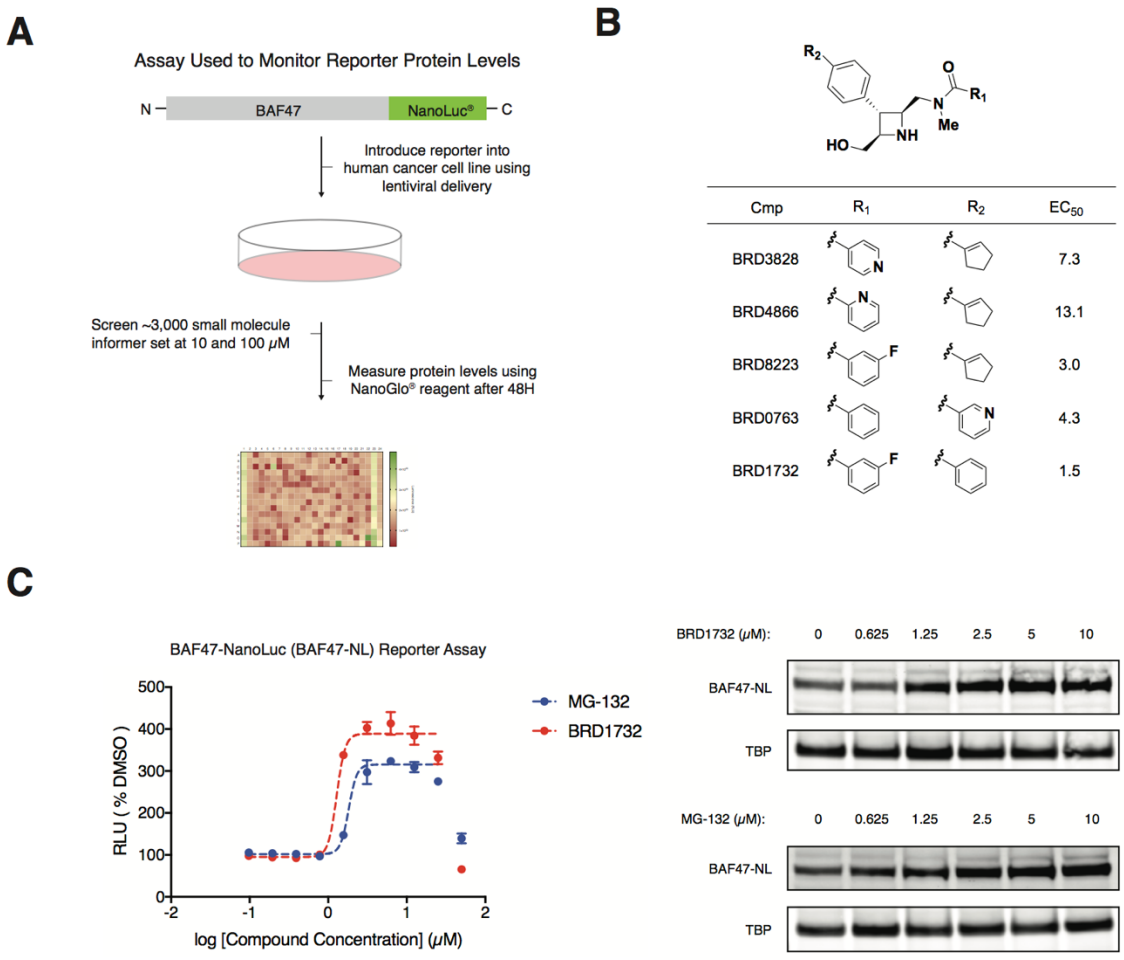


Figure 4.3. BRD1732 is a small-molecule that prevents the degradation of BAF47. (A) Outline of performed high-throughput screen for BAF47-NanoLuc (BAF47-NL) protein stabilizers. (B) Medicinal chemistry results for BRD1732. (C) Dose-response curve for BRD1732 in the BAF47-NL assay (left) compared to MG132, a compound known to increase the protein levels of BAF47. (right) Whole-cell lysate immunoblot of Yamato for the reporter protein BAF47-NL and TBP.

A

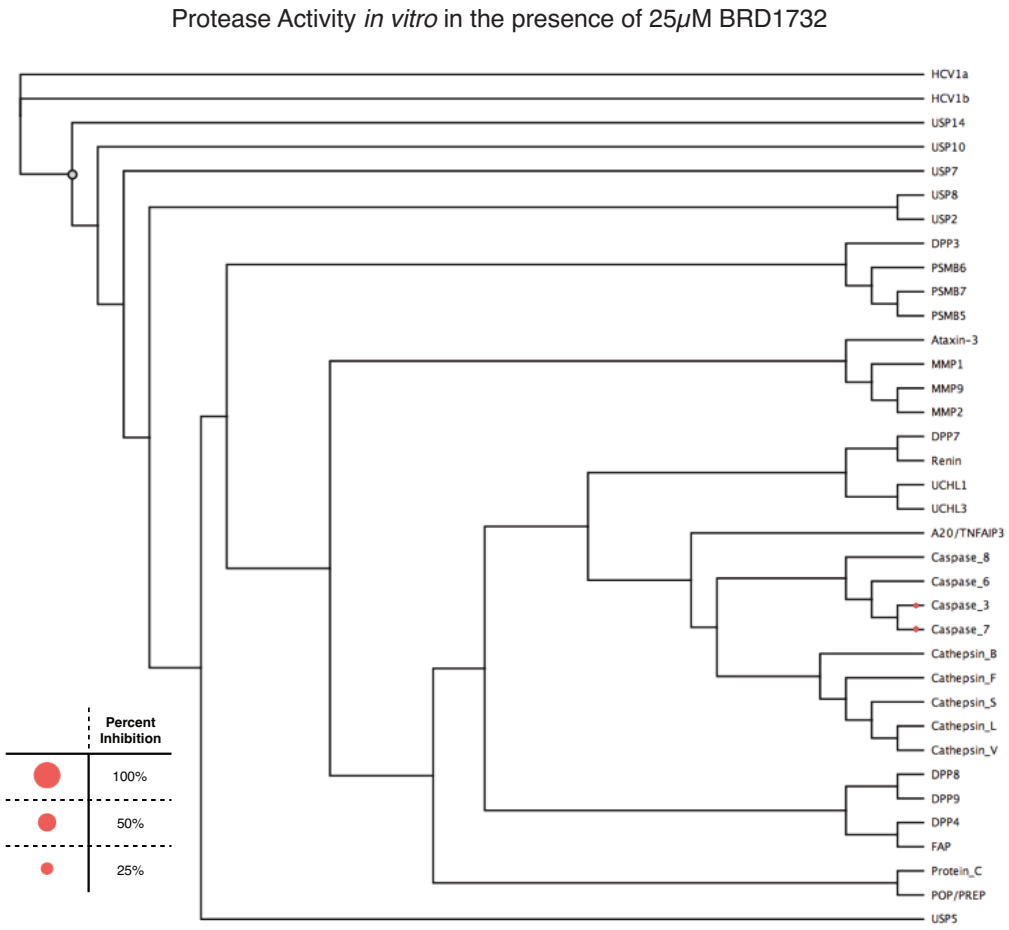


Figure 4.4. BRD1732 is not active in a panel of 36 proteases. (A) Phylogenetic tree for the 36 proteases tested in vitro for inhibitory activity, with percent inhibition observed with BRD1732 at 25μM overlaid.

A

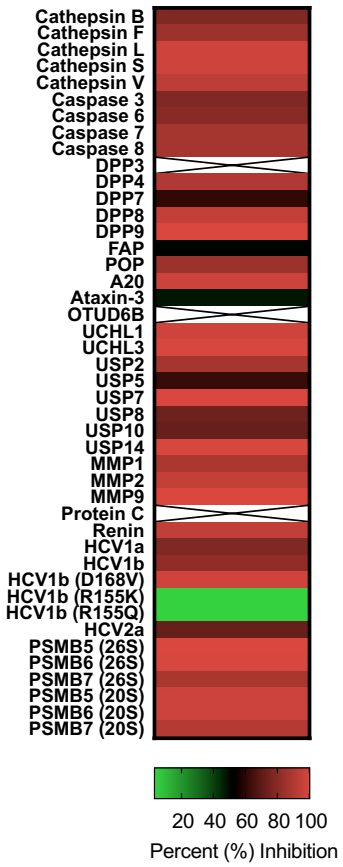


Figure 4.5. Positive Controls for Protease Panel. (A) Percentage inhibition of protease activity for 36 proteases (as in Figure 4.4) following treatment with positive controls. If available, each protease was treated with known inhibitors of their activity.

Chapter 4.4: Methods

Chapter 4.4.1: Reporter Construct Generation

DNA containing the coding-domain sequence for BAF47 Isoform A (RefSeq: NP_003064.2) was amplified from 293T cDNA and ligated to NanoLuc® (Promega) at the C-terminus of BAF47, to generate BAF47-NanoLuc, using the In-Fusion HD Cloning Kit (Takara Bio). Colonies were screened using PCR with Phusion HF DNA Polymerase (New-England Biolabs) and primers for the N- and C-terminus of BAF47 and NanoLuc, respectively. Positive colonies were isolated, expanded, and DNA was purified using Plasmid Maxiprep Kits (Qiagen). Resulting constructs were validated for integrity using Sanger DNA Sequencing (Genewiz).

Chapter 4.4.2: Cell Culture and Lentiviral Production

Cells were grown in DMEM cell culture media (DMEM (Gibco) supplemented with 10% heat-inactivated FBS (Omega Scientific), 1mM Sodium Pyruvate (Gibco), and 1mg/mL Penicillin-Streptomycin (Gibco)) and allowed to reach confluency before transfection. Lentivirus was prepared in 293T cells by transfecting the cells with lentivirus packaging plasmids in conjuction with the

BAF47-NL construct. Cells were grown for an additional 3 days, and resulting virus was isolated from the supernatant via 0.22μM filtration (Corning). Lentivirus was added to Yamato cells at 75% confluency and allowed to grow for 2 days before removing virus and adding blastomycin selection agent at 1 μg/mL. Expression of BAF47-NL was confirmed through immunoblotting.

Chapter 4.4.3: Phenotypic Screening

Yamato cells containing BAF47-NL were plated on white 384-well plates (Corning) at a density of 0.2 x 10^6 cells / mL in 50μL of media (10,000 cells per well) and allowed to grow for 24 hours. Volume transfer was performed using a 0.5μL of compound from the Performance-Diverse Library was then added with a pinning tool (CyBio Vario) to each well and cells were incubated for another 48 hours. To read protein levels 25μL of Nano-Glo® reagent (Promega) was added to each well, incubated for 10 minutes, and luminescence measured in an Envision Multilabel Plate Reader (Perkin Elmer).

Chapter 4.4.4: Immunofluorescence

Yamato cells containing BAF47-NL were plated on black transparent-bottom 384-well plates (Corning) at a density of 0.4 x 10^6 cells / mL in 50μL of media

(20,000 cells per well) and allowed to grow for 24 hours. Cells were fixed by adding para-formaldehyde (ThermoFisher) into the media to a final concentration of 4% and incubating for 10 minutes at 37ºC. Media was removed and cells were washed with PBS. Staining was performed using an anti-NanoLuc antibody generously provided by Promega at a concentration of 0.01 mg/mL overnight at 4ºC, and nuclear staining was achieved with DAPI before imaging in an Opera Phenix High Content confocal-microscope (Perkin Elmer).

Chapter 4.4.5: Immunoblotting

Cells were pelleted and 100μL of lysis buffer (10mM Tris-HCl pH 8.0, 1mM EDTA, 1% Triton X-100, 0.1% sodium deoxycholate, 0.1% SDS, and 150mM NaCl + cOmplete Protease Inhibitors (Roche) + PhosSTOP (Roche)) was added to 2 x 10^6 cells, incubated on ice for 30 min and cleared in a micro-centrifuge (17,000xg for 15 min). 30μg of the supernatant was separated using gel electrophoresis, transferred into a PVDF membrane (Millipore), blotted for the target protein and analyzed using an IR imaging system (LI-COR Odyssey CLx).

Chapter 4.4.6: Protease Profiling

Characterization of BRD1732 activity against 36 different proteases was performed by BPS Bioscience at a single concentration of 25μM.

Chapter 4.4: Conclusions

In an effort to identify compounds that could become therapeutics for SS I designed a phenotypic screen to monitor the protein levels of tumor suppressor BAF47. This reporter responded strongly to loss of SS18-SSX and proteasome inhibition, with a dynamic range and Z' (>0.5) suitable for high-throughput screening. The original hypothesis was that small molecule inhibition of SS18-SSX activity would lead to protein level increases of BAF47. This approach has one major caveat: protein stabilization alone is not sufficient to induce toxicity in SS (Kadoch & Crabtree, 2013), hence hits from the assay that prevent the degradation of BAF47 would not immediately translate to a SS therapeutic. Nonetheless, these compounds could serve as tools to understand the protein homeostasis of BAF subunits, a largely unexplored field.

Screening of the unique performance-diverse library yielded a collection of 9 hits that could stabilize BAF47-NL more than 2.5-fold over DMSO, a significant

increase that resembles proteasome inhibition. I de-prioritized 4 of these 9 hits because they were known HDAC inhibitors, particularly HDAC1 and HDAC2. While I consider these hits worthy of further study, I prioritized others hits based on the potential novelty of their MOA. The 5 hits from the azetidine-scaffold series contained potent compounds, with EC_{50} as low as 8.8μM. A medicinal chemistry campaign succeeded in increasing this potency to 1.5μM with BRD1732, the lead compound resulting from this screen.

None of the azetidine-derived compounds exhibited promiscuous activity in screens performed at the Broad, and a panel of 36 proteases tested in vitro yielded no activity for BRD1732. These results warranted further investigation into the mechanism of action of BRD1732, specifically on how it is able to increase the protein levels of BAF47.

References

Betz, B. L., Strobeck, M. W., Reisman, D. N., Knudsen, E. S., & Weissman, B. E. (2002). Re-expression of hSNF5/INI1/BAF47 in pediatric tumor cells leads to G1 arrest associated with induction of p16ink4a and activation of RB. *Oncogene*, *21* (34), 5193–5203. http://doi.org/10.1038/sj.onc.1205706

Ito, J., Asano, N., Kawai, A., & Yoshida, A. (2016). The diagnostic utility of reduced immunohistochemical expression of SMARCB1 in synovial sarcomas: a validation study. *Human Pathology*, *47* (1), 32–37.

http://doi.org/10.1016/j.humpath.2015.09.010

Kadoch, C., & Crabtree, G. R. (2013). Reversible disruption of mSWI/SNF (BAF) complexes by the SS18-SSX oncogenic fusion in synovial sarcoma. *Cell*, *153* (1), 71–85. http://doi.org/10.1016/j.cell.2013.02.036

Machleidt, T., Woodroofe, C. C., Schwinn, M. K., Méndez, J., Robers, M. B., Zimmerman, K., et al. (2015). NanoBRET--A Novel BRET Platform for the Analysis of Protein-Protein Interactions. *ACS Chemical Biology*, *10* (8), 1797–1804. http://doi.org/10.1021/acschembio.5b00143

Roberts, C. W. M., Leroux, M. M., Fleming, M. D., & Orkin, S. H. (2002). Highly penetrant, rapid tumorigenesis through conditional inversion of the tumor suppressor gene Snf5. *Cancer Cell*, *2* (5), 415–425.

Wawer, M. J., Li, K., Gustafsdottir, S. M., Ljosa, V., Bodycombe, N. E., Marton, M. A., et al. (2014). Toward performance-diverse small-molecule libraries for cell-based phenotypic screening using multiplexed high-dimensional profiling. *Proceedings of the National Academy of Sciences of the United States of America*, *111* (30), 10911–10916. http://doi.org/10.1073/pnas.1410933111

Chapter 5: BRD1732 is a Chemical Probe of the Ubiquitin-Proteasome System

All work, analysis, and interpretation was performed by Enrique Miguel García-Rivera except for the following experiments. Medicinal chemistry and all compound syntheses were performed by Micah Maetani. Connectivity Map of BRD1732 (by L1000) was performed by the Broad's Cancer Program. TMT® mass spectrometry was performed by Dr. Joel Chick. Viability effects of BRD1732 on bortezomib-resistant cancer cell lines were measured by Dr. Geoffrey Matthews. Generation of KP-4 cells with Cas9 and genome-wide CRIPSR guides was performed by Matthew Ryan, and genomic DNA isolation was performed by Dr. Shubroz Gill.

Chapter 5.1: Introduction

Given the potent effect BRD1732 had on BAF47-NL protein levels I set out to identify its MOA. Because I used the Performance-Diverse Library for the screen, I was able to access rich biological assay annotations for the five hits derived from the azetidine-scaffold. This included morphological and transcriptional profiles related to compound treatment (Wawer et al., 2014). Having these sorts of annotations dramatically reduced the time to hypothesis in terms of MOA for BRD1732, narrowing it down to a single biological pathway. By comparing these annotations across different small molecule treatments (with known MOA), one can get a connectivity map that could hint at a compound's mechanism (Lamb et al., 2006).

Interrogation of BRD1732's cellular activity was performed in human cell lines, including cancer cell lines and non-diseased fibroblasts. It had a potent phenotype that was indicative of perturbation of the ubiquitin-proteasome system. This pathway is the major mechanism by which cells degrade proteins, and has proven instrumental in the treatment of diseases that are dependent on protein turnover (e.g. multiple myeloma) (Manasanch & Orlowski, 2017). The activity of BRD1732 was starkly different than canonical proteasome inhibition, suggesting

a novel MOA that could further expand our understanding of the ubiquitin-proteasome system in disease.

Chapter 5.2: BRD1732 Disrupts the Ubiquitin-Proteasome System

To understand the MOA of BRD1732 I first looked at the biological annotation data that was available from the Performance-Diverse Library. These annotations of gene expression profiles are compared to other perturbations performed at the Broad, with the goal of determining which other perturbations (including small molecule treatment, gene knockdown, and gene overexpression) can induce a transcriptional profile that is similar to BRD1732. Surprisingly, the majority of perturbations that connected to BRD1732 were related to the ubiquitin-proteasome pathway (**Table 5.1**). Several said knockdown connections were proteasome subunits, i.e. loss of these subunits causes transcriptional changes that are similar to BRD1732 treatment (**Figure 5.1A**).

Table 5.1. Results of BRD1732 Connectivity Map. (A-C) Top 20 perturbations found to connect strongly with BRD1732 treatment. These set of perturbations include compound treatments (A), transcriptional knockdown (B), and gene overexpression (C).

A

pert_id	pert_iname	pert_type	average
BRD-K88510285	bortezomib	compound	99.4
BRD-K15935639	z-leu3-VS	compound	99.2
BRD-K78659596	MLN-2238	compound	99.1
BRD-K74402642	NSC-632839	compound	98.5
BRD-K60230970	MG-132	compound	98.1
BRD-K60870698	BRD-K60870698	compound	97.7
BRD-K36007650	puromycin	compound	97.3
BRD-K92317137	BRD-K92317137	compound	97.3
BRD-A55484088	BNTX	compound	96.6
BRD-K50234570	EMF-bca1-16	compound	96.4
BRD-K78599730	manumycin-a	compound	96.1
BRD-K13169950	NSC-3852	compound	96.0
BRD-A20697603	thiostrepton	compound	95.9
BRD-K02130563	panobinostat	compound	95.8
BRD-K06765193	BRD-K06765193	compound	95.7
BRD-K86472598	MD-II-051	compound	95.5
BRD-A68065211	BRD-A68065211	compound	95.5
BRD-A28970875	puromycin	compound	95.3
BRD-K42308740	ST-056792	compound	95.1
BRD-K04853698	LDN-193189	compound	95.0

B

pert_id	pert_iname	pert_type	average
CGS001-5690	PSMB2	shRNA	98.0
CGS001-5682	PSMA1	shRNA	97.9
CGS001-5707	PSMD1	shRNA	97.4
CGS001-4817	NIT1	shRNA	96.8
CGS001-7316	UBC	shRNA	96.1
CGS001-1054	CEBPG	shRNA	95.9
CGS001-8607	RUVBL1	shRNA	94.6
CGS001-5709	PSMD3	shRNA	94.2
CGS001-51160	VPS28	shRNA	94.1
CGS001-29978	UBQLN2	shRNA	94.0
CGS001-5684	PSMA3	shRNA	94.0
CGS001-4172	MCM3	shRNA	93.9
CGS001-10450	PPIE	shRNA	93.5
CGS001-670	BPHL	shRNA	92.9
CGS001-5689	PSMB1	shRNA	92.7
CGS001-26039	SS18L1	shRNA	92.5
CGS001-641	BLM	shRNA	92.3
CGS001-9146	HGS	shRNA	91.7
CGS001-5695	PSMB7	shRNA	90.5
CGS001-10972	TMED10	shRNA	90.3

C

pert_id	pert_iname	pert_type	average
ccsbBroad304_01388	RELB	overexpression	95.1
ccsbBroad304_05982	CDX2	overexpression	93.6
ccsbBroad304_02451	HOXB13	overexpression	93.1
ccsbBroad304_09396	TIRAP	overexpression	92.6
ccsbBroad304_05098	MAGEB6	overexpression	92.5
ccsbBroad304_02048	BCL10	overexpression	92.1
ccsbBroad304_01710	TRAF2	overexpression	91.5
ccsbBroad304_06038	CRK	overexpression	89.9
ccsbBroad304_00763	HNF4A	overexpression	89.6
ccsbBroad304_02012	FADD	overexpression	89.3
ccsbBroad304_00348	MAP3K8	overexpression	88.8
ccsbBroad304_06260	GATA3	overexpression	87.9
ccsbBroad304_03441	UGT1A9	overexpression	87.6
ccsbBroad304_06648	CNOT3	overexpression	87.4
ccsbBroad304_04780	GPR139	overexpression	86.7
ccsbBroad304_00259	CD40	overexpression	86.1
ccsbBroad304_06318	GPER	overexpression	84.3
ccsbBroad304_00954	LYN	overexpression	84.0
ccsbBroad304_02691	PUF60	overexpression	84.0
ccsbBroad304_01688	TNFRSF1A	overexpression	83.8

Because the screen identified compounds that prevent the degradation of a protein, it was not unreasonable to explore whether BRD1732 could inhibit the ubiquitin-proteasome system. One of the hallmarks of proteasome inhibition is the accumulation of poly-ubiquitinated proteins. In contrast to MG132 treatment, BRD1732 induced a massive accumulation of free ubiquitin, including free ubiquitin chains (**Figure 5.1B**). This free ubiquitin accumulation occurred simultaneously with the increase of BAF47-NL, suggesting it is linked to the MOA of the compound and not an off-target effect (**Figure 5.1C**). Furthermore it is a rapid phenotype, with free ubiquitin accumulating within an hour of treatment with BRD1732 (**Figure 5.1D**). I validated the observed increase in free ubiquitin with BRD1732 treatment in an alternative cancer cell line (293T) and saw the same phenotype (**Figure 5.2A**).

Despite the deviation from canonical proteasome inhibition I still suspected BRD1732 could be inhibiting proteasome activity. Using human purified proteasome particles, both 20S and 26S, I measured the catalytic activity of the proteasome using fluorescent peptide substrates over time, and saw no impact from the addition of BRD1732 (**Figure 5.1E**). This included all three major catalytic activities of the proteasome: chymotrypsin-line, trypsin-like, and caspase-like. Given this result it is unlikely that BRD1732 binds that catalytic active site of the proteasome. Further phenotypical characterization showed that

BRD1732 inhibited the unfolded-protein response (UPR). Canonical proteasome inhibition by MG132 leads to a steady induction of XBP1, the major regulator of the UPR. Upon accumulation of unfolded proteins XBP1 is spliced by the ER-bound IRE1 enzyme into its active form as a transcription factor (Poothong, Tirasophon, & Kaufman, 2017). BRD1732, again in contrast to MG132, does not induce XBP1 expression or splicing (**Figure 5.1F**). I extended this further by actively inducing the UPR with tunicamycin, an inhibitor of protein glycosylation that causes the accumulation of unfolded proteins (Lumley et al., 2017). With the co-treatment of BRD1732 and tunicamycin there was attenuated XBP1 splicing but similar expression of the chaperone BiP when compared to tunicamycin alone (**Figure 5.1G**).

Other cellular responses were similar to proteasome inhibition, complicating the interpretation of BRD1732's MOA. One feature of proteasome disruption is the depletion of ubiquitin from the nucleus, frequently found covalently bound to various histones (Dantuma, Groothuis, Salomons, & Neefjes, 2006). Interestingly BRD1732 was able to deplete ubiquitination at histone H2A residue K119, with more potency than MG132, suggesting the cell is responding in a manner that mimics loss of ubiquitin outside of the nucleus (**Figure 5.1H**). Similar to nuclear ubiquitin depletion, inhibition of NFκB signaling is a hallmark of proteasome inhibition, with the inhibitor of NFκB (IkB) being a canonical substrate of the

proteasome (Shah et al., 2001). In a luciferase reporter assay, where an NFκB response element was fused to NanoLuc®, BRD1732 inhibited signaling following induction of NFκB with recombinant TNF-α (**Figure 5.1I**).

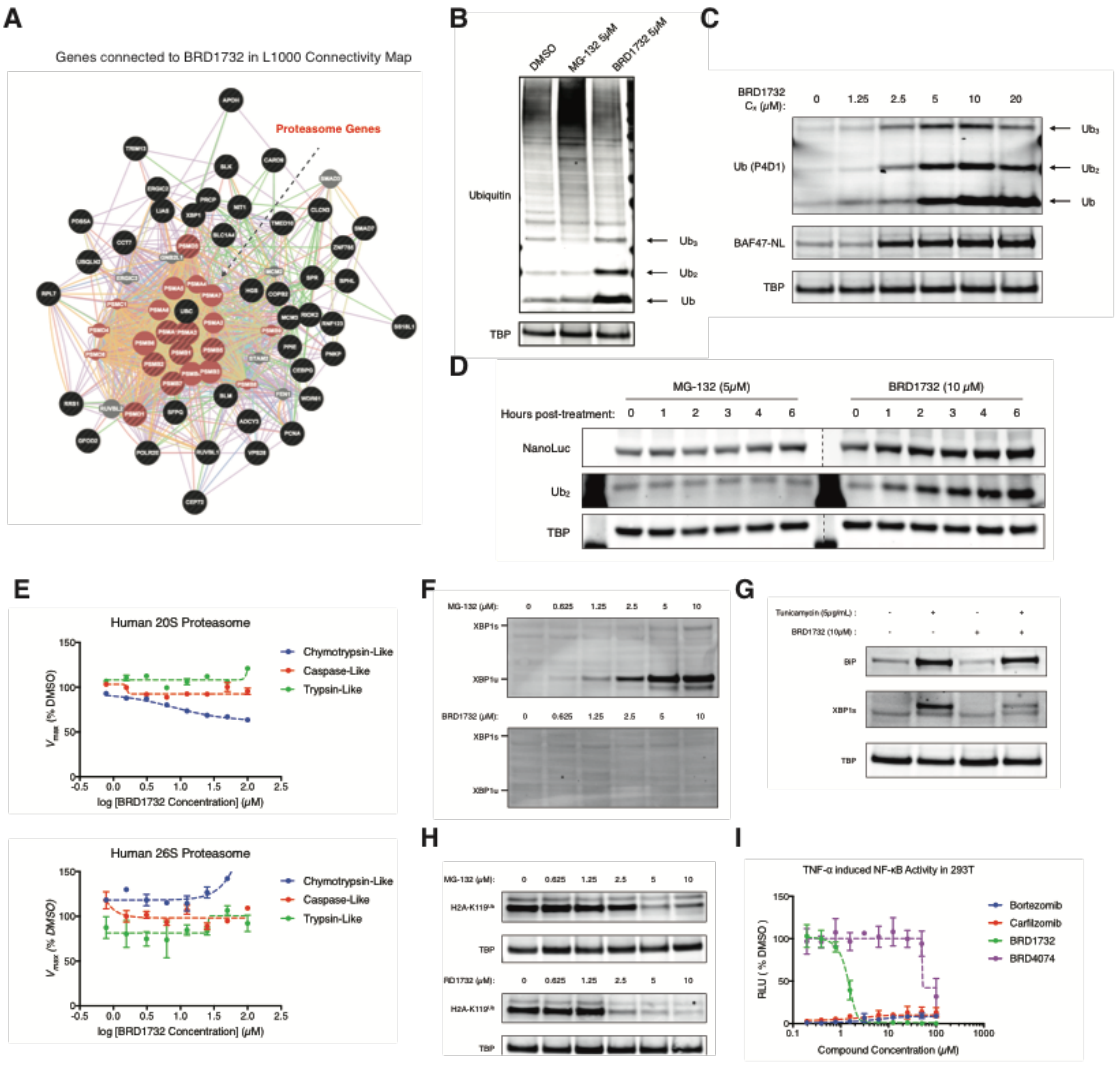


Figure 5.1. BRD1732 disrupts proteasome-regulated pathways without inhibiting the Human proteasome. (A) Connectivity Map for BRD1732 highlighting a strong connection between the compound and knockdown of proteasomal subunits. (B) Whole-cell immunoblot of Yamato for Ubiquitin following compound treatment for 24 hours. (C) Same as in (B) but performed in dose for BRD1732 and blotted for BAF47-NL.

Figure 5.1 (Continued). (D) Immunoblot for BAF47-NL and Ubiquitin of whole-cell lysate from Yamato cells treated at different time points with MG132 or BRD1732. (E) In vitro activity of human purified 20S and 26S proteasome particles using fluorescent peptides. (F) Immunoblot for XBP1 of whole-cell lysates from Yamato cells treated with compound for 48 hours. (G) Immunoblot for BiP and XBP1 of whole-cell lysates from Yamato treated concomitantly with Tunicamycin and BRD1732 or vehicle for 48 hours. (H) Immunoblot for H2A-K119Ub of whole-cell lysates from Yamato cells treated with compound for 48 hours. (I) Activity of compounds in luciferase-based reporter assay for NFκB activity following stimulation of NFκB with recombinant TNF-α.

One compound that counteracts protein degradation is cycloheximide, a known inhibitor of protein translation that prevents protein synthesis through inhibition of peptide elongation and release in the ribosome (Roy & Wonderlin, 2003). Co-treatment with cycloheximide completely blocked BRD1732's activity, including loss of free ubiquitin increase and BAF47-NL stabilization (**Figure 5.2B**). As expected cycloheximide blocked the accumulation of poly-ubiquitinated substrates with MG132 treatment in the same setting.

In concordance with the results from human purified proteasome activity, I tested the proteasome activity in cell lysates that were treated with BRD1732 and saw no inhibition of the chymotrypsin-like activity (**Figure 5.2C**). Furthermore, BRD1732 failed to induce the formation of aggresomes at doses where BAF47-NL is significantly stabilized, suggesting the proteotoxic stress caused by BRD1732 is significantly lesser than MG132 (**Figure 5.2D**).

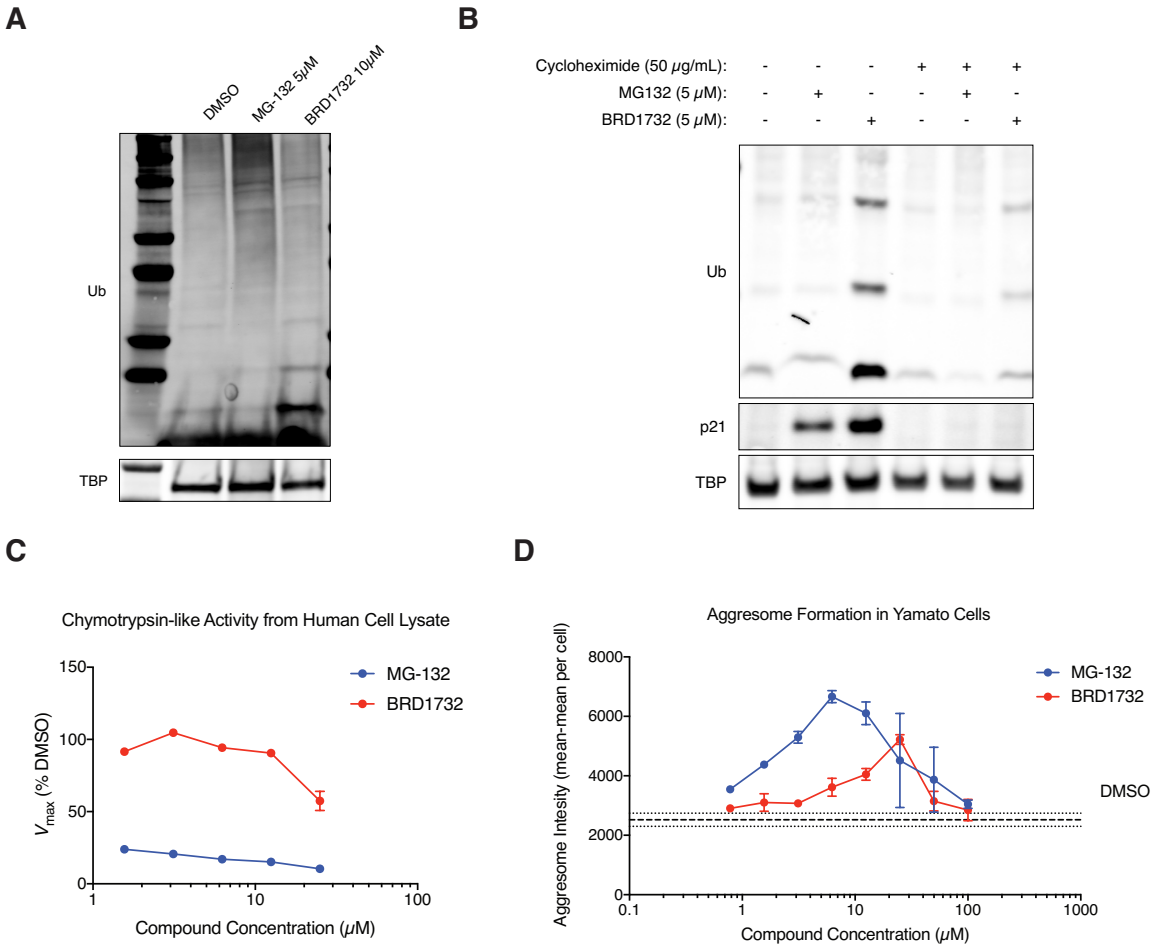


Figure 5.2. BRD1732 perturbs the ubiquitin-proteasome pathway. (A) Whole-cell immunoblot for ubiquitin and TBP from 293T cells following 48 hour treatment with MG132 or BRD1732. (B) Whole-cell immunoblot for ubiquitin, p21, and TBP from Yamato cells treated first with cyclohexime or vehicle for 24 hours, after which MG132 or BRD1732 was added for an additional 24 hours. (C) Chymotrypsin-like activity in lysates from Yamato cells treated with BRD1732 or MG132 for 24 hours, measured using fluorescent peptides.

Figure 5.2 (Continued). (D) Aggresome formation measured in Yamato cells treated with compound for 48 hours, measured using a protein-aggregate specific dye and fluorescence microscopy.

Further reaffirming that BRD1732 does not inhibit the proteasome (at least completely), pulse-chase experiments showed poor inhibition of total protein breakdown in cells. This assay consists of first pulsing with radio-labeled phenylalanine, chasing with unlabeled phenylalanine, and monitoring the radioactivity in the supernatant with and without compound treatment over time. As expected, MG132 caused a significant reduction in the percentage of protein breakdown (radioactivity in media relative to radioactivity in cells) when compared to vehicle, whereas BRD1732 had little impact (**Figure 5.3A-B**).

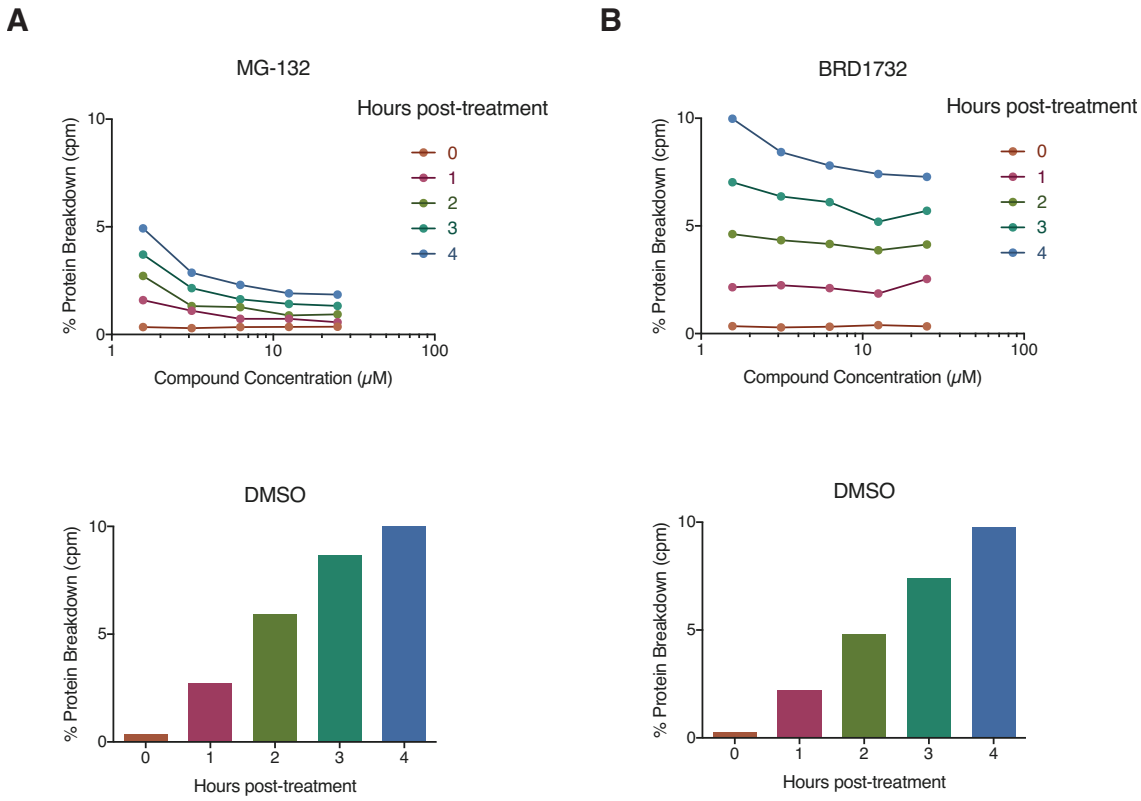


Figure 5.3. BRD1732 does not significantly inhibit total protein breakdown in cells. (A) Protein breakdown in Yamato cells measured using a pulse-chase with phenylalanine, L-[2,3,4,5,6-^{3}H]. Percentage of protein breakdown (cpm in media over cpm in cells) after treatment with MG132 for different time lengths (top). Expected protein breakdown for vehicle control is also shown (bottom). (B) Same as in (A) but with BRD1732.

Chapter 5.3: BRD1732 does not Prevent *in vitro* Ubiquitin Ligation

Because BRD1732 causes such a dramatic increase in free ubiquitin, I tested its ability to inhibit ubiquitin ligation in vitro. First I used a HeLa S100 cytoplasmic extract which contains all proteins necessary to ubiquitinate substrate present in the exctract it self. This was performed in a proteasome-null background (with MG132) to enhance the signal from ubiquitin ligation. In this setting BRD1732 had no impact on protein ubiquitination, both globally or K48- and K63-linkage types (**Figure 5.4A**). I also tested the activity of BRD1732 against recombinant ubiquitin ligases, including the major human E1 and 26 E2 enzymes. This assay allows for monitoring of E1 activity by detecting ubiquitin loading into E2 enzymes, and E2 activity by monitoring auto-ubiquitin loading by the E2. None of the enzymes tested were inhibited by BRD1732, and both E1 loading and E2 auto-ubiquitin loading were unperturbed (**Figure 5.4B**).

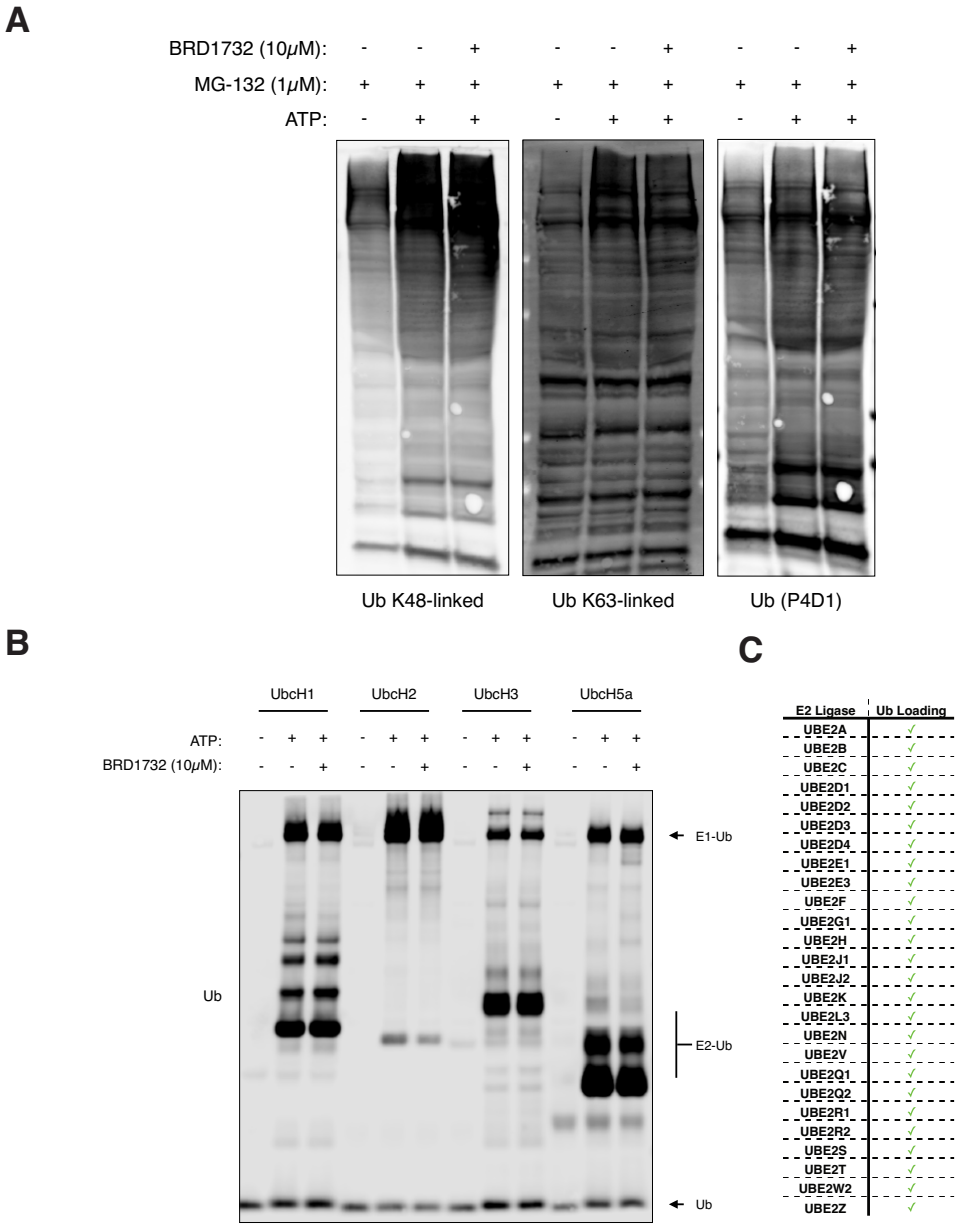


Figure 5.4. BRD1732 does not inhibit ubiquitin ligase activity in vitro. (A) Immunoblot for Ubiquitin of HeLa S100 fraction following addition of ATP and Ubiquitin, in combination with BRD1732.

Figure 5.4 (Continued). (B) Recombinant E2 auto-ubiquitination was performed in vitro in the presence of recombinant E1, biotinylated-Ub and BRD1732. Reaction products were visualized following PAGE using Streptavidin-IR. (C) Results of same assay shown in (B) in the presence of BRD1732 at 10μM for various E2 ligases.

Chapter 5.4: BRD1732 Induces Transcriptional and Proteome-wide Changes that are Distinct from Proteasome Inhibition

In the previous results it is clear that BRD1732 has a unique MOA, with both similarities and differences to canonical proteasome inhibition. To clarify further what BRD1732 is doing in cells I performed two key experiments in parallel on the same human cell line: transcriptional profiling by RNA-Seq and proteomics profiling by TMT-MS (**Figure 5.5A**). This enabled a head-to-head comparison of proteasome inhibition by MG132 and BRD1732. These compounds both induced transcriptional changes that were dramatically different from each other, as assessed by Principal Component Analysis (**Figure 5.5B**). In addition, MG132 and BRD1732 exhibited little correlation in terms of gene expression (**Figure 5.5C**). Despite this, of the most variable genes in both treatments those that did overlap between MG132 and BRD1732 were changed in the same direction, suggesting in fact that there are some commonalities in the compound's function

as was seen previously. Of the ~4,000 genes significantly change by BRD1732, 1,786 were also changed with MG132 treatment, with 615 and 1076 being upregulated and downregulated in both conditions, respectively (**Figure 5.5D**). Because of the parallel proteomics data I could use the transcriptional data to identify which proteins changed significantly only at the protein level and not its RNA. Both MG132 and BRD1732 caused significant accumulation of proteins that had little change in their RNA abundance, including key cell cycle regulators such as CDKN1A and CDKN1B (**Figure 5.5E-F**). Stabilization of these cell cycle proteins was dramatic, with BRD1732 increasing more than 5-fold CDKN1A, CDKN1B, CDKN2A, and BCL6, with a larger magnitude than MG132 and little changes at the RNA level (**Figure 5.5G**). At the gene-set level both MG132 and BRD1732 caused changes in genes associated with NFkB signaling, corroborating previous results showing inhibition of this pathway by BRD1732 (**Figure 5.5H**).

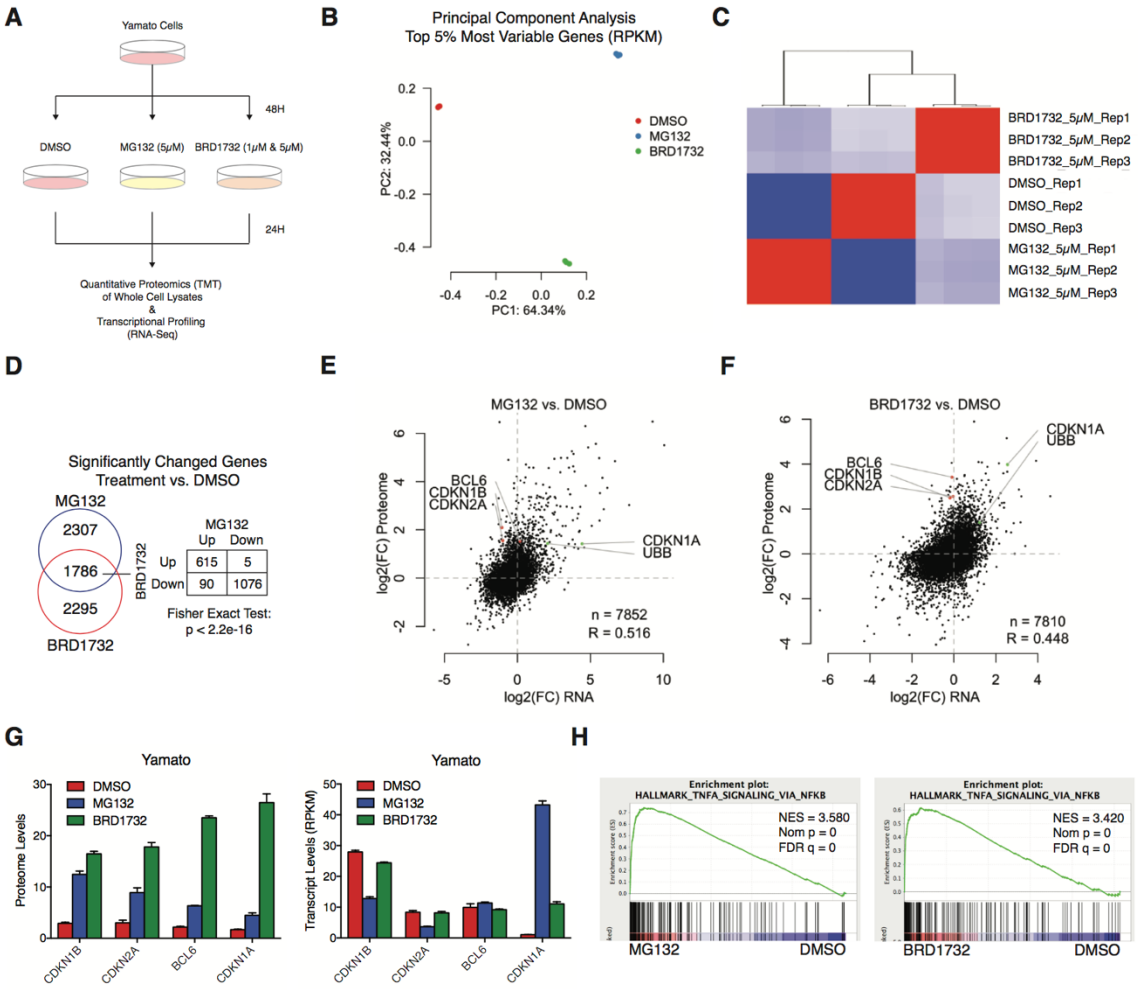


Figure 5.5. BRD1732 induces a transcriptional and proteome-wide change that is distinct from proteasome inhibition. (A) Outline of performed proteomics and transcriptional profiling of Yamato cells following compound treatment. (B) Principal component analysis (PCA) of gene expression in Yamato cells after treatment with BRD1732 or MG132. (C) Gene expression correlation for the top 5% most variable genes under each treatment condition.

Figure 5.5 (Continued). (D) Number of significantly changed genes for each compound normalized to vehicle. Table highlights the directionality of change for genes that are variable under both BRD1732 and MG132 treatment. (E-F) Scatter plot of fold-change at the protein and RNA level for MG132 (left) and BRD1732 (right). Highlighted are key genes that change predominantly at the protein level only. (G) Protein (left, relative abundance) and expression levels (right, RPKM) for key genes that change with BRD1732 treatment. (H) Gene-set Enrichment Analysis (GSEA) for genes that change with MG132 (left) or BRD1732 (right) treatment.

At the protein level alone there were numerous changes that were different between MG132 and BRD1732 (**Figure 5.6A**). The protein that was most increased by BRD1732 was the potent cell cycle inhibitor CDKN1A, a stabilization that was nearly 6-times more than the change caused by MG132 (**Figure 5.6B**). Other proteins increased included CCNF, BCL6 and FBXO3, in addition to multiple proteins known to be located in the nucleus. Unlike BRD1732, MG132 selectively increased levels of proteins associated to proteotoxic stress, including HSPA6 and HSPA7 (**Figure 5.6B**).

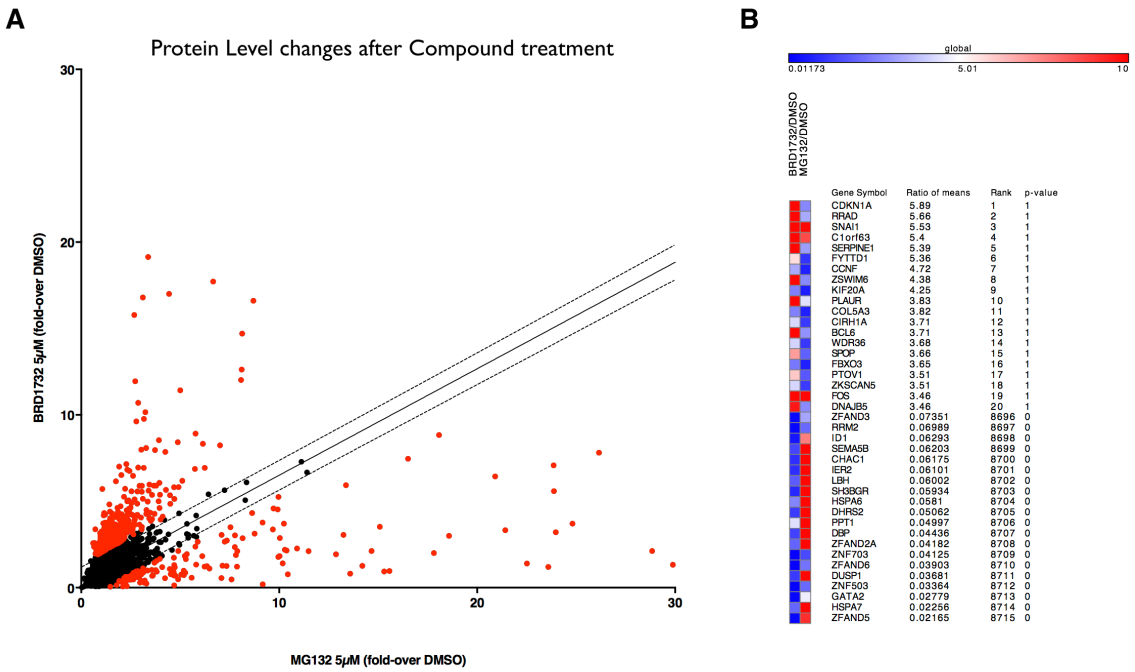


Figure 5.6. BRD1732 stabilizes a unique set of proteins that are different from MG132. (A) Scatter plot of protein levels following BRD1732 or MG132 treatment normalized to DMSO (fold Relative Abundance). (B) Proteins found to differentiate BRD1732 and MG132 treatment ranked by the ratio of means (BRD1732 over MG132).

Transcriptional changes caused by BRD1732 and MG132 are distinct, with MG132 response being dominated by genes responding to proteotoxic stress, e.g. HSPA6 and HSPA7 (as seen with the proteomics) (**Figure 5.7A**). Gene-ontology analysis reveals that MG132 transcriptional changes are mostly associated to the unfolded protein response, including response to unfolded protein stress and PERK-mediated UPR (**Figure 5.7B**). This is in contrast to BRD1732, whose transcriptional profile changes are enriched for genes associated to the cell cycle, including cell division and mitosis (**Figure 5.7C**). This is exemplified by upregulation of TOP2A and AURKB. Interestingly there were some ubiquitin-proteasome related genes upregulated by BRD1732, such as UBE2C and UBE2S.

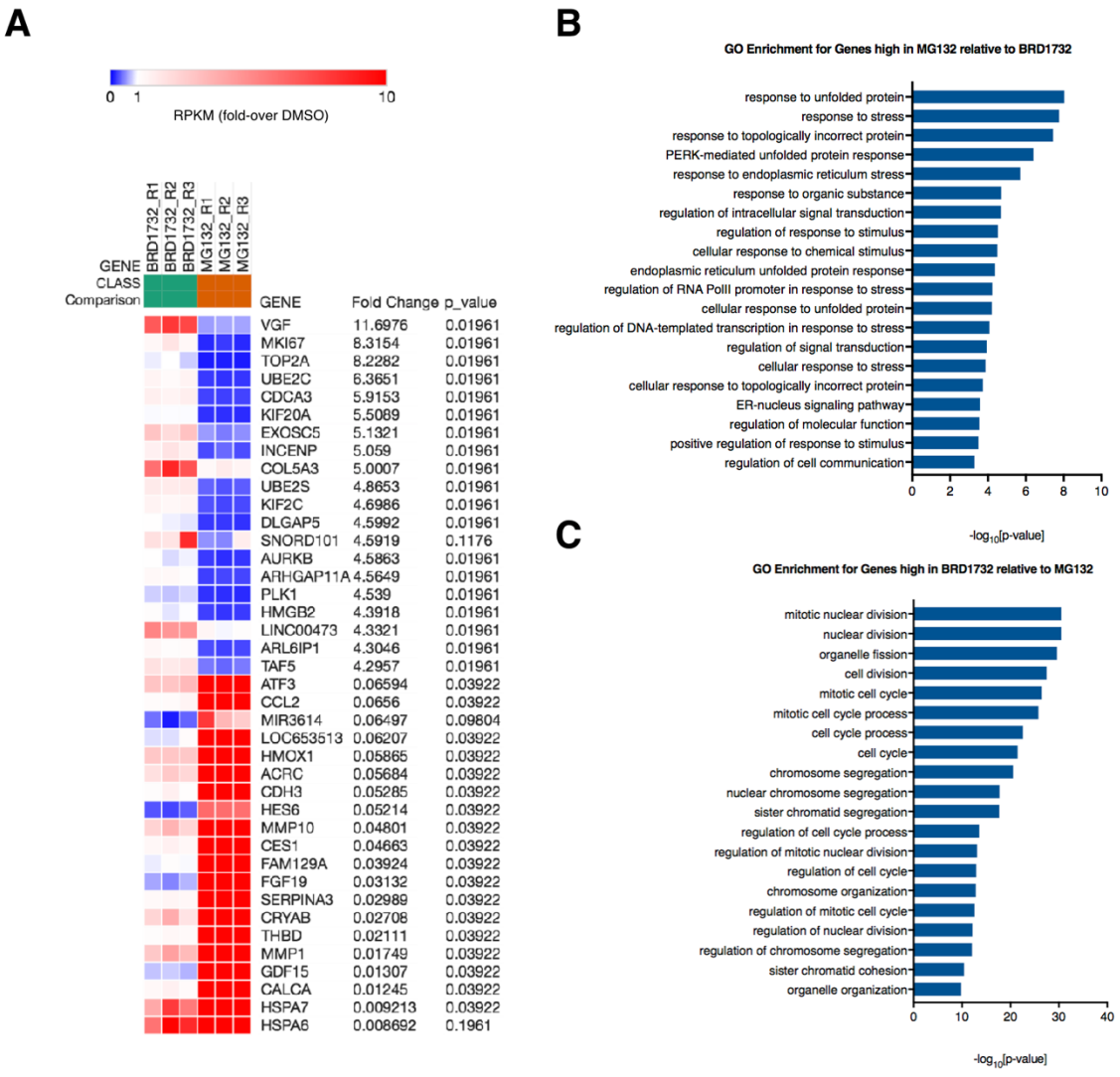


Figure 5.7. BRD1732 causes transcriptional changes that are distinct from MG132. (A) Identification of genes that are significantly changed differently in BRD1732 as compared to MG132, ranked by fold-change (normalized to DMSO). (B) Gene-ontology enrichment for genes significantly upregulated by MG132 treatment when compared to DMSO. (C) Same as in (B) but with BRD1732 treatment.

Chapter 5.5: BRD1732 Induces Cell-Cycle Arrest

One of the more striking features of BRD1732 was its ability to stabilize the cell cycle inhibitors p21 (CDKN1A) and p27 (CDKN1B), two tumor suppressors known to induce senescence in cancer cell line models (Wang et al., 2015). This increase was dramatic, being more than 10-fold over DMSO and 6-fold over MG132, even more than what was seen for the BAF47-NL reporter (**Figure 5.8A**). Cell cycle profiling showed that BRD1732 was able to induce accumulation of cells in the S-phase after 24 hours of treatment, a faster arrest than what was seen with MG132 (**Figure 5.8B**). Not surprisingly BRD1732 was able to prevent the growth of various cancer cell lines, the most the affected being the AML line PEER, even those that did not respond to MG132 (i.e. MCF7 and A549) (**Figure 5.8C**).

Given these results, one potential avenue for BRD1732 clinical development is as a therapeutic for patients that are refractory to proteasome inhibition. One such example occurs in multiple myeloma, where bortezomib resistance is frequently observed. To emulate such cases I used a multiple myeloma cell line that has a mutation linked to bortezomib resistance. ANBL6-V5R, which is bortezomib resistant, and its parental line ANBL6 were treated with either BRD1732 or bortezomib for three different time points up to 72H. ANBL6-V5R did

not show a differential response to BRD1732 when compared to the parental line, while response to bortezomib was attenuated in this genetic background (**Figure 5.8D**).

To determine if BRD1732 would be amenable to in vivo studies I tested its stability in human and mouse microsomes. This measurement serves as a proxy to bioavailability, and good microsomal stability is key in assessing a molecule's pharmacokinetic (PK) properties (Crawford et al., 2016). In both human and mouse microsomes BRD1732 had very poor stability, with a half-life of 23.8 and 20.7 minutes respectively. Remaining compound after 60 min in the presence of human microsomes was 17.6%, much less than what is necessary for in vivo treatments. This suggests that further medicinal chemistry will be necessary before it is possible to treat mice, and subsequently humans, with BRD1732.

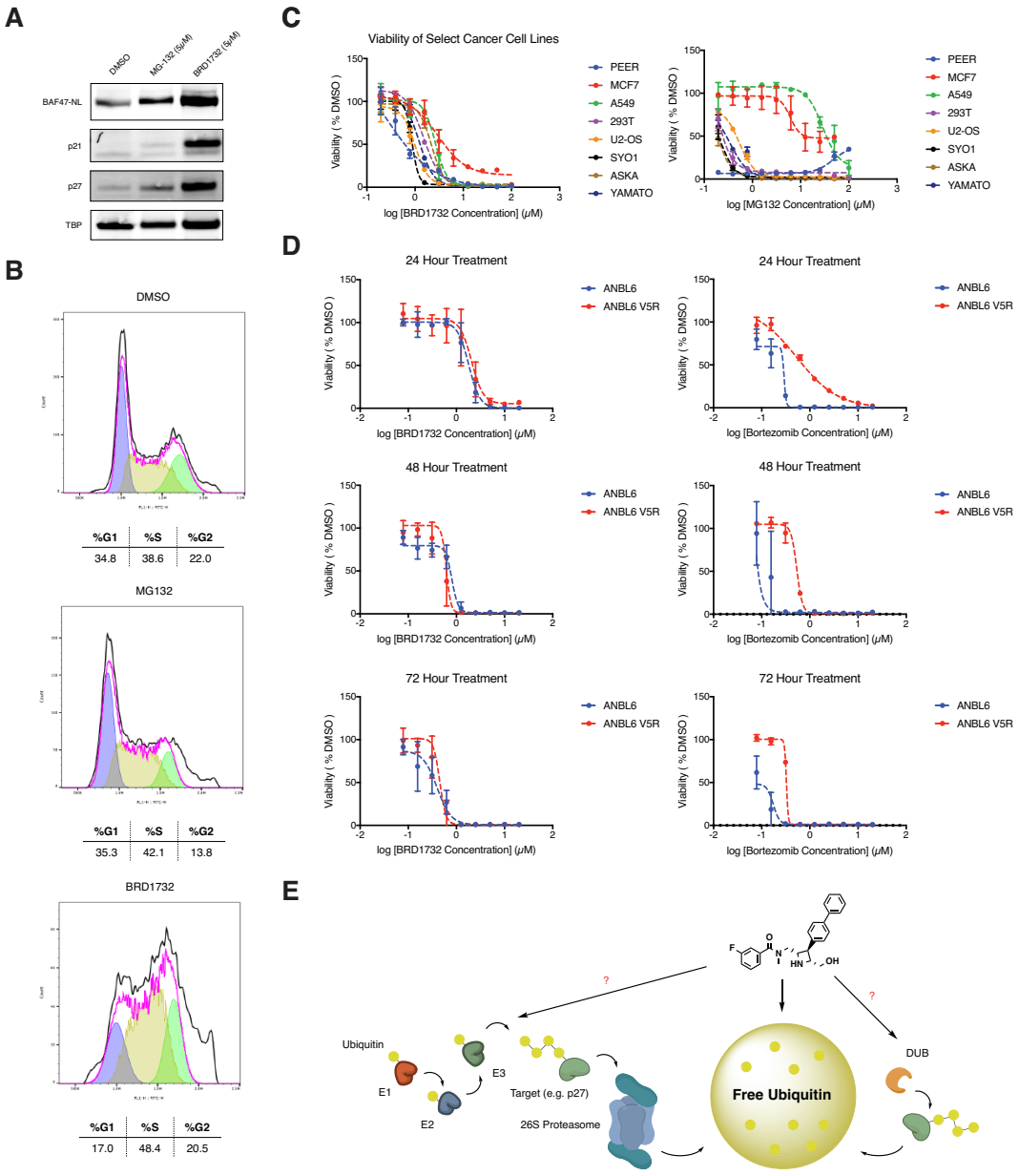


Figure 5.8. BRD1732 inhibits cancer cell line proliferation through protein stabilization of cell-cycle inhibitors. (A) Whole-cell immuno- blot of Yamato lysates for the reporter BAF47-NL and cell-cycle inhibitors p21 and p27 following 24 hours of compound treatment.

Figure 5.8 (Continued). (B) Cell-cycle profiling of Yamato cells treated with compound for 24 hours using fluorescent DNA dyes. (C) Viability of select cancer cell lines measured with CellTiterGlo following compound treatment for 48 hours. (D) Viability of ANBL6 cell line and its bortezomib-resistance daughter cell line ANBL6 V5R following treatment with MG132 or BRD1732 over different time points. (E) Proposed MOA of BRD1732.

Chapter 5.6: Target ID Efforts for BRD1732

Chapter 5.6.1: Biotinylated Analogs of BRD1732

Identifying the target of BRD1732 is necessary for fully comprehending its MOA. Several methods exist for this purpose, and I employed a variety of assays with limited success, focusing on affinity-based methods and resistance screens. First I coordinated the generation of two BRD1732 analogs that contained a biotin molecule linked to the azetidine-scaffold through a covalent linker. These were prepared by Micah Maetani, the same scientist that performed the medicinal chemistry efforts that yielded BRD1732. Both of these compounds had activity in the BAF47-NL screen, albeit it was significantly reduced when compared to BRD1732 (**Figure 5.9A**). One compound had the biotin placed on the amide near the azetidine-ring, N- (((2S,3R,4R)-3- (4'-fluoro-[1,1'-biphenyl]-4-yl)-4-

(hydroxymethyl)azetidin-2-yl)methyl)-N-methyl-6- (5- ((3aS,4S,6aR)-2-oxohexahydro-1H-thieno[3,4-d]imidazol-4-yl)pentanamido)hexanamide, while the other was linked to biotin through the free alcohol at the azetidine-ring, ((2R,3R,4S)-3- ([1,1'-biphenyl]-4-yl)-4- ((3-fluoro-N-methylbenzamido)methyl)azetidin-2-yl)methyl (2- (2- (2- (5- ((3aS,4S,6aR)-2-oxohexahydro-1H-thieno[3,4-d]imidazol-4-yl)pentanamido)ethoxy)ethoxy)ethyl)carbamate (**Figure 5.9B**). Despite the decreased potency I tested the ability of these compounds to capture their target by affixing them to streptavidin beads and subsequently flowing cell lysate through them in the presence or absence of BRD1732. Neither was able to produce a significant protein enrichment that was lost in the presence of competitor, and an exemplary gel of the experiment is shown (**Figure 5.9C**). I also attempted to determine if any protein was being enriched at low abundances using mass spectrometry, but this gave non-conclusive results. Several variations in the experimental conditions were also unsuccessful, including lysate amount, buffers used, and washing conditions of the affinity media.

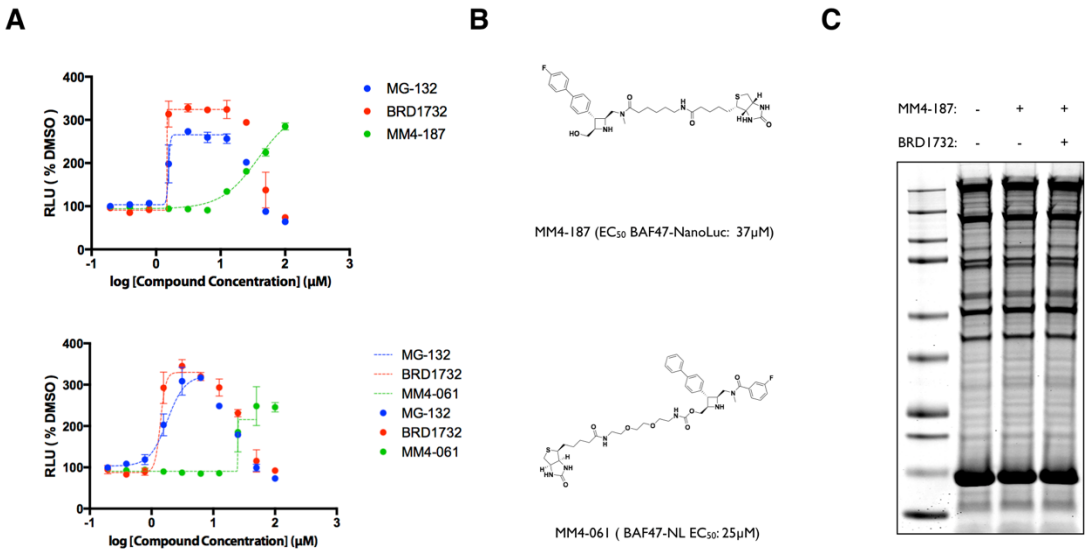


Figure 5.9. Two active biotinylated analogs of BRD1732. (A) Activity of two biotinylated analogs of BRD1732, MM4-187 and MM4-061, in comparison to BRD1732 and MG132. (B) Structure of aforementioned analogs and their EC_{50} in the BAF47-NL assay. (C) Exemplary gel of performed affinity capture experiments using these analogs and Yamato cell lysates.

Chapter 5.6.2: Identifying Resistance Mechanisms to BRD1732 using CRISPR

BRD1732 treatment causes toxicity in the majority of cell lines I tested. It then follows that inducing resistance to this treatment through genetic manipulation could hint at the target of BRD1732. I set out to perform a genome-wide CRISPR screen for resistance to compound treatment in a prostate cancer cell line background. I picked this cell line due to its ease of use and availability, in addition to the fact that it had been used in the past with the AVANA CRISPR library that was employed.

BRD1732 had a half-maximal growth inhibitory concentration of 4.5μM, and this was equal to that observed with MG132. Once the KP-4 cells were infected with the genome-wide CRISPR guide library, they were treated with BRD1732 at 10μM for 3 days, causing the death of approximately 90% of the cells. After the cells recovered I identified which guides were enriched using genome sequencing. Only the guides for one gene showed significant enrichment in the cells that survived BRD1732 treatment, and those were for RNF19B (**Figure 5.10A**).

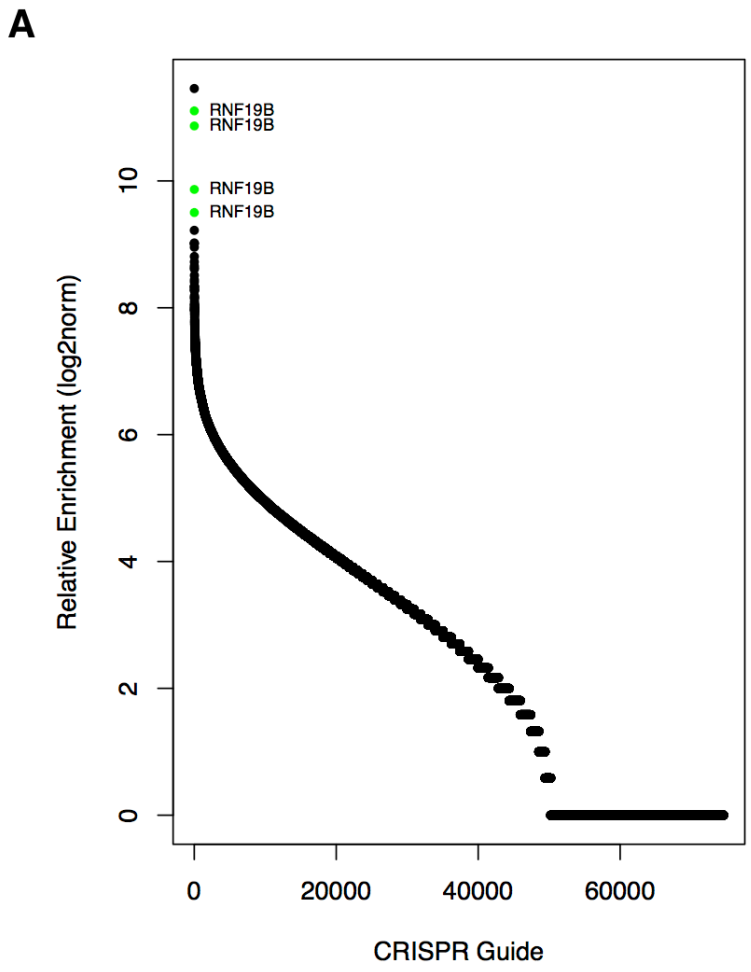


Figure 5.10. Loss of RNF19B Causes Resistance to BRD1732. (A) CRISPR guide relative enrichment in samples treated with BRD1732 at 10μM for 3 days. The abundance of guide was normalized to that found in DMSO treated cells under the same conditions.

Chapter 5.7: Methods

Chapter 5.7.1: Cell Culture

All cells were grown in DMEM (Gibco) (supplemented with GlutaMax, 10% FBS (OmegaScientific), 1 mM sodium pyruvate (Gibco), and 1 mg/mL penicillin-streptomycin (Gibco)), except PEER and KP-4 cells which were grown in RPMI-1640 (Gibco) media (supplemented with 10% FBS (OmegaScientific) and 1mg/mL penicillin-streptomycin (Gibco)).

Chapter 5.7.2: Immunoblotting and Compound Treatment

Cell pellets were lysed in RIPA Buffer (supplemented with cOmplete Protease Inhibitors (Roche)) and cleared by micro-centrifugation (17,000 x g for 20 min). Protein concentration was measured using a DC Protein Assay (Bio-Rad). 40μg of cell lysate was separated using Bolt PAGE (Life Technologies) and transferred onto Immobilon-FL PVDF membrane (Millipore) using a wet transfer protocol. Proteins were detected using antibodies used at a concentration of 1 μg/mL (all antibodies were obtained from CellSignaling) and detected using an Odyssey CLx Imaging System (LI-COR).

Chapter 5.7.3: In vitro Proteasome Activity

Human purified 20S and 26S proteasome particles were obtained from a commercial vendor (Boston Biochem), and used at a concentration of 1nM in all assays. 20S activity was measured in 20S Assay Buffer (50mM Tris pH 7.5, 25mM KCl, 10mM NaCl, 1mM MgCl2, and 0.01% SDS) using LLVY-AMC, LLE-AMC, and LRR-AMC peptide substrates (Enzo LifeSciences) at 20μM to measure the chymotrypsin-like, caspase-like, and trypsin-like activities, respectively. 26S activity was measured in 26S Assay Buffer (30mM Tris pH 7.5, 10mM MgCl2, 1mM ATP, and 1mM DTT) using the same peptide substrates. Measurements for 20S and 26S assays were taken in kinetic mode for 60 minutes in a SpectraMax M5 Microplate Reader (MolecularDevices), and kinetic parameters were obtained using the device's software fitting tools.

Chapter 5.7.4: NFκB Activity Reporter

A construct with five copies of an NFκB response element that drive a destabilized form of NanoLuc® (pNL3.3.NF-kB-RE/Hygro, Promega) was transfected into 293T cells. Cells were plated in a 384-well plate at a density of $0.4x10^6$ cells / mL and allowed to adhere for 24 hours. NFκB signaling was induced with recombinant TNF-α (SigmaAldrich), used at 2 μg/mL, for 6 hours.

Subsequent induction of NanoLuc® was measured by the addition of NanoGlo® reagent (Promega), and luminescence was detected after 10 minutes in an Envision Multi-label Plate Reader (Perkin Elmer).

Chapter 5.7.5: Aggresome Formation

Yamato cells were added to a 96-well black clear-bottom plate (Corning) at a density $0.2x10^6$ cells / mL and allowed to adhere for 24 hours. Cells were subsequently treated with compound for 24 hours. Aggresome formation was measured using the ProteoStat® dye (Enzo LifeSciences), and the experiment was performed according to the manufacturer's protocol. Induced signal from the dye was measured using a confocal Opera Phenix High Content Screening System (Perkin Elmer).

Chapter 5.7.6: Transcriptional Profiling

Yamato BAF47-NL cells were plated in 15cm dishes at a density of $2x10^6$ cells / mL and allowed to grow for 48 hours or until 75% confluency was reached. These cells were then treated with BRD1732 at 5μM, MG132 at 5μM, or DMSO in triplicate at a final DMSO concentration of 1% v/v, and incubated for 24 hours.

RNA extraction, RNA-Seq and data processing was performed as previously described (see Chapters 2.5.3 and 2.5.4).

Chapter 5.7.7: Whole-lysate Proteomics

Yamato BAF47-NL cells were plated in 10cm dishes at a density of $2x10^6$ cells / mL and allowed to grow for 48 hours or until 75% confluency was reached. These cells were treated with BRD1732 at 1 or 5 μM, MG132 at 5μM, or DMSO for 24 hours at a final DMSO concentration of 1% v/v. Cells were harvested, washed with ice-cold PBS, and lysed in 200μL of RIPA (5omM Tris-HCl pH 7.5, 150mM NaCl, 1% Triton X-100, 0.1% SDS, 0.5% sodium deoxycholate, 1mM DTT, and cOmplete Protease Inhibitors (Roche)). Protein concentrations were measured using the DC Protein Assay (Bio-Rad). Samples were submitted for quantification via Tandem Mass Tag (TMT) mass spectrometry, performed by Steve Gygi's group at Harvard Medical School.

Chapter 5.7.8: Cell-cycle Profiling

Yamato cells were plated in 10cm dishes at a density of $2x10^6$ cells / mL and allowed to grow for 48 hours or until 75% confluency was reached. These cells were treated with BRD1732 at 5 μM, MG132 at 5μM, or DMSO for 24 hours at a final DMSO concentration of 1% v/v. Cells were harvested, and $1x10^6$ cells were re-suspended in 1mL of PBS and incubated with 1μL of DyeCycle® Violet (Life Technologies) for 30 minutes at 37ºC. Fluorescence in cells was then measured using a CytoFLEX Flow Cytometer (Beckman Coulter), and the data was analyzed using FlowJo (FlowJo).

Chapter 5.7.9: CRISPR Resistance Screen

KP-4 cells expressing Cas9 were infected with the AVANA genome-wide sgRNA library (Doench et al., 2016) and plated in T175 flasks at a density of $2x10^6$ cells / mL and allowed to adhere for 48 hours. Cells were then treated with BRD1732 at 10μM or DMSO for 3 days, and allowed to recover from treatment for additional 7 days. Following recovery cells were harvested and genomic DNA was isolated using Maxi kits according to the manufacturer's protocol (Qiagen). Next-generation sequencing was performed by the Genomics Platform at the Broad Institute.

Chapter 5.8: Conclusions

In this chapter I have described the cellular activity of BRD1732, a novel small molecule that can dramatically increase the protein levels of tumor suppressor BAF47. Through the use of higher-level biological annotations, I observed that transcriptional changes induced by BRD1732 were very similar to those caused by loss of the ubiquitin-proteasome system, both through gene knockdown and pharmacological inhibition. Surprisingly, BRD1732 does not cause the accumulation of poly-ubiquitin proteins, but rather a stark increase in the levels of free ubiquitin and ubiquitin-chains in the cell. This is remarkably different to canonical inhibition, and is a phenotype that has not been previously described in the literature. This increase occurs simultaneously with protein stabilization. It is also quite fast, with free ubiquitin increasing after an hour of treatment with BRD1732.

Given this observation it was not surprising that BRD1732 did not inhibit the proteasome in vitro, as this phenotype is not related to canonical proteasome inhibition. Nonetheless I cannot rule out that proteasome activity is being perturbed by BRD1732. For one, all in vitro assays I performed used fluorescent peptides, an artificial set of substrates that does not resemble a fully ubiquitinated substrate since its degradation does not require activity of the 19S

regulatory particle. Further studies should explore BRD1732's activity in reconstituted proteasome assays where a ubiquitinated substrate is used. Second, the proteasome is a massive and complicated protein complex whose regulation is still being explored today. BRD1732 could easily be affecting a yet unknown part of proteasome function that when inhibited leads to the observed phenotype. Lastly, BRD1732 could be activating parts of the proteasome, e.g. its deubiquitinase activity.

Interestingly BRD1732 appears to induce a cellular response that mimics loss of ubiquitin, even though there is an accumulation of free ubiquitin in the cell. This is exemplified by an accumulation of proteins with NEDD8 conjugated, which is seen in cases where ubiquitin is depleted (Leidecker, Matic, Mahata, Pion, & Xirodimas, 2012). In addition, nuclear ubiquitin is lost with an almost complete removal of ubiquitin from histone H2A at K119. This latter modification has been shown to be a major storage of ubiquitin that is only accessed in the event of ubiquitin loss in the cytosol (Dantuma et al., 2006). This is despite evidence that BRD1732 does not induce severe proteotoxic stress at relevant doses, both from a lack of XBP1 induction and no accumulation of aggresomes. In addition, global protein breakdown was not significantly altered by BRD1732. Since no single protein has been described to have such a profound effect on the ubiquitin-proteasome system, one possibility is that BRD1732 is inhibiting a family of

ubiquitin ligases. Such a multi-target effect could explain the various, and at times paradoxical, responses.

None of the early stages in the ubiquitin ligation process were inhibited by BRD1732 in vitro, including E1 and E2 activities. To explore ubiquitin ligation in more detail, a series of key biochemical and cellular experiments need to be performed. It is still unclear what the ubiquitination state of proteins that are stabilized by BRD1732 is. If these proteins are indeed losing ubiquitin, and hence cannot be degraded by the proteasome, this would implicate ubiquitin ligation as a major component of BRD1732's MOA. On the other hand, if ubiquitin is still present in these proteins it is more likely that BRD1732 is preventing their degradation further downstream in the pathway. This can be teased out in vitro using reconstituted assays, e.g. using 26S proteasome particles with ubiquitinated full-length protein substrates.

It is clear that BRD1732 functions distinctly from proteasome inhibitors, and this was confirmed by exploring transcriptional and proteome-wide changes caused by each treatment. MG132 induced a cell state that was characterized by increase in genes and proteins associated with a response to proteotoxic stress, whereas BRD1732's response was dominated by cell cycle genes. This latter effect could be due to induction of cell senescence by p21/p27 accumulation, and

hence not a direct effect of the BRD1732's target. Performing similar experiments at earlier time points could help tease out the secondary and tertiary cellular responses from BRD1732's target inhibition.

From a translational point of view BRD1732 is very interesting, causing growth arrest in various cancer cell lines, including some that do not respond to MG132 and have acquired resistance to bortezomib. This is likely due to NFkB signaling inhibition and stabilization of cell cycle inhibitors, both potent mechanisms of cancer cell growth inhibition (Manasanch & Orlowski, 2017). Further medicinal chemistry will look to improve the potency of BRD1732 in addition to its bioavailability, with the aim of performing pre-clinical studies as a cancer therapeutic.

The efforts performed to date for the identification of BRD1732's target have not been successful, most likely due to the weak potency exhibited by the biotin analogs of the compound. As such an effort needs to be made to use label-free methods that can harness the full potency of BRD1732. One of these is thermal proteome profiling, which attempts to identify proteins that have a shift in thermal stability in the presence of a small molecule, with the assumption that this is a consequence of the compound's binding (Saxena, 2016).

If I can identify the target of BRD1732, it will make for a valuable addition to the chemical toolset available to study the ubiquitin-proteasome system. Currently there are no small molecules or genes known to display this phenotype, with an impressive accumulation of free ubiquitin and wide-spread (but not global) protein stabilization effect. Such tools can further our understanding of this pathway and advance its therapeutic relevance, not only for cancer but other malignancies that are linked to protein degradation.

References

Crawford, T. D., Romero, F. A., Lai, K. W., Tsui, V., Taylor, A. M., de Leon Boenig, G., et al. (2016). Discovery of a Potent and Selective in Vivo Probe (GNE-272) for the Bromodomains of CBP/EP300. *Journal of Medicinal Chemistry*, *59* (23), 10549–10563. http://doi.org/10.1021/acs.jmedchem.6b01022

Dantuma, N. P., Groothuis, T. A. M., Salomons, F. A., & Neefjes, J. (2006). A dynamic ubiquitin equilibrium couples proteasomal activity to chromatin remodeling. *The Journal of Cell Biology*, *173* (1), 19–26. http://doi.org/10.1083/jcb.200510071

Doench, J. G., Fusi, N., Sullender, M., Hegde, M., Vaimberg, E. W., Donovan, K. F., et al. (2016). Optimized sgRNA design to maximize activity and minimize off-target effects of CRISPR-Cas9. *Nature Biotechnology*, *34* (2), 184–191. http://doi.org/10.1038/nbt.3437

Lamb, J., Crawford, E. D., Peck, D., Modell, J. W., Blat, I. C., Wrobel, M. J., et al.

(2006). The Connectivity Map: using gene-expression signatures to connect small molecules, genes, and disease. *Science (New York, N.Y.)*, *313* (5795), 1929–1935. http://doi.org/10.1126/science.1132939

Leidecker, O., Matic, I., Mahata, B., Pion, E., & Xirodimas, D. P. (2012). The ubiquitin E1 enzyme Ube1 mediates NEDD8 activation under diverse stress conditions. *Cell Cycle (Georgetown, Tex.)*, *11* (6), 1142–1150. http://doi.org/10.4161/cc.11.6.19559

Lumley, E. C., Osborn, A. R., Scott, J. E., Scholl, A. G., Mercado, V., McMahan, Y. T., et al. (2017). Moderate endoplasmic reticulum stress activates a PERK and p38-dependent apoptosis. *Cell Stress & Chaperones*, *22* (1), 43–54. http://doi.org/10.1007/s12192-016-0740-2

Manasanch, E. E., & Orlowski, R. Z. (2017). Proteasome inhibitors in cancer therapy. *Nature Reviews. Clinical Oncology*, *28*, 9270. http://doi.org/10.1038/nrclinonc.2016.206

Poothong, J., Tirasophon, W., & Kaufman, R. J. (2017). Functional analysis of the mammalian RNA ligase for IRE1 in the unfolded protein response. *Bioscience Reports*, *37* (2), BSR20160574. http://doi.org/10.1042/BSR20160574

Roy, A., & Wonderlin, W. F. (2003). The permeability of the endoplasmic reticulum is dynamically coupled to protein synthesis. *The Journal of Biological Chemistry*, *278* (7), 4397–4403. http://doi.org/10.1074/jbc.M207295200

Saxena, C. (2016). Identification of protein binding partners of small molecules using label-free methods. *Expert Opinion on Drug Discovery*, *11* (10), 1017–1025. http://doi.org/10.1080/17460441.2016.1227316

Shah, S. A., Potter, M. W., McDade, T. P., Ricciardi, R., Perugini, R. A., Elliott, P. J., et al. (2001). 26S proteasome inhibition induces apoptosis and limits growth of human pancreatic cancer. *Journal of Cellular Biochemistry*, *82* (1), 110–122.

Wang, Y., Luo, Z., Pan, Y., Wang, W., Zhou, X., Jeong, L. S., et al. (2015). Targeting protein neddylation with an NEDD8-activating enzyme inhibitor MLN4924 induced apoptosis or senescence in human lymphoma cells. *Cancer Biology & Therapy*, *16* (3), 420–429. http://doi.org/10.1080/15384047.2014.1003003

Wawer, M. J., Li, K., Gustafsdottir, S. M., Ljosa, V., Bodycombe, N. E., Marton, M. A., et al. (2014). Toward performance-diverse small-molecule libraries for cell-based phenotypic screening using multiplexed high-dimensional profiling. *Proceedings of the National Academy of Sciences of the United States of America*, *111* (30), 10911–10916. http://doi.org/10.1073/pnas.1410933111

Chapter 6: Concluding Remarks

Chapter 6.1: Summary and Impact of Dissertation

In this thesis, I have presented two impactful scientific discoveries: (1) that the MET oncogene is a dependency in some cases of biphasic synovial sarcomas, and (2) that BRD1732 is novel small molecule probe of the ubiquitin proteasome system. This first finding could be a real benefit in the clinic, given that SS treatment remains a largely unmet need. I identified that two SS cancer cell lines that were particularly sensitive to MET inhibition, even when the sensitivity in 860 other cancer cell lines was taken into consideration. This sensitivity was recapitulated by genetic knockdown of MET, and MET was found to be amplified in these sensitive lines. In addition, these cells exhibited an active AKT pathway that was dependent on MET activity. This dependency could also be targeted in vivo using the MET inhibitor SGX-523. I explored the translational aspect of MET activity in SS by examining SS patient biopsies, and observed that MET is indeed expressed in SS tumors. This expression was exclusive to the epithelial compartment of biphasic SS, the same histology of the 2 SS cancer cell lines that responded to MET inhibition. Lastly, I compared the transcriptional impact of MET inhibition to loss of SS18-SSX, the fusion protein linked to the oncogenesis of SS. Both perturbations caused pathway changes that resembled differentiation and the epithelial-to-mesenchymal transition. Together the results suggest that MET potentiates SS18-SSX in these SS cancer cell lines, and inhibition of MET

could prove therapeutically useful in biphasic SS cases that harbor MET expression.

The second major finding here presented is the discovery of BRD1732, a small molecule that causes a massive accumulation of free ubiquitin in cells and prevents the degradation of a wide-array of protein substrates. This occurs despite no apparent inhibition of human 20S or 26S proteasome activity in vitro, suggesting a novel MOA. In addition, BRD1732 does not inhibit ubiquitin ligation in vivo, with no activity against human E1 or E2 enzymes. It also had no activity in vitro against 36 proteases, which included cathepsins, deubiquitinases, and caspases. Paradoxically, treatment with BRD1732 resembles a cellular response to loss of ubiquitin, with near complete depletion of nuclear ubiquitin from histones. It can also impair the growth of various cancer cell lines, even those that are relatively resistant to proteasome inhibition. Most likely this is achieved through inhibition of NFkB signaling and upregulation of p21 and p27, both potent effects of BRD1732 treatment. This positions BRD1732 as an attractive alternative for patients who are refractory to bortezomib, the proteasome inhibitor that is widely used in treatment of multiple myeloma.

Chapter 6.2: Future Directions

It remains to be seen if the mechanisms that led to MET inhibitor sensitivity in SS cell lines, mainly amplification of the MET gene, also occur in patients. This can be addressed using fluorescence in-situ hybridization (FISH) using a MET probe to determine if MET is amplified in biphasic SS patient tumors. If amplification is observed, it would suggest that what was observed in the cell lines is representative of the patient biology. Alternatively if there is no amplification found in patients that would suggest that amplification of MET could be an artifact of cancer cell line generation, and further studies would be necessary to determine if MET is relevant to SS progression. Furthermore, it is unclear how SS generates a biphasic tumor with two distinct histological compartments even when both of these harbor the fusion protein SS18-SSX (Nishio et al., 2001). One possibility is that subsequent chromosomal events or mutations differentiate the two populations, such as amplification of MET, which would explain why MET is only expressed in a single compartment; in this scenario expression of a receptor tyrosine kinase follows generation of SS18-SSX. Another avenue would be if SS18-SSX had a stochastic mechanism of action, in which two stable states exist that are highly dependent on the cell origin. Some cells would transform into epithelial cells while the rest would become spindle-like cells. To address this it would be necessary to establish a robust in vivo model of biphasic SS, either

from patient derived samples or cancer cell lines. Current xenografts do not recapitulate both compartments seen in biphasic SS, and an accurate model would permit interrogation of the mechanisms that give rise to the two distinct histological types of SS.

Further work into BRD1732 must focus on identifying its target and MOA, which has so far remained elusive and complex. The biotin analogs did not display enough potency to warrant further investigation, and as such there should be a focus on label-free methods. This includes thermal proteome profiling to determine what proteins have a change in thermal stability in the presence of BRD1732, a property indicative of binding. These targets can be subsequently validated using the cellular-thermal shift assay (CETSA), which has shown to be a useful tool in small molecule target ID (Alshareef et al., 2016; Martinez Molina et al., 2013). Complementary to this would be a CRISPR screen for mechanisms of resistance that could hint at the target of BRD1732. Genes that when lost cause resistance to BRD1732 would be intimately linked to the target of the compound. Similarly, one would look for loss of sgRNAs relative to DMSO control, which would hint at the genes that augment the potency of BRD1732, one of which could be the target it self. This would be performed in parallel with MG132 treatment to identify a mechanism of resistance that is unique to BRD1732.

Two additional comparison experiments can be performed to illuminate BRD1732's target, with the compounds MLN4924 and MLN7243. The first is a NEDD8 inhibitor which prevents activity of E3 enzymes that depend on this modification (e.g. cullins). If co-treatment of BRD1732 with MLN4924 prevented the increase of poly-ubiquitin chains, it would hint at a mechanism where these chains are being generated but cannot be placed on the protein substrate, e.g. through direct inhibition of an E3 complex. MLN7243 is a recently discovered inhibitor of UBA1, the E1 enzyme responsible for ubiquitin activation. If E1 activity were to be required for BRD1732 activity, then the results would again point to conjugation as a critical step that is being perturbed by BRD1732. On the other hand, if co-treatment with MLN7243 had no activity, it would suggest that the observed accumulation of chains is being caused by their active removal from proteins. Likewise, BRD1732 could target an E1-E2 complex, and co-treatments with MLN7243 could aid in ruling out such a possibility.

To expand on the therapeutic potential of BRD1732 it is necessary to understand which specific subtypes of cancer respond most strongly to the compound. While I did look at several cell lines, it was not a sufficient sample size to make a significant conclusion. This can be addressed using large-scale cancer cell line profiling, such as what is obtained with the PRISM method. Being much faster than traditional screening methods, PRISM pools cancer cell lines that have been

DNA barcoded and treats them collectively, dramatically shortening the amount of time and reagents it takes to get a comprehensive profiling (Yu et al., 2016). Out of ~500 cancer cell lines, PRISM will allow for the identification of those that respond strongly to BRD1732, helping guide its translational development. This will be complemented with a set of viability measurements performed in cell lines derived from patients that are refractory to bortezomib treatment. Lastly, an extensive medicinal chemistry campaign must be launched to improve BRD1732's potency and bioavailability. Only then could pre-clinical studies could be undertaken and the full potential of BRD1732 be explored. With these insights BRD1732 could become an invaluable tool for probing the ubiquitin-proteasome system and its function in human malignancies.

References

Alshareef, A., Zhang, H.-F., Huang, Y.-H., Wu, C., Zhang, J. D., Wang, P., et al. (2016). The use of cellular thermal shift assay (CETSA) to study Crizotinib resistance in ALK-expressing human cancers. *Scientific Reports*, *6* (1), 33710. http://doi.org/10.1038/srep33710

Martinez Molina, D., Jafari, R., Ignatushchenko, M., Seki, T., Larsson, E. A., Dan, C., et al. (2013). Monitoring drug target engagement in cells and tissues using the cellular thermal shift assay. *Science (New York, N.Y.)*, *341* (6141), 84–87. http://doi.org/10.1126/science.1233606

Nishio, J., Iwasaki, H., Ishiguro, M., Ohjimi, Y., Isayama, T., Naito, M., & Kikuchi, M. (2001). Identification of syt-ssx fusion transcripts in both epithelial and spindle cell components of biphasic synovial sarcoma in small tissue samples isolated by membrane-based laser microdissection. *Virchows Archiv : an International Journal of Pathology*, *439* (2), 152–157.

Yu, C., Mannan, A. M., Yvone, G. M., Ross, K. N., Zhang, Y.-L., Marton, M. A., et al. (2016). High-throughput identification of genotype-specific cancer vulnerabilities in mixtures of barcoded tumor cell lines. *Nature Biotechnology*, *34* (4), 419–423. http://doi.org/10.1038/nbt.3460

Page intentionally left blank